Crustal thickening in Gansu-Qinghai, lithospheric mantle subduction, and oblique, strike-slip controlled growth of the Tibet plateau

B Meyer, P Tapponnier, F Bourjot, F D Métivier, G Gaudemer, G Peltzer, Guo Shunmin, Chen Zhitai

Geophys. J. Int. (1998) **135,** 1–47

Crustal thickening in Gansu-Qinghai, lithospheric mantle subduction, and oblique, strike-slip controlled growth of the Tibet plateau

B. Meyer,[1] P. Tapponnier,[1] L. Bourjot,[2] F. Métivier,[1] Y. Gaudemer,[1] G. Peltzer,[3] Guo Shunmin[4] and Chen Zhitai[5]

[1] *Laboratoire de Tectonique,* CNRS-UMR 7578, *Institut de Physique du Globe,* 4 *place Jussieu,* 75252 *Paris cedex* 05, *France*

[2] *Université de Savoie, Chambéry,* 73000, *France*

[3] *Jet Propulsion Laboratory,* 4800 *Oak Drive, Pasadena,* CA 91109, *USA*

[4] *State Seismological Bureau,* 63 *Fuxing Road, Beijing, China*

[5] *Institute of Seismology,* 20 *Donggangxi Road, Lanzhou, China*

Accepted 1998 February 7. Received 1997 December 19; in original form 1997 August 1

SUMMARY

Fieldwork complemented by SPOT image analysis throws light on current crustal shortening processes in the ranges of northeastern Tibet (Gansu and Qinghai provinces, China). The ongoing deformation of Late-Pleistocene bajada aprons in the forelands of the ranges involves folding, at various scales, and chiefly north-vergent, seismogenic thrusts. The most active thrusts usually break the ground many kilometres north of the range-fronts, along the northeast limbs of growing, asymmetric ramp-anticlines. Normal faulting at the apex of other growing anticlines, between the range fronts and the thrust breaks, implies slip on blind ramps connecting distinct active décollement levels that deepen southwards. The various patterns of uplift of the bajada surfaces can be used to constrain plausible links between contemporary thrusts downsection. Typically, the foreland thrusts and décollements appear to splay from master thrusts that plunge at least 15–20 km down beneath the high ranges. Plio-Quaternary anticlinal ridges rising to more than 3000 m a.s.l. expose Palaeozoic metamorphic basement in their core. In general, the geology and topography of the ranges and forelands imply that structural reliefs of the order of 5–10 km have accrued at rates of 1–2 mm yr^{-1} in approximately the last 5 Ma.

From hill to range size, the elongated reliefs that result from such Late-Cenozoic, NE–SW shortening appear to follow a simple scaling law, with roughly constant length/width ratio, suggesting that they have grown self-similarly. The greatest mountain ranges, which are over 5.5 km high, tens of kilometres wide and hundreds of kilometres long may thus be interpreted to have formed as NW-trending ramp anticlines, at the scale of the middle–upper crust. The fairly regular, large-scale arrangement of those ranges, with parallel crests separated by piggy-back basins, the coevality of many parallel, south-dipping thrusts, and a change in the scaling ratio (from ≈ 5 to 8) for range widths greater than ≈ 30 km further suggests that they developed as a result of the northeastward migration of large thrust ramps above a broad décollement dipping SW at a shallow angle in the middle–lower crust. This, in turn, suggests that the 400–500 km-wide crustal wedge that forms the northeastern edge of the Tibet–Qinghai plateau shortens and thickens as a thick-skinned accretionary prism decoupled from the stronger upper mantle underneath.

Such a thickening process must have been coupled with propagation of the Altyn Tagh fault towards the ENE because most thrust traces merge northwestwards with active branches of this fault, after veering clockwise. This process appears to typify the manner in which the Tibet–Qinghai highlands have expanded their surface area in the Neogene. The present topography and structure imply that, during much of that period,

the Tibet plateau grew predominantly towards the northeast or east-northeast, but only marginally towards the north-northwest. This was accomplished by the rise, in fairly fast succession, of the Arka Tagh, Qiman Tagh, Mahan shan, Tanghenan Shan, and other NW-trending mountain ranges splaying southeastwards from the Altyn Tagh, isolating the Aqqik-Ayakkum Kol, Qaidam, Suhai and other catchments and basins that became incorporated into the highland mass as intermontane troughs. The tectonic cut-off of catchments and the ultimate infilling of basins by debris from the adjacent ranges, a result of tectonically forced internal drainage, have thus been essential relief-smoothing factors, yielding the outstandingly flat topography that makes Tibet a plateau.

Using Late-Mesozoic and Neogene horizons as markers, the retrodeformation of sections across the West Qilian Ranges and Qaidam basin implies at least ≈ 150 km of N30°E Neogene shortening. On a broader scale, taking erosion into account, and assuming isostatic compensation and an initial crustal thickness comparable to that of the Gobi platform (47.5 ± 5 km), minimum amounts of Late-Cenozoic crustal shortening on NE sections between the Kunlun fault and the Hexi corridor are estimated to range between 100 and 200 km. In keeping with the inference of a deep crustal décollement and with the existence of Mid-Miocene to Pliocene plutonism and volcanism south of the Kunlun range, such values suggest that the lithospheric mantle of the Qaidam plunged obliquely into the asthenosphere south of that range to minimum depths of the order of 200–300 km. A minimum of ≈ 150 km of shortening in the last ≈ 10 Ma, consistent with the average age of the earliest volcanic–plutonic rocks just south of the Kunlun (≈ 10.8 Ma) would imply average Late-Cenozoic rates of shortening and regional uplift in NE Tibet of at least ≈ 15 mm yr^{-1} and ≈ 0.2 mm yr^{-1}, respectively. Such numbers are consistent with a cumulative sinistral offset and slip rate of at least ≈ 200 km and ≈ 2 cm yr^{-1}, respectively, on the Altyn Tagh fault east of 88°E. The fault may have propagated more than 1000 km, to 102°E, in the last 10 Ma.

Our study of ongoing tectonics in northeast Tibet is consistent with a scenario in which, while the Himalayas-Gangdese essentially 'stagnated' above India's subducting mantle, much of Tibet grew by thickening of the Asian crust, as propagation of large, lithospheric, strike-slip shear zones caused the opposite edge of the plateau to migrate far into Asia. The Asian lithospheric mantle, decoupled from the crust, appears to have subducted southwards along the two Mesozoic sutures that cut Tibet north of the Gangdese, rather than to have thickened. The Bangong-Nujiang suture was probably reactivated earlier than the Jinsha-Kunlun suture, located farther north. Overall, the large-scale deformation bears a resemblance to plate tectonics at obliquely convergent margins, including slip-partioning along large strike-slip faults such as the Altyn Tagh and Kunlun faults. Simple mechanisms at the level of the lithospheric mantle are merely hidden by the broader distribution and greater complexity of strain in the crust.

Key words: deformation, fault propagation, fold and mountain growth, plate tectonics, plateau building, Tibet.

1 INTRODUCTION

The high elevation and great crustal thickness of the Tibet plateau, between the Himalayas and the Kunlun, are generally assumed to result from the India–Asia collision, but the processes that have led to the situation observed today remain unclear. While Ni & Barazangi (1984) or Zhao & Morgan (1985) relate the formation of the plateau to wholesale underthrusting (Argand 1924), or to injection of the crust of India beneath that of Asia, most authors view distributed shortening and thickening of the Asian crust to have been the dominant mechanism (e.g. Dewey & Burke 1973; Molnar & Tapponnier 1978; Mattauer 1986a,b; Molnar & Lyon-Caen 1988). Some (e.g. Molnar *et al.* 1993; England & Houseman 1986, 1989; Dewey *et al.* 1988) also invoke homogeneous thickening and shortening of the Asian lithospheric mantle, followed by convective removal of its lower part.

The lack of detailed mapping of Tertiary thrust zones within Tibet, the lack of high-resolution seismic studies of its deep crustal and upper-mantle structure, the lack of convincing evidence documenting the way in which its elevation changed since the Cretaceous, and the fact that it has been the site of E–W crustal extension since the beginning of the Quaternary (e.g. Tapponnier *et al.* 1981; Armijo *et al.* 1986) have set the stage for enduring controversy. Besides, most extant models addressing the formation of Tibet share a serious bias: they

focus on deformation in the Himalayas and within the plateau (Zhao *et al.* 1993; Nelson *et al.* 1996; Owens & Zandt 1997) rather than along its northern rim.

Active crustal shortening, however, occurs prominently along and north of the Kunlun range, over much of northern Qinghai and Gansu provinces, from the Qaidam basin to the Tarim, Gobi and Alashan platforms (Fig. 1). This broad mountainous region forms the northeastern edge of the Tibet highlands. North, east and west of the Qaidam, it is composed of roughly parallel NW–SE-trending ranges, several hundreds of kilometres long and a few tens of kilometres wide (Qilian Shan, Taxueh Shan, Sulenan Shan, Tanghenan Shan, Qiman Shan, etc., Fig. 1). The ranges tower to 5500–6000 m, more than 4000 m above the Gobi desert. They are separated by intermontane basins with altitudes between 2000 and 4000 m. The average topographic elevation (approximately 3500 m), the presence of Quaternary folds and thrust faults (Guo & Xian 1985; Xu *et al.* 1989; Tapponnier *et al.* 1990a; Meyer 1991; Zhang *et al.* 1991), the level of historical and instrumental seismicity (Institute of geophysics 1976), and thrust fault-plane solutions (Tapponnier & Molnar 1977; Molnar & Lyon-Caen 1989; Ekström 1987; Chen *et al.* 1996) (Fig. 1) concur to indicate that these mountain ranges are still growing, to accommodate thickening of the crust. In the Qaidam basin, seismic profiles and borehole data suggest that thrust faulting and folding began after the Cretaceous, were most active in the Mio-Pliocene, and continue at present (Bally *et al.* 1986).

The region located north of the Kunlun is thus well suited to study the mechanisms by which thickening of the crust of Asia now takes place, as well as whether and how the lithospheric mantle is involved. A strong incentive for such a study is that this region may be viewed as a young outgrowth of the Tibet plateau proper, with which it is contiguous (e.g. Molnar & Tapponnier 1978). Hence, deformation mechanisms at work here today may resemble those that have contributed to the formation of the plateau.

As a step towards elucidating such mechanisms and their bearing on the growth and uplift of orogenic high plateaus, we document here the existence, extent, and geometry of active thrusts and growing folds in some of the mountains of Qinghai and Gansu. Our study is based on fieldwork, guided and complemented by SPOT image analysis. Two regions, at the northern foot of Taxueh Shan, and of Tanghenan Shan, were targets of more detailed investigation and mapping. Particular attention was given to quantitative assessment of the morphology, using either topographic maps (at scales of $1:10^5$ and $1:10^6$) or levelled surface profiles.

We combine geological and structural observations with measurements of surface warping and deformation to clarify fold growth, the relationship between folding and faulting, and to constrain plausible shapes of active thrusts down-section. We then use the insights gained on the geometry of thrust faulting along the Taxueh and Tanghenan Shan, with additional evidence from the Qilian Shan (Peltzer *et al.* 1988; Tapponnier *et al.* 1990a; Meyer 1991; State Seismological Bureau 1993) and the Qaidam basin, to draw inferences on the growth of the mountain ranges and thrusts, on the large-scale organization of crustal shortening, and on its relationship to strike-slip faulting. We finally attempt to place bounds on the amounts and rates of Late Neogene shortening and faulting north of the Kunlun, and discuss the role played by the mantle in the shortening process, the way in which the Tibet plateau developed, and the origin of its flat topography.

2 GROWING RAMP ANTICLINES, ACTIVE DÉCOLLEMENTS AND BRANCHING THRUSTS IN THE FORELANDS OF THE TAXUEH AND TANGHENAN RANGES

2.1 Morphology and age of the mountain piedmonts

Steep mountain range fronts in NE Tibet (Fig. 1) generally rise 2–3 km above piedmont bajadas of great size. Such broad, gently sloping Quaternary aprons result from the coalescence of alluvial fans fed by the many streams that flow out of the ranges. The bajada shown in Fig. 2(a), along the northern piedmont of the Taxueh Shan, south of Changma, is a typical example. The fanglomerates that compose its apron have been deposited as fluvial or fluvio-glacial terraces. While all of them are of Late Quaternary age, they are not coeval. To a first order, on the SPOT image and in the field, three groups of deposits of increasing relative ages (a3, younger than a2, itself younger than a1) may be distinguished on the basis of clast size and consolidation, colour and relative elevation of the surfaces that cap them, and degree of incision of such surfaces by erosion.

On the images of Figs 2, 3, 4 and 5, for instance, the dark linear swaths correspond to the flood channels of the contemporary drainage, floored by the youngest (lowest) deposits of the bajada (a3). The dark-grey colour results from denser vegetation due to more abundant seasonal and subsurface water in the stream beds. Typically, such streams have incised several metres below the average level of the bajada.

The surface that forms the bulk of the bajada apron (a2) has a rather uniform light-grey hue on the SPOT image (Fig. 2a). It has little internal relief, with only small rills, generally less than a couple of metres deep, meandering on its top. Due to loess accumulation in them, the rills are a lighter shade of grey. In the field, much of a2 itself is in fact coated by a thin blanket of loess, a few centimetres to over one metre thick. The blanket becomes thicker southwards, as reflected by its smoother texture and lighter, more even colour on the image (Figs 2a,b). Farther south, near the foot of the range, the uniform, barren bajada blends with a more densely incised and vegetated (darker) surface. We interpret the more rugged morphology to result from the proximal accumulation of coarser debris of morainic origin, reworked by the streams that fan out when escaping the glacial valleys that reach the range front (Fig. 2).

The oldest bajada fanglomerates are exposed along two narrow, ESE-trending zones that are conspicuous on the SPOT image (Figs 2a,b, and for greater detail, Figs 4a,b, and 5a,b). In both zones, such fanglomerates lie above, and are more incised than the rest of the bajada apron (Fig. 4c), even though they appear to merge with it upstream or, at places, downstream. Occasionally, the surfaces that top them stand at somewhat different levels, a few metres apart (Fig. 4e). Overall, however, these levels may be seen as only slightly diachronous components of a distinct terrace surface (a1), which forms the highest and oldest geomorphological unit of the bajada.

The relative age inferred from morphological evidence for each of the three units is consistent with the aspects of the fanglomerates in outcrop. Loose gravel and pebbles mixed

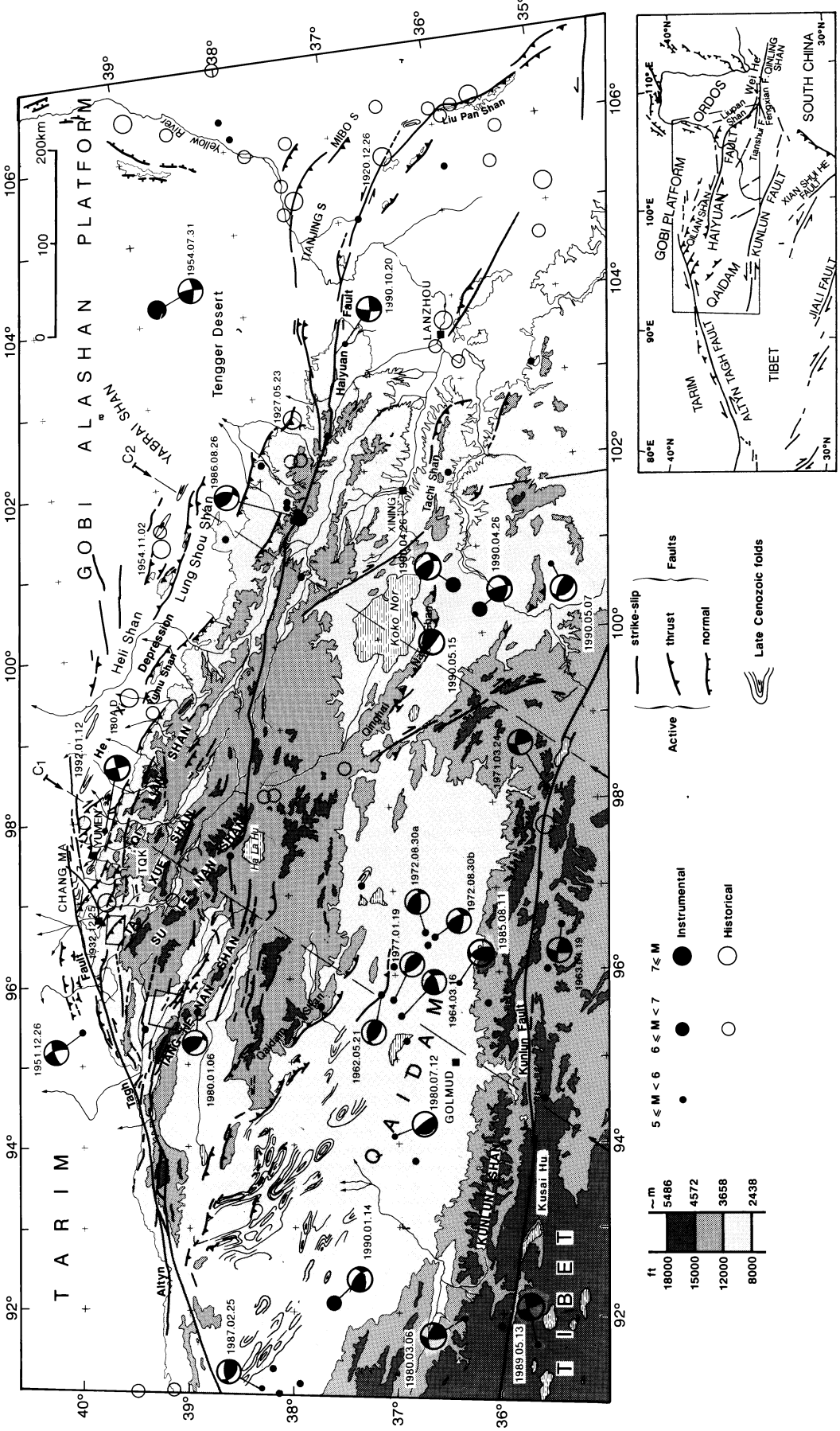

Figure 1. Seismotectonic map of Qinghai–Gansu highlands. The insert shows the location of the region relative to Tibet and within eastern Asia. Active and Quaternary features (faults and folds) are from our fieldwork and Landsat and SPOT image analysis. Elevation contours are from ONC chart G8 (Defense Mapping Agency 1973, 1989). Earthquake epicentres are from the catalogue of strong shocks of China (Institute of geophysics 1976; Gu *et al.* 1989). Fault-plane solutions are from Molnar & Lyon-Caen (1989). Boxes with numbers refer to areas of Figs 2 and 9. Thin dashed lines are sections in Fig. 17. TQK is Ta Quen Kou basin, where piedmont bajada surface loess has been dated (Meyer 1991).

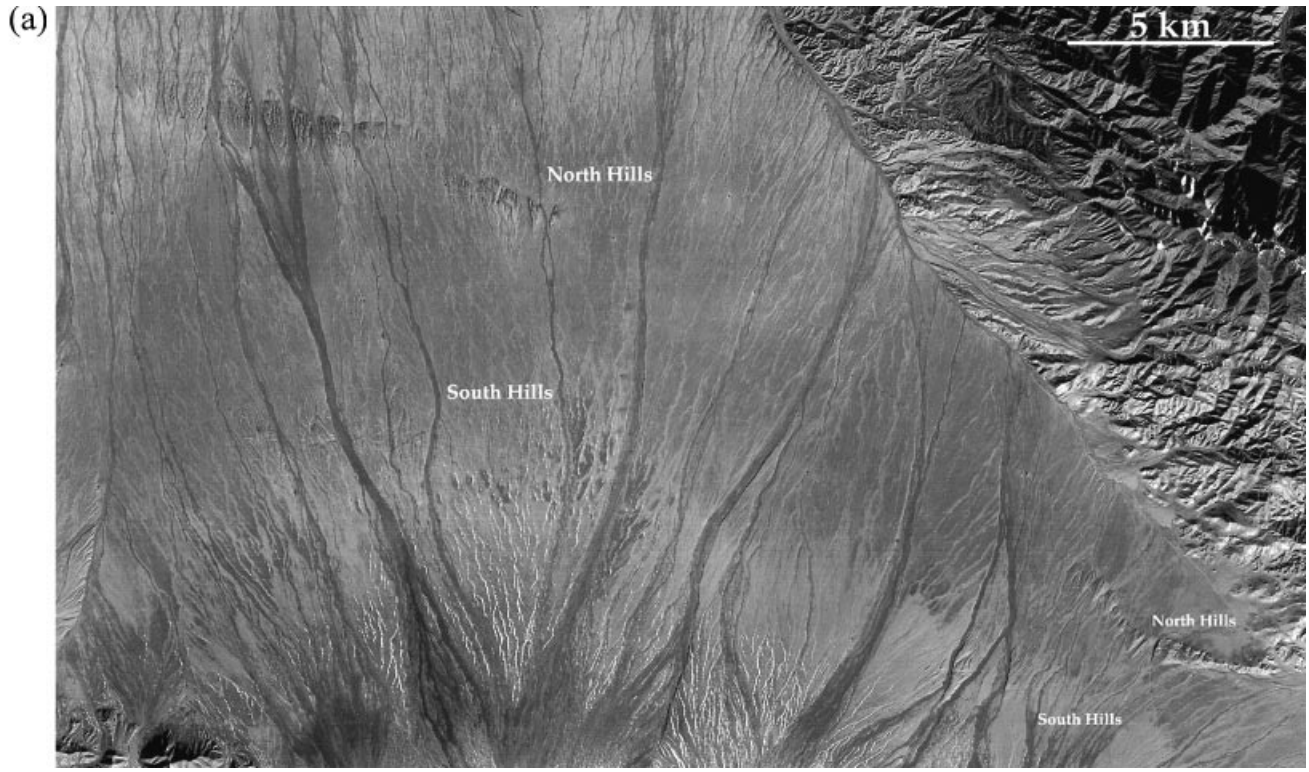

Figure 2(a). Part of panchromatic SPOT scene KJ 240–270 (12/11/87; pixel-size, 10 m).

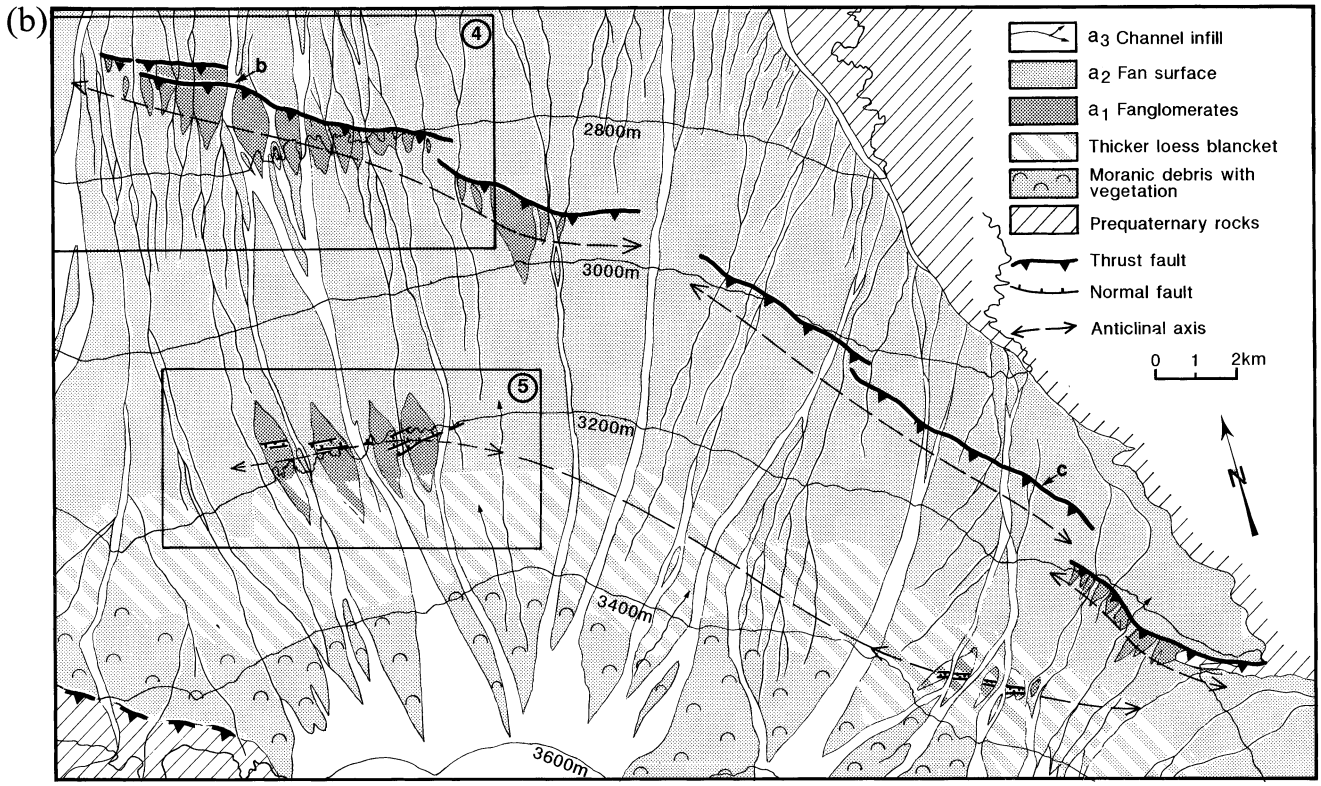

Figure 2(b). Morphotectonic map of Fig. 2(a). Taxueh Shan piedmont is mantled by large postglacial bajada. Three fanglomerate units and surfaces of different ages are distinguished: a3, contemporary stream-channels; a2, coalescent fans of main bajada surface; a1, oldest fanglomerates along narrow EW zones of tectonic uplift corresponding to growing anticlines (thin dashed lines, anticlinal axes). Elevation contours are from PRC $1:10^5$ topographic maps, Chang Ma and Sandou Gou sheets. Boxes indicate locations of Figs 4 and 5.

Figure 3(a). South-looking view of Taxueh Shan Piedmont. The growing north-hills anticline is in the foreground, with the emergent thrust activated by the 1932 Chang Ma earthquake along its front (see Fig. 3b). The south-hills anticline is discernable in the right-middleground. The highest peak of the Taxueh Shan range (5681 m) dominates the background. (**b**). Southeast-looking views of the 1932 Chang Ma earthquake surface break (white arrows) at site b in Fig. 2(b). (**c**). As (b), for site c.

with sand and silt fill the a3 channels, while alternating layers of sandy and pebbly conglomerate characterize a2. Better cemented, more consolidated, cobbly conglomerate is associated with a1.

The average elevation of the Taxueh Shan piedmont is high ($\approx$3100 m). From about 3600 m at the foot of the range (Fig. 2) the bajada descends regularly northwards to about 2600 m (at the NW corner of Fig. 2), with a slope averaging $\approx 2.85^\circ$ over a distance of $\approx$20 km. On the north flank of Taxueh Shan, whose summit peaks at 5681 m, the tips of contemporary glacier tongues reach down to 4200–4300 m, approaching to within 5–6 km of the range front. The present-day snowline roughly follows the 4700 m elevation contour, while the permafrost line, the lower limit of the periglacial zone, is near 3700 m (Wang & Derbyshire 1987). Where fresh-looking and well preserved, the lowest Würm terminal moraines in the northern Taxueh Shan stand at about 3600 m, 800–900 m below the present ones (Peltzer *et al.* 1988). Hence, during the last glacial maximum, large Würm glaciers probably flowed out of the range onto the uppermost part of the piedmont, while much of that piedmont was within the periglacial domain, a situation similar to that in the Ta Quen Kou basin (TQK, Fig. 1), 90 km to the east (Peltzer *et al.* 1988). We thus infer the morainic debris along the foot of Taxueh Shan (Fig. 2) to be mostly of late Würm age (20–15 ka BP, e.g. Duplessy *et al.* 1988; Bard *et al.* 1990). At that time, much of the piedmont surface was probably smoothed out by efficient, periglacial mass transport processes (e.g. cryoplanation, gelifluction, etc.). Such superficial processes would not have allowed preservation of small-scale relief such as the fine incision network now visible on a1 or a2. Hence, that pluvial network, as well as the surfaces that bear it and their loess blanket, ought to postdate the Würm glacial retreat.

Thermoluminescence dating, with one-year-long dosimeter calibrations, of a comparable loess blanket, approximately 90 cm thick, sampled at two sites in the nearby Ta Quen Kou basin corroborates this inference. Both sampling sites yield comparable, upward-decreasing age sequences of 11.5 ± 1.5 ka, 6.6 ± 2.2 ka, 3.6 ± 0.6 ka, and 9.4 ± 1 ka, 4.4 ± 0.7 ka, 1.8 ± 0.35 ka, at shallowing depths of 80, 55, and 30 cm (Meyer 1991). The loess layer thus postdates 10.7 ± 2.3 ka BP, and most of the a2 fanglomerates of the bajada were deposited as a result of increased run-off in the piedmont prior to 8.4 ka BP, around the beginning of the Holocene. Even the oldest surface (a1) probably represents remnants of a terrace emplaced after deglaciation started ($\approx$14 ka BP, Fairbanks *1989*; Bard *et al.* 1990).

Together with the Yumu Shan bajada, 300 km eastwards (Fig. 1), whose age also appears to be mostly Holocene (e.g. Tapponnier *et al.* 1990a), the Taxueh Shan bajada is the foreland fanglomerate apron that we studied in most detail. We infer, however, from their similar aspect on SPOT images and topographic maps, that many other Quaternary bajadas that reach elevations $\geq$2000 m at the foot of the great ranges of northeastern Tibet have a similar age and origin. In particular, we assume that large areas of the northern foreland of Tanghenan Shan (Fig. 1) are mantled by postglacial or holocene fanglomerates.

2.2 Shortening in the Taxueh Shan piedmont

The two narrow zones where the highest terrace (a1) is exposed across the Taxueh Shan piedmont trend roughly perpendicular to the drainage direction (Fig. 2). In the field, both zones thus form rows of hills separated by contemporary drainage channels (Fig. 3a). The hills stand above the average surface of the bajada apron (a2), interrupt its continuity, and break its otherwise uniform slope (Figs 2, 3, 4 and 5). There is ample evidence, described below, that such hill rows are of tectonic origin and mark the top of two actively growing anticlinal

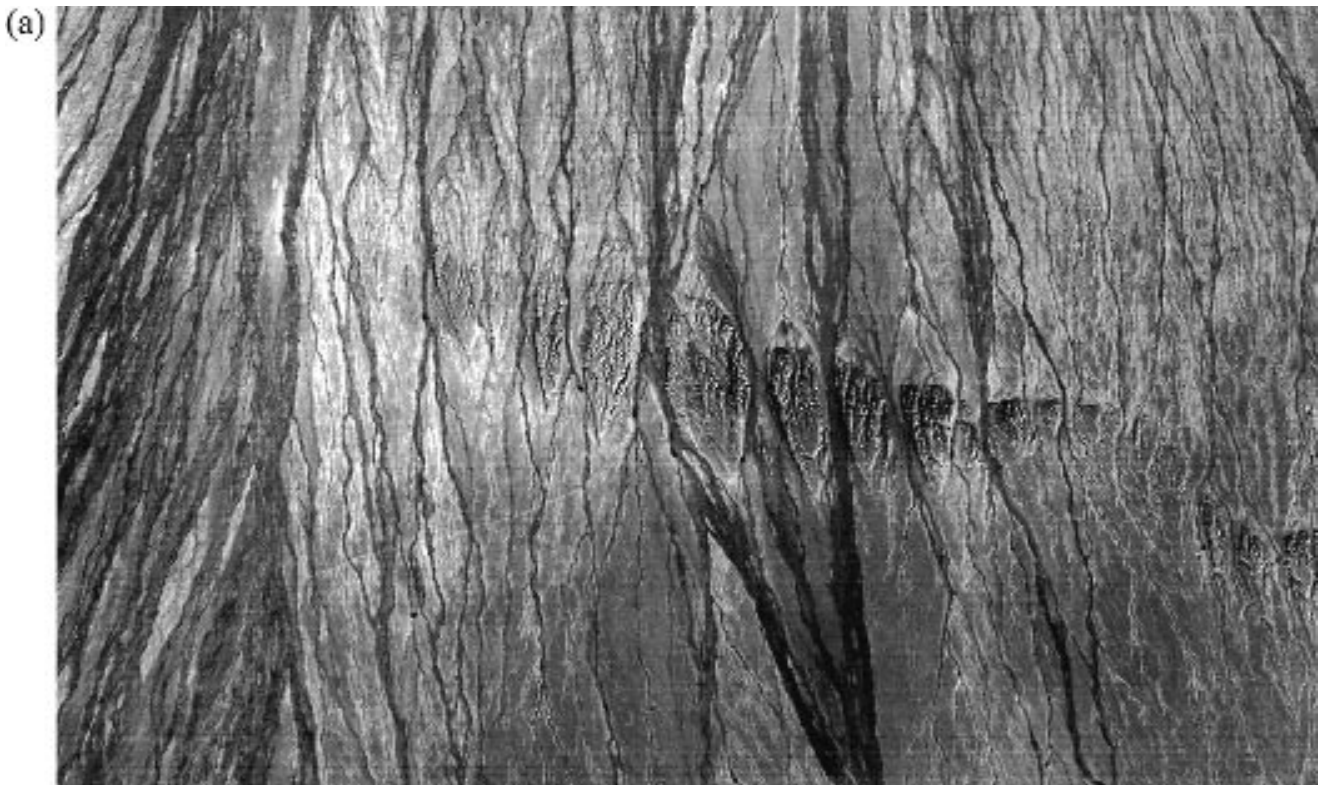

Figure 4(a). Detail of panchromatic SPOT scene KJ 240–270 (12/11/1987; pixel size, 10 m).

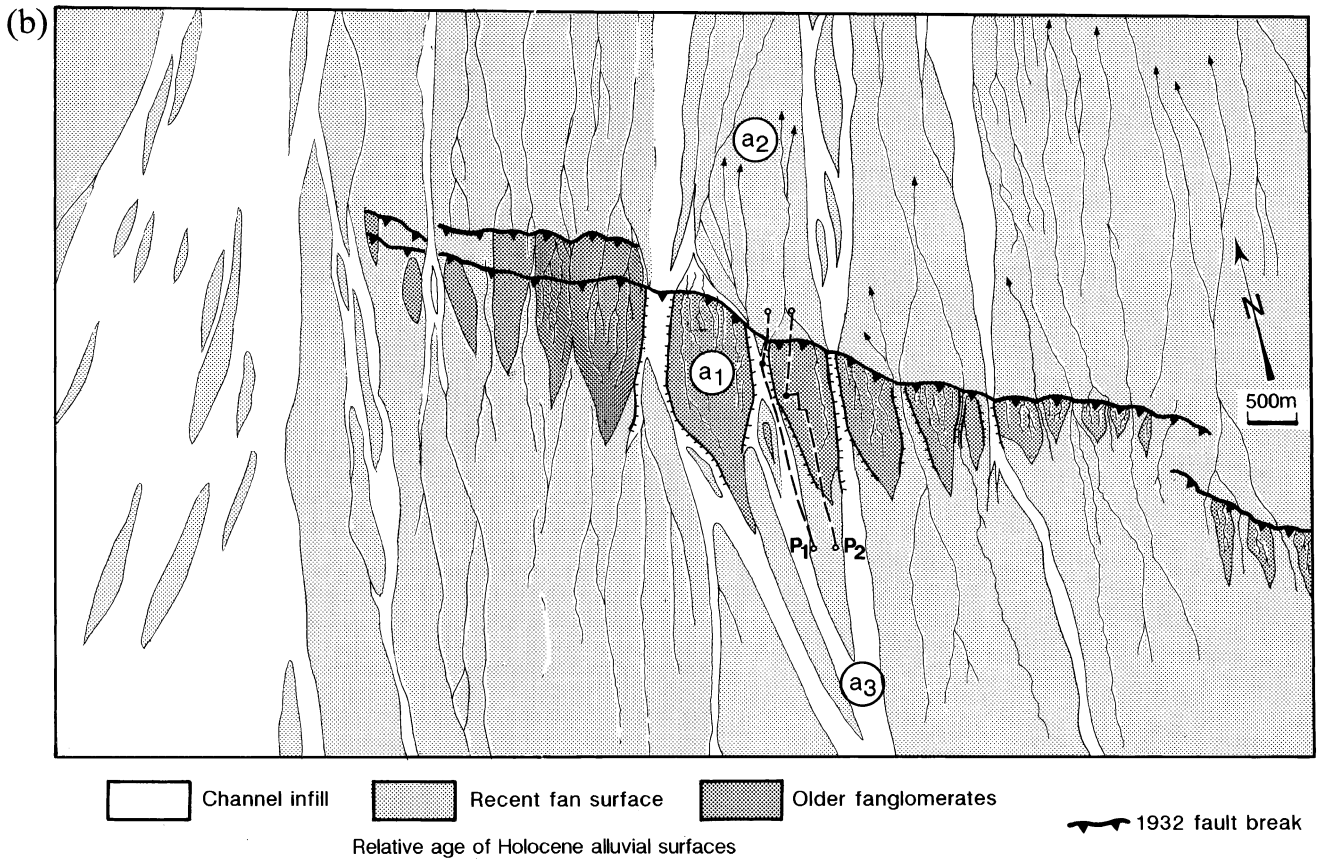

Figure 4(b). Morphotectonic map of (a). Spearheaded, almond-shaped tongues of uplifted terrace a1, separated by bottleneck cluses of contemporary streams, signal the growth of the north-hills anticline south of the festooned thrust trace. Such tongues vanish where thrust-trace segment terminates or steps over, or where depositional surface is younger. Thin dashed lines are streambed and hilltop profiles of Fig. 4(f).

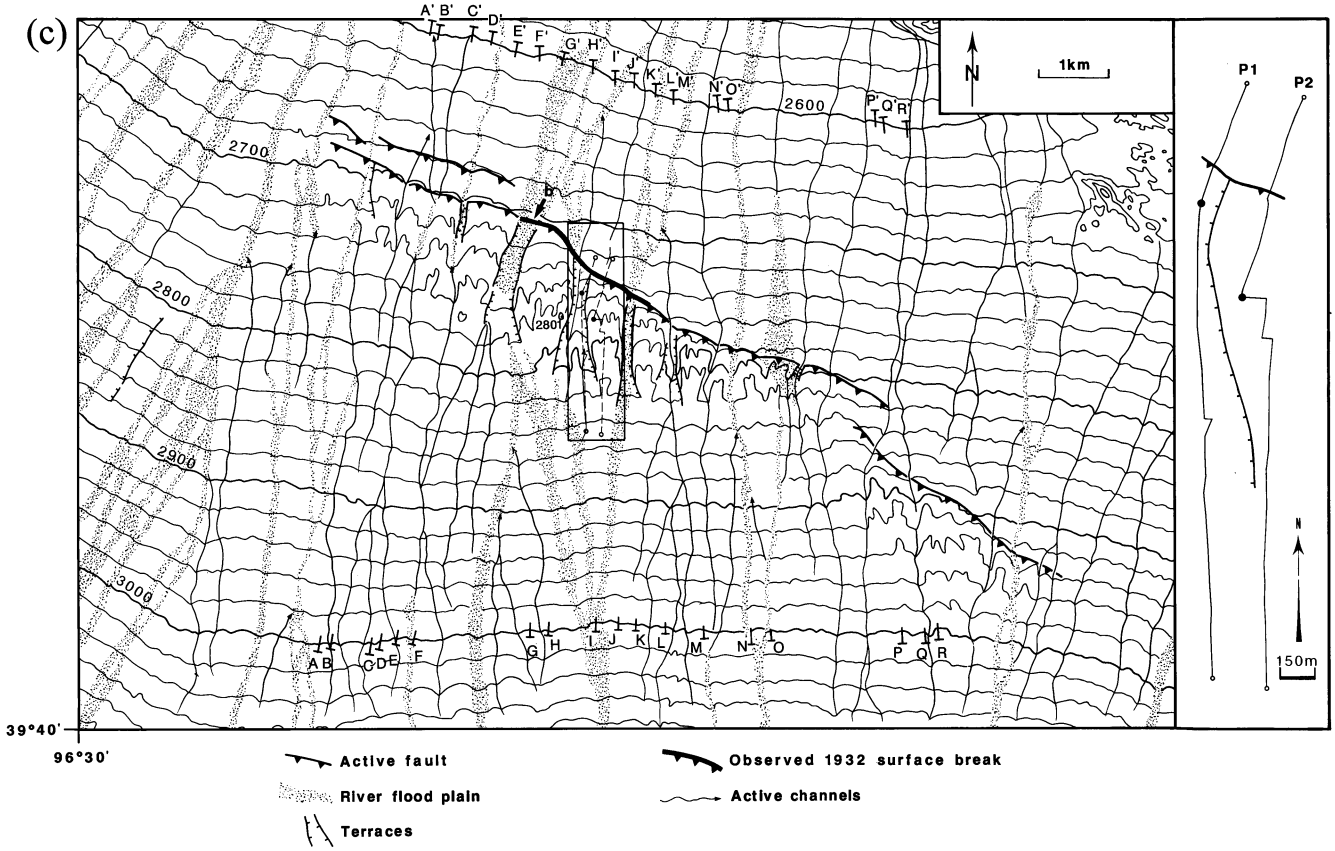

Figure 4(c). Detail of $1:10^5$ topographic map in the north-hills anticline area. Tees with capital letters mark extremities of profile pairs of Fig. 4(d). Inset on right shows precise location and trace of levelled field profiles.

ridges above south-dipping thrust ramps. For lack of local toponyms to designate these features, we refer to them as the north- and south-hills anticlines.

2.2.1 *North-hills (Beishanzi) anticline*

The north side of the northern hill row, about 16 km north of the range front, is bounded by a thrust fault—the Taxueh Shan piedmont thrust—whose trace is conspicuous on the SPOT image (Figs 2 and 4a,b). The thrust trace, about 30 km long, is composed of right-stepping, en échelon segments with festooned shape (Figs 2 and 3c). The segments along the biggest hills display clear south-pointing cusps at intersections with main stream channels (Figs 2 and 4), as expected for a south-dipping thrust. At both ends of the thrust trace (NW and SE corners of Figs 2a,b) we found, and followed for a few kilometres in the field, a north-facing, 30–75 cm high scarp (Figs 3b,c). The freshness of that scarp [exposed gravels on its rather steep face (25–30°N), small bushes aligned along its base, or in places loose soil without turf, as if freshly plowed, and small pressure ridges poked with rodent holes] implies that it is a surface break of the 1932 December 25, $M=7.6$, Chang Ma earthquake, making the Taxueh Shan piedmont thrust one of five large fault strands ruptured by that great earthquake (Meyer 1991).

The maps and sections of Fig. 4 display the morphology and superficial structure of the northern hill row, as well as the geometry of the underlying anticline (north-hills anticline) and of the thrust ramp compatible with that structure. In map view, the stream channels that wander within the generally divergent fan pattern of the bajada tend to converge into fewer channels as they cross the hill zone. Water flow is thus funnelled into bottleneck narrows, or 'cluses', that separate (Fig. 3a) almond-shaped patches of uplifted terrace (a1), elongated in the direction of flow (Figs 4a,b and c). Upstream, such terrace patches merge smoothly with the bajada surface (a2), forming spearheaded tongues, as the amount of relative uplift between a1 and a2 gradually decreases (Figs 4b and c). Downstream, by contrast, the active thrust sharply truncates the patches at their widest. On the images, on the $1:10^5$ topographic map (Figs 4a and c) and in the field, there is good evidence that the stream channels crossing the north-hills anticlinal ridge became narrower and deeper, and hence more localized, by successively abandoning older terrace levels on the sides. The existence of such levels adds to the composite, locally diachronic nature of a1.

Sections along stream channels show the uppermost fanglomerates, which roughly parallel the top surface of terrace a1, unconformably capping gently folded, more consolidated fanglomerates (Figs 4e and f). The angle of unconformity is in general small, varying across section from a few degrees in the south to about 10° in the north. Steeper dips (up to 30°N) locally exist near the cumulative thrust scarp (Fig. 4f). Folding of the Late Quaternary piedmont fanglomerates thus appears to increase with deposition age and is asymmetric (north-facing), a straightforward consequence of north-vergent thrusting. Although exposure is limited to cliffs at most ≈ 20 m high (Figs 4c and e), it is likely that the degree and asymmetry of

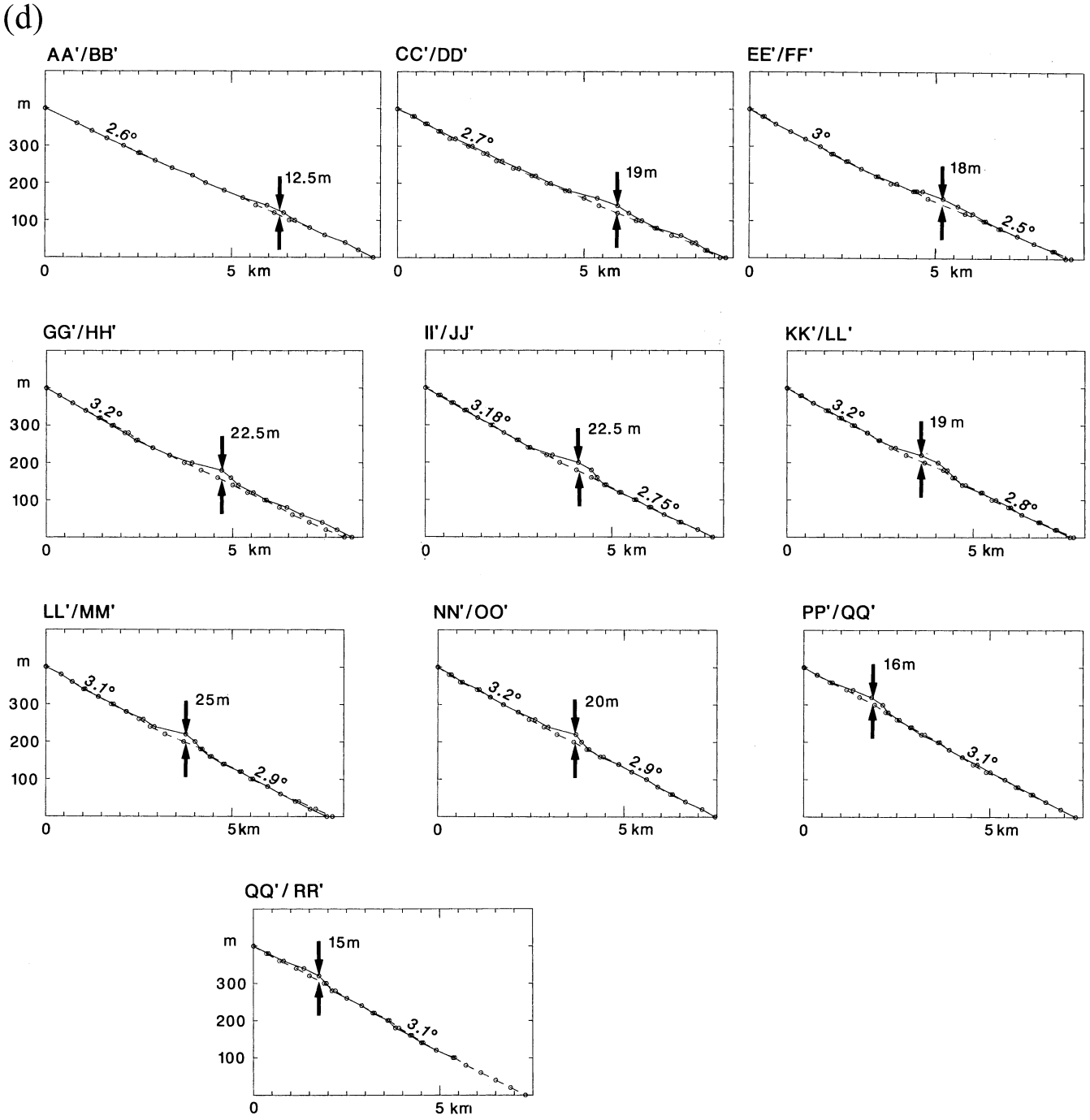

Figure 4(d). Hilltop/streambed profile pairs derived from map of Fig. 4(c). The shape of the north-hills anticlinal bulge is visible on all profiles. Parameters derived from the profiles are summarized in Table 1.

folding increase further with depth. 15 km to the northeast, at Xiao Kouzi, in the hanging wall of another north vergent active thrust, the Changma thrust (Meyer 1991), a tight recumbent fold of Cretaceous red beds (Gansu Geological Bureau 1975) is exposed under the gently warped, distal fanglomerates of the Taxueh Shan Bajada, here only a few tens of metres thick (Meyer 1991). Hence, we infer the base of the much thicker fluvio-glacial Quaternary sequence beneath the northern hill row to be folded in a comparable tight manner (Fig. 4f), within the faulted, asymmetric core of the north-hills anticline. The uppermost part of the section suggests that the most prominent unconformities within that sequence ought to correspond chiefly to the onsets of interglacial periods (for example, the folded $\approx$125 ka unconformity represented in Fig. 4f).

In summary, the northern hill row is a remarkable example of the geomorphic expression of an active fault-propagation anticline in a rather dynamic environment of fluvial deposition. Because of its exceptional location within a periglacial area, it provides a 'snapshot' (with a geological 'exposure time' of about 14 ka) of a ramp anticline caught in the process of active growth and uplift, complete with 'bottleneck cluses' separating

Figure 4(e). East-looking view of the slight angular unconformity of a1 upon gently south-dipping upper-Pleistocene fanglomerate beds on the southern top part of the north-hills anticline.

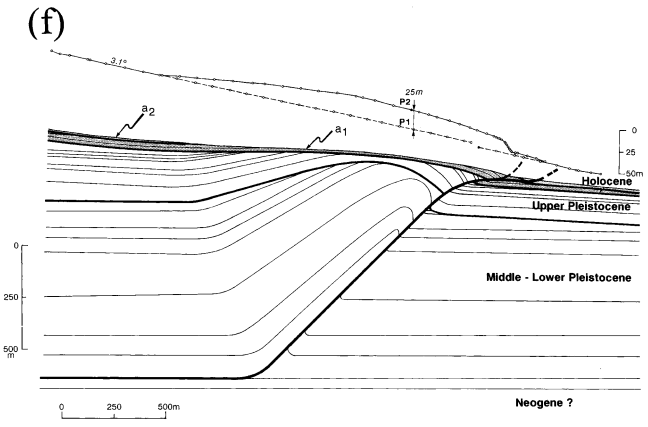

Figure 4(f). Top: difference between hilltop (P2) and streambed (P1) profiles near the centre of the north-hills anticline (location on Figs 4b,c). Small circles are levelling points. Both profiles are projected on N–S- and N21°E-striking vertical planes, south and north of the black circles, respectively (see also inset in Fig. 4c). Bottom: cross-section of the anticline beneath the profile, derived from field observations and regional geological evidence. The degree of folding increases with depth. The progressive growth of the anticline accounts for thinning of sedimentary layers above the thrust ramp, taken to dip 45°S. Unconformities are assumed to correspond to the onset of the last two interglacials. The thickness of Quaternary is taken to be similar to that in neighbouring sites where stratigraphic log is known (Gansu Geological Bureau 1975; Xu *et al.* 1989). Postglacial fanglomerates are shaded. See discussion in text.

'spearheaded', 'almond-shaped' terrace tongues, all of them truncated by fresh surface scarps that testify to seismic movement on the thrust ramp underneath.

Since the Taxueh Shan piedmont thrust splays and shallows near the surface (Figs 3c, 4b,f), its average dip under the north-hills anticline may only be estimated. In general, dips of active continental thrust ramps in sediments vary between 30° and 70° (e.g. Yeats 1983, 1986; Suppe 1983; Philip & Meghraoui 1983; Tapponnier *et al.* 1990a; Meyer *et al.* 1990; Chen *et al.* 1996). Avouac *et al.* (1993) found such thrust ramps to dip 55 ± 5°S along the Dzungarian piedmont of the Tien Shan, in a Quaternary tectonic environment broadly comparable to that of western Gansu. Dips measured by Zhang *et al.* (1991) in the Liupan Shan, east of Gansu, range mostly between 40° and 60°. More specifically, where exposed in a small gully east of Sange Quan, ≈ 20 km east of the north-hills anticline, the measured dip of the Changma thrust, closest neighbour of the Taxueh Shan piedmont thrust, is 40°S (Meyer 1991; State Seismological Bureau 1993). 80 km eastwards, the Ta Quen Kou fault, which may be considered an eastern splay of the Taxueh piedmont Shan thrust, dips $55° \pm 5$°S (Peltzer *et al.* 1988). We thus take $45° \pm 15$°S to be the most plausible dip of that thrust under most of the northern hill row.

It is possible to infer more about the depth and kinematics of thrusting with a quantitative assessment of the relief above it. The amount of surface warping recorded by the visible uplift of the postglacial terraces may be obtained, at complementary scales, from the $1:10^5$ topographic maps and from levelling in the field. The difference between paired profiles roughly perpendicular to the thrust, one across a given hill (a1), the other along an adjacent stream channel (a3), yields the width and amplitude of the anticlinal bulge relative to the contemporary depositional surface. Fig. 4(d) shows 10 pairs of 7–9 km long profiles across the western part of the north-hills anticline, derived from the map of Fig. 4(c). Although precision is limited by the equidistance of the elevation contours on that map (20 m), the anticlinal shape of the hills is clear on all the profiles, being constrained by at least three point pairs. The anticlinal bulge makes only a local disturbance, up to 25 m high and 1.4–2.1 km wide, on the otherwise regular bajada surface (Fig. 4d, Table 1). As befits sedimentary fans, the bajada is in general slightly concave upwards, with a slope angle of as much as 3.2°N south of the anticline and as little as 2.5°N north of it (Fig. 4d, Table 1). The width and height of the bulge diminish both eastwards and westwards (Fig. 4d, Table 1), towards the extremities of the corresponding thrust segment, in keeping with the decrease in length of the a1 terrace tongues (Fig. 4b).

A more accurate shape of the anticlinal bulge was obtained by levelling, using a digital-recording theodolite distancemeter (Wild T 2000-DI 3000), two approximately NS profiles about 2.5 km long (P1 and P2, Figs 4b,c and f) across a typical spearheaded terrace tongue and adjacent bottleneck cluse near the centre of the thrust segment (for technical details and measurement errors, which are less than 20 cm in height and less than 2 m in horizontal position, see Peltzer *et al.* 1988, Avouac *et al.* 1993 and Gaudemer *et al.* 1995). The highest stand of terrace a1 on the hill top lies 25 ± 0.5 m above the stream bed below (a3). The asymmetric shape of the anticlinal bulge comes out clearly on the hill-top profile. The gentle (≈ 1.2°N), undisrupted slope of the south limb, ≈ 1.9° less than the local bajada slope, contrasts with the rather steep (≈ 20–25°N on average), ≈ 10–12 m high cumulative scarp to the north. The zone of uplift is ≈ 1.6 km wide, close to the average bulge width (≈ 1.8 km) visible on the SPOT image and derived from Figs 4(c and d) (Table 1). Although there is ≈ 4 m of local entrenchment of the contemporary stream-bed near the cumulative scarp, there seems to be no detectable cumulative vertical offset of the bajada slope upstream and downstream from the anticline, within the precision of our measurements. Nor is there any great change in the bajada slope gradient (≈ 3.1°N upstream, and ≈ 2.6°N downstream), whose average (2.85°N) is identical to the 20 km average and to the long-profiles slope average (Table 1). The topographic measurements thus support quantitatively the observation, in

Figure 5(a). Detail of panchromatic SPOT scene KJ 240–270 (12/11/1987; pixel size, 10 m).

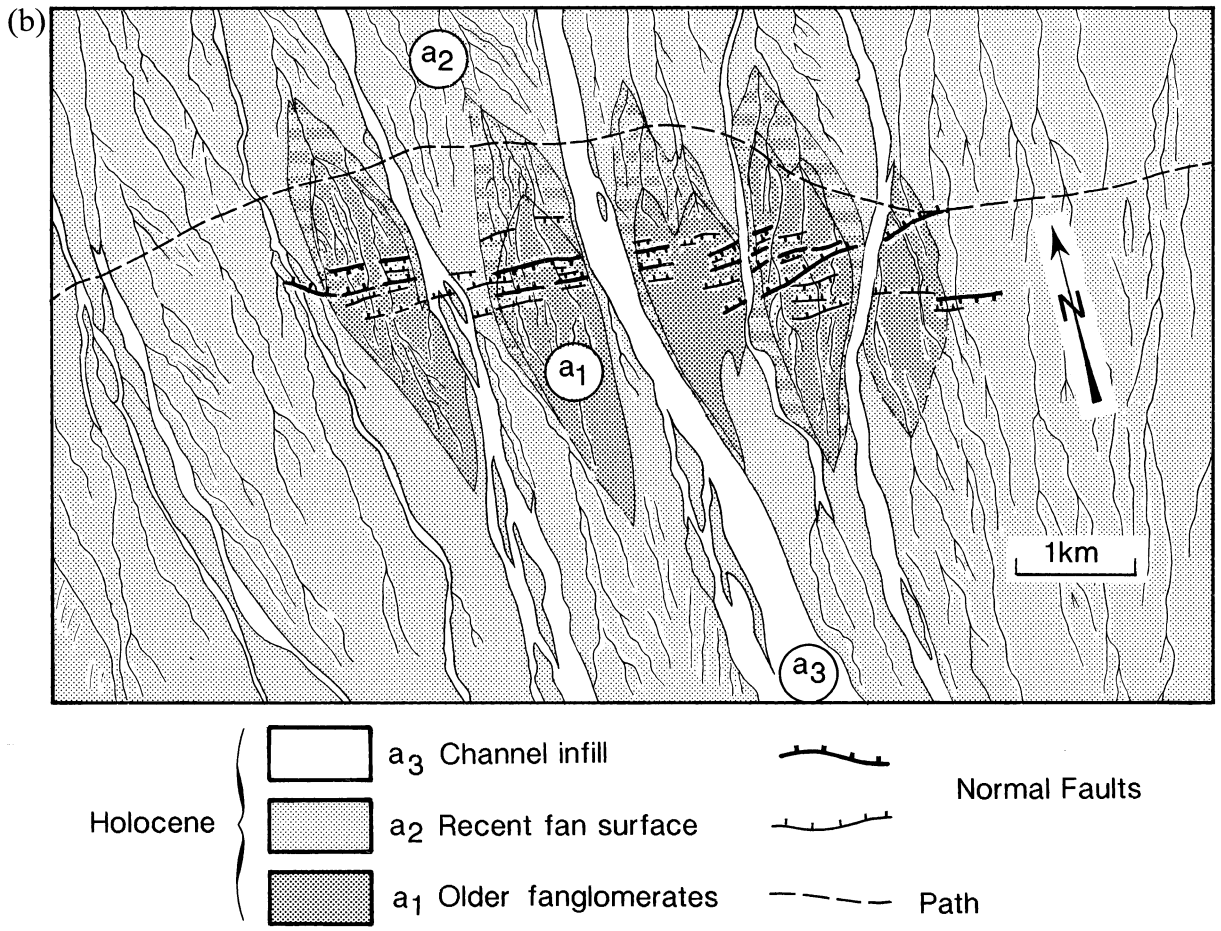

Figure 5(b). Morphotectonic map of Fig. 5(a). Spearheaded almond-shaped tongues of uplifted a1 and a1–2 (stripes) terraces, due to fold growth, are not truncated by thrust trace. Roughly parallel scarps facing south (sunlit) or north (shaded) along the anticline apex (see Fig. 5a) testify to active surface deformation, in all likelihood normal faulting, near its hinge.

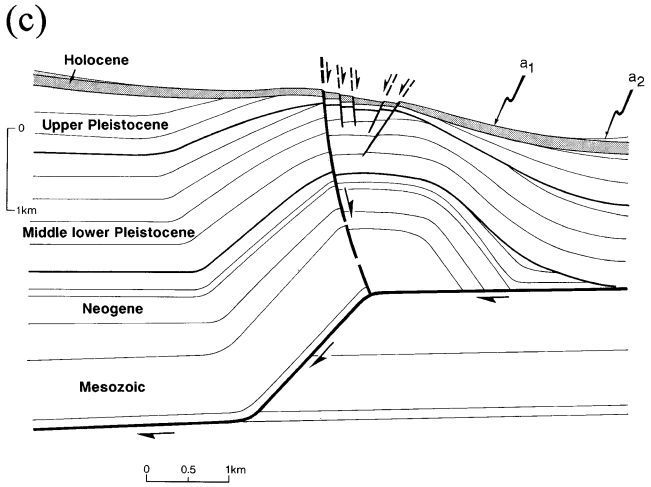

Figure 5(c). Plausible cross-section of the south-hills anticline consistent with surface observations on the SPOT image. The south-hills anticline is inferred to result from fault-bend folding above blind ramp linking two active décollement levels. Kinematic compatibility results in hinge-normal faulting. Triple junction instability may cause hanging-wall normal faults to stop and move passively towards the foreland (e.g. Avouac *et al.* 1992). Stratigraphy, as in Fig. 4(f). Due to lack of field measurements, this section is more qualitative than that of Fig. 4(f) (see discussion in text).

map view on the SPOT image, that a1 and a2 merge upstream and that stream channels are not deeper south than north of the anticline.

That the bajada slope is not offset or warped on a large scale, except within a few hundred metres of the cumulative thrust scarp on the stream-bed profile, implies either that the thrust plane terminates downwards at a shallow depth, at most of the order of the anticlinal bulge width, or that it kinks rather sharply at such depth into a décollement (Fig. 4f). Given the accuracy of our field profiles, such a décollement would have to dip at a very shallow angle. Assuming the thrust ramp under the north-hills anticline to dip 45°S, and resolving the 25 m surface uplift of a1 on the deeper part of that ramp implies ≈33 m of postglacial slip on it. This amount of slip on a décollement dipping 10°S would have generated ≈7.5 m of cumulative uplift south of the anticline. Since the bajada surface (a2) is younger than a1, the vertical uplift of its slope could plausibly be a few metres only, an amount no greater than the entrenchment of a3 near the thrust scarp and probably small enough to have been smoothed out by deposition or erosion processes away from the thrust. It seems doubtful, however, that such processes could smooth out more than a few metres of uplift. We conclude that a décollement south of the north hills would be unlikely to dip south by more than ≈10°, and take 5°±5° as the most plausible value. With the rules commonly used to constrain the geometry of growing fault-propagation folds (e.g. Suppe 1983; Jamison 1987) and the dip assumed for the thrust ramp, bulge widths of 1.6–1.8 km would imply depths of ≈1.1–1.2 km for the ramp termination or ramp-to-flat kink (Fig. 4f), appropriate for it to lie in the weak upper-Neogene mudstones under the coarse, competent lower Quaternary conglomerates (Xiyu fm.) that characterize the regional late-Cenozoic sedimentation here, as in much of western China (e.g. near Yumen, State Seismological bureau 1993; in the Tien Shan, Avouac *et al.* 1993).

2.2.2 *South-hills (Nanshanzi) anticline*

About halfway between the trace of the emergent Taxueh Shan piedmont thrust ramp and the range front, ≈8 km south of the north-hills anticline, bottleneck cluses in the drainage, separating almond-shaped patches of uplifted, incised terrace fanglomerates (a1) signal the existence of another contemporary anticline, the south-hills anticline, whose growth has formed the other hill row of the piedmont (Figs 2 and 5).

The morphology of the southern hill row, which we could not reach in the field, differs from that of the northern one. On the SPOT image, the terrace tongues have a more symmetrical shape, with spearheaded tips both upstream and downstream, and no trace of an active thrust trace truncating them either to the north or south (Figs 5a and b). Many parallel ≈EW-striking fault scarps cut the upper surface of the almond-shaped terrace patches where they are widest and highest, therefore roughly at the apex of the anticline. The scarps tend to be right-stepping, slightly oblique to the anticlinal axis. In general, the northernmost scarps are lit by the sun, i.e. face towards the south, while the southernmost ones are shaded and face north (Figs 5a and b). The scarps that face north tend to be more continuous and prominent than those that face south. To the east, a particularly large, north-facing, ENE-striking scarp appears to crosscut smaller scarps that more closely parallel the average strike of the anticlinal axis.

Table 1. Dimensions of north-hills anticlinal bulge, derived from sections in Fig. 4.

Hilltop/streambed profiles	Profiles length (km)	Upstream slope (°)	Downstream slope (°)	Bulge width (km)	Bulge height (m)
BB′/AA′	9	2.6	—	1.5	12.5
CC′/DD′	9	2.7	—	2.1	19
EE′/FF′	8.5	3	2.5	2.1	18
GG′/HH′	8	3.2	—	1.9	22.5
II′/JJ′	7.75	3.2	2.75	2	22.5
KK′/LL′	7.75	3.2	2.8	2	19
MM′/LL′	8	3.1	2.9	2	25
OO′/NN′	7.5	3.2	2.9	1.5	20
PP′/QQ′	7.5	—	3.1	1.7	16
RR′/QQ′	7.25	—	3.1	1.4	15
Average	≈8 km	≈3°	≈2.85°	≈1.82 km	≈19 m
P2/P1	2.5	3.1°	2.6°	1.62	25

With the SPOT image as sole source of information, we can assess only qualitatively the main traits of the structure of the south-hills anticline, by comparison with that along the north hills. The length of the uplifted terrace patches is about 3.5 km on average, everywhere greater than the maximum width of the north-hills anticline (2.1 km), (Figs 2, 4 and 5). The channels that separate these patches, and certain rills that incise their surface, seem to have somewhat greater depths and steeper sides than channels and rills in the north hills. The spearheaded a1 tongues north of the anticlinal axis tend to be shorter than those south of it, reflecting some degree of asymmetry, with the north limb of the anticline being somewhat steeper than the southern one.

The multiple scarps along the axis of the anticline must result from contemporary faulting because they can be traced across most of the rills that incise the terrace surface. The rectilinearity of their traces suggest faulting on steep planes. By comparison with the rills they cut, we infer these scarps to be a few to several metres high, a cumulative result of repeated slip during earthquakes comparable to, and in all likelihood including, that of 1932. Although the location of the scarps implies that they reflect deformation during incremental fold growth, the exact deformation mechanism is harder to assess short of detailed fieldwork. The simplest interpretation is that the scarps result from roughly conjugate normal faulting at the apex of the anticline (Fig. 5c). A somewhat greater amount of downthrow towards the north would account for the slight pre-eminence of the north-facing scarps and a small component of left-slip, for their right-stepping, en échelon arrangement (Figs 5a and b). This overall geometry is closely comparable to that of the normal fault array at the apex of the anticline along the central segment of the Ech Cheliff thrust, in Algeria, that was activated by the 1980 October 10 El Asnam earthquake (e.g. King & Vita-Finzi 1981; Philip & Meghraoui 1983; Meyer *et al.* 1990; Avouac *et al.* 1992). A different interpretation might be that such scarps, which are numerous, closely parallel to one another, and south- or north-facing, respectively, north or south of the anticline axis, result from flexural slip between competent beds in steep fold-limbs hidden beneath a relatively thin layer of unconformable Quaternary fanglomerates. Such a mechanism of deformation (Yeats *et al.* 1981) is common in young, growing folds north of the Qilian Shan and Tien Shan (Tapponnier *et al.* 1990a; Avouac *et al.* 1993). We doubt that it operates here, however, at least near the surface, because the most prominent scarps lie within a few hundred metres of the fold axis, in a narrow belt following the fold hinge, and because the thickness of rather gently dipping mid-upper Pleistocene fanglomerates close to the range front is unlikely to be less than a few hundred metres (Fig. 5c) (Gansu Geological Bureau 1975; Xu *et al.* 1989).

In summary, the evidence visible on the SPOT image implies that the southern hill row is the surface expression of a fairly broad feature, about twice the width of its counterpart along the northern hill row, and with somewhat greater amplitude. It probably folds a sedimentary pile about twice as thick. Like the north-hills anticline, the south-hills anticline is asymmetric (north-facing), which is consistent with north-directed slip on an underlying thrust ramp. The more subdued asymmetry than that visible across the north-hills anticline, however, implies that the upper tip of that ramp is fairly deep (e.g. Suppe 1983; Stein & King 1984). That seismic slip currently occurs on such a blind ramp is attested by the existence of fresh, steep, conjugate surface scarps along the hinge of the anticline. Such scarps are most simply interpreted to reflect compatibility normal faulting due to bending of the strata within a seismically growing fault-bend fold (Fig. 5c) (e.g. Avouac *et al.* 1992). Despite the lack of topographic profiles, the apparent incision depth on the SPOT image suggests that, like the north-hills anticline, the south-hills anticline is a localized bulge within the bajada apron (Fig. 2). Hence, the blind ramp beneath it extends downwards to only limited depth. The section drawn on Fig. 5(c), which we find to be, for reasons discussed below, most consistent with surface evidence, depicts the blind ramp linking two décollement levels at different depths within the sedimentary cover (Fig. 5c).

2.2.3 *Overall geometry of thrusting*

That contemporary shortening north of the Taxueh Shan involves the coeval growth of two different, roughly parallel, ramp anticlines, 20–30 km long and as much as 8 km apart within the piedmont bajada (Figs 2 and 6a,b), makes it worth examining whether they are related to one another, and how.

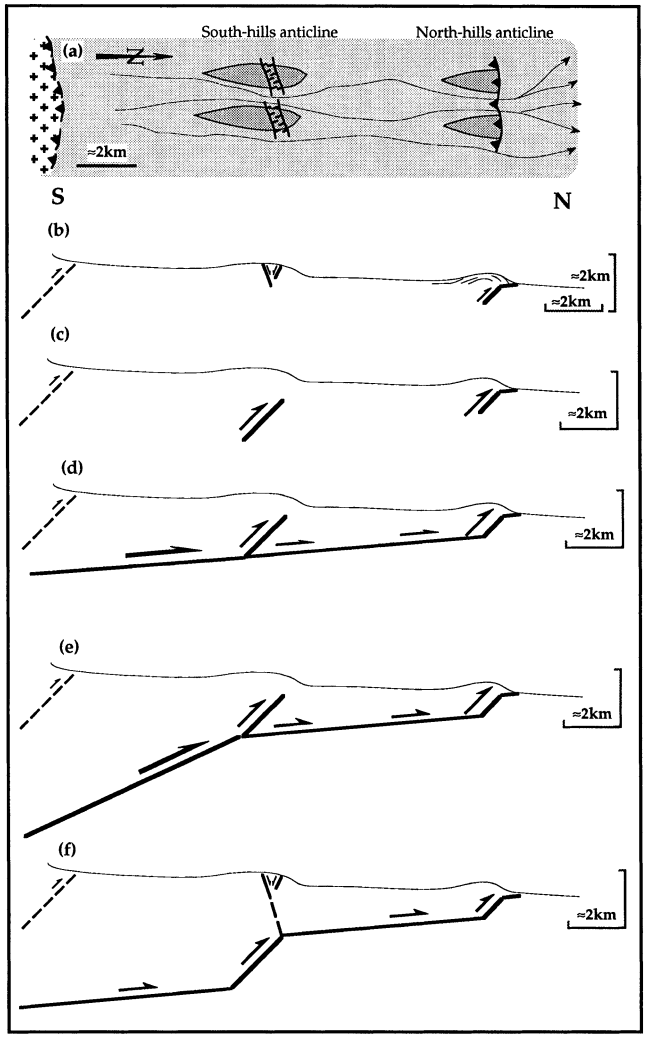

Figure 6. Sketch showing how observed warping and faulting in map view (a) and in cross-section (b) might result from distinct thrust geometries at depth (c,d,e,f). (f) is the most likely geometry, see text for discussion.

Although such anticlines could reflect active thrusting on two independent ramps (Fig. 6c), we find this hypothesis untenable. Given the limited width of the anticlinal bulges, the ramps, whose most plausible dips are $\leq 60°$, are unlikely to reach depths greater than ≈ 5–6 km and probably terminate short of the metamorphic basement, within Meso-Cenozoic sediments. The north-hills ramp, which bears a surface break unquestionably related to the $M \approx 7.6$ Changma earthquake, could not reach deeper than about 2 km, and more likely extends 1.1–1.2 km down, to near the base of the Quaternary conglomerates (Fig. 4f). From a mechanical point of view, it is doubtful that such a shallow thrust could have been activated by such a large event without being physically connected to a deeper seismogenic structure. Therefore, we infer both ramps to be linked with a deep thrust fault, beneath the mountain basement to the south, by means of shallower-dipping flats, as shown in the sections of Figs 6(d)–(f).

Further support for the hypothesis of interconnected south-dipping ramps and flats comes from the observation that the distances between the north- and south-hills anticlines, and between them and the range front, decrease as the Taxueh Shan foreland basin narrows, and hence shallows towards the east (Fig. 2). This implies that the depths of certain horizons, which depend on sedimentary thickness, exert a strong control on faulting (e.g. Armijo *et al.* 1986): the fold axes and underlying ramps converge because the diminishing thickness of the sedimentary cover causes such guiding horizons to shallow. Concurrently, the widths of the anticlinal bulges also decrease from west to east (Fig. 2).

The observed surface deformation, combined with kinematic compatibility requirements, makes the section of Fig. 6(f) preferable to those of either Fig. 6(d) or (e). Section 6(d), in which both the north- and south-hills ramps are inferred to splay from the same flat, provides no plausible explanation for the fundamental difference between the two anticlines, i.e. for the fact that the southern ramp remains blind, with only normal faults at the surface. Rather, it maximizes internal shortening above the junction between that ramp and the flat, and ought to induce reverse faulting. Section 6(e), which depicts a thrust triple-junction under the south-hills anticline, minimizes such shortening but raises another problem. Since the height of the south-hills anticline—hence the amount of postglacial slip on the ramp beneath—appears to be at least of the order of that of the north-hills anticline, slip-conservative kinematics at the junction require that the 5°–10°S-dipping foreland flat steepens by at least 15°–20° after meeting with the lower tip of the 40°–50°S-dipping south-hills ramp. Such steepening would result in visible uplift, hence deeper incision, of the bajada surface south of the south-hills anticline, which is not observed. A flat linking the north-hills ramp to the upper tip of the south-hills ramp as shown in Fig. 6(f), on the other hand, would be the simplest way to transfer surface slip to that ramp, then to a deeper flat, eventually allowing a single thrust surface to reach deep enough within the crust to rupture in a large earthquake. The geometry of section 6(f) also accounts most simply for the blindness of the ramp beneath the south-hills anticline and for the occurrence of normal faulting, compatible with rough conservation of slip at depth, at the apex of that anticline (e.g. King & Vita-Finzi 1981; Meyer *et al.* 1990; Avouac *et al.* 1992; Lacassin *et al.* 1993).

The schematic section drawn in Fig. 7(a) summarizes our preferred interpretation of present-day shortening and thrusting in the Taxueh Shan. It outlines the simplest way to account for surface observations without subsurface information or geodesy. Although the range front is marked by a distinct break in topographic slope, there is only subdued, discontinuous evidence for Late Quaternary surface faulting along that slope break (Fig. 2). Hence, while the youthful mountain range must be underlain by a prominent Late Cenozoic thrust ramp (F), bringing Precambrian basement on top of Cretaceous and Neogene sediments (Gansu Geological Bureau 1975), the trace of that ramp at the foot of the range (R1) is no longer the primary site of movement. Instead, most of the present-day slip appears to be transferred towards the north by a shallow south-dipping décollement. We infer this décollement (D1) to be guided by a flattish sedimentary interface several kilometres deep, possibly an unconformity at the base of the Mesozoic cover, or within Palaeozoic basement rocks. 8 km north of the range front, beneath the south-hills anticline, the thrust ramps up (R2) to a shallower décollement (D2), probably located near the Neogene–Lower Quaternary interface. Emergence of the active thrust eventually occurs as much as 16 km north of the range front, along the north-hills ramp (R3).

The most robust feature of the simplified section of Fig. 7(a) is the overall geometry of the Taxueh Shan piedmont thrust,

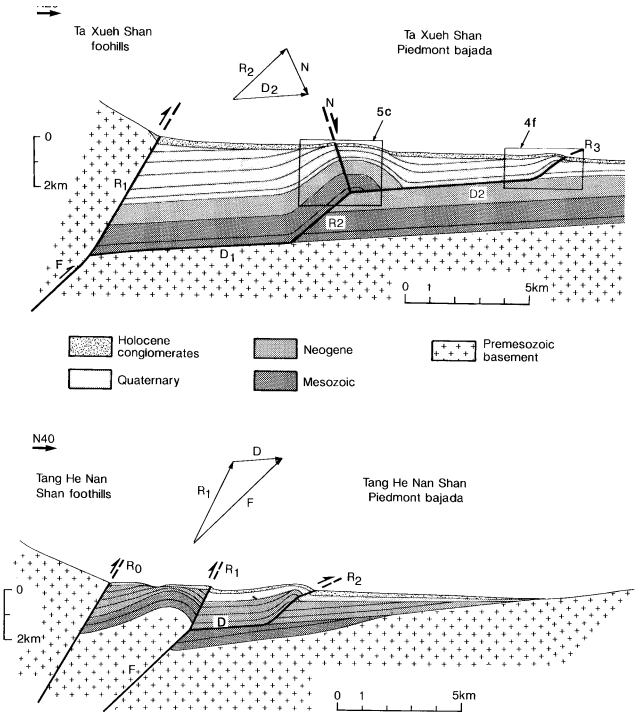

Figure 7. Schematic sections showing the most plausible geometry of active Taxueh Shan (a) and Tanghenan Shan (b) thrusts. In both cases, foreland décollements (D1–D2, D, inferred to dip 5°S) splay from deep thrust ramps under mountain ranges (F). Fault-propagation and fault-bend anticlines that fold piedmont bajada fanglomerates are due to the occurrence of shallower, blind (R2, section a) or emergent ramps (R3, section a; R2, section b). F, R2 and R3 are inferred to dip 45°S; R0 and R1, 60°S. Inset vector diagrams indicate the inferred composition of slip components at fault triple junctions. Stratigraphic thicknesses are compatible with those known in western Hexi-corridor drill-logs (Gansu Geological Bureau 1975; Xu *et al.* 1989). Crosses only represent pre-Mesozoic basement, without inference on rock type. Boxes are sections of Figs 4(f) and 5(c).

which seems inescapable. The section itself, however, is not uniquely constrained because the dips—which are tied to the depths—of the ramps and flats are not precisely known, even though the values chosen (45° and 5°S, respectively) yield décollement-horizon depths consistent with known stratigraphic thicknesses in the western Hexi corridor (Gansu Geological Bureau 1975; Xu *et al.* 1989) (Fig. 8). Such limitations taint the inferences derived below.

As drawn, the section implies at least ≈ 7 km of structural throw on the deepest part of the thrust (F), much of it probably since deposition of the Neogene mudstones, in keeping with the observation that the Taxueh Shan range is one of the largest, highest, and thus presumably fastest-rising wedges of crust in the region. Although the contemporary geometry suggests migration of the thrust away from the range and fairly recent localization of R3, our data are insufficient to assess the timing and detailed mechanism of such a sequential development. It suffices, however, to place plausible bounds on the Holocene slip rate and age of the thrust. We take the age of the top surface in the north-hills, which we infer to be younger than the Würm glacial retreat (≈ 14 ka BP) but older than the bajada loess layer ($\approx 10.7 \pm 2.3$ ka BP), to be 11.2 ± 2.8 ka BP. With D2 at a depth of ≈ 1.1 km (Figs 4f and 7a), the cross-sectional area of the north-hills anticlinal bulge on P1–2 ($\approx 25.5 \times 10^3$ m^2, Fig. 4f) implies about 23 m of horizontal shortening during that time, which translates into Holocene rates of shortening—or slip on D2—of $\approx 2.1 \pm 0.6$ mm yr^{-1}. With slip conserved from D2 to D1 across R2 (inset vector diagram, Fig. 7a), and negligible contemporary movement on R1, the thrust rate on the deep ramp (F) underlying the Taxueh Shan would be the same. Assuming F to dip 45°S would imply that rocks in the mountain range have been tectonically uplifted at a rate of about 1.5 ± 0.4 mm yr^{-1} relative to distal piedmont deposits during the Holocene. If such an uplift rate had been uniform prior to the Holocene, 5 ± 1.3 million years would have been sufficient to create the minimum Late Cenozoic structural relief on the north flank of the range. As drawn, the section would imply coeval movement on R1 and R2 during much of the recent uplift history of the Taxueh Shan, hence probably slower slip on the foreland thrust than now, but the inference that most of the relief of the mountain might be of Plio-Quaternary age finds support in the sharp change of sedimentation rate recorded in a comparable foreland basin, about 50 km to the ENE. The Late Mesozoic–Cenozoic stratigraphic thicknesses

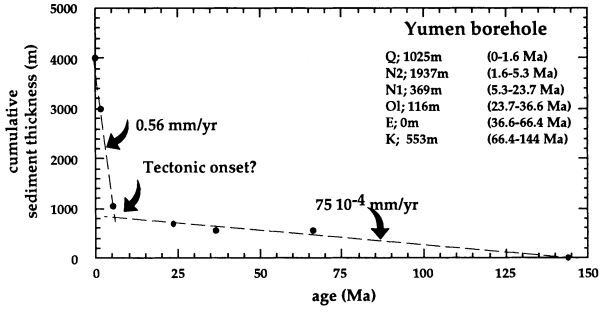

Figure 8. Maximum thicknesses of post-Devonian sediments as a function of age from the Yumen drillhole in Hexi corridor (after Xu *et al.* 1989). Dots represent cumulative thicknesses, plotted at the end of main geological periods and epochs. Note the sharp increase in average deposition rate around 6 Ma BP.

reported in the log of the Yumen drill-hole (Gansu Geological Bureau 1975) (Fig. 8), and those depicted on sections across the western Hexi corridor, at the foot of the Qilian Shan (Xu *et al.* 1989) (Fig. 1), reveal a drastic surge of that rate in the Latest Miocene, most probably around 5–6 Ma. Even allowing for compaction, the surge implies a many-fold increase of detrital influx in the basins. Short of a change towards a wetter climate, for which there is little evidence at that time in central Asia (Métivier & Gaudemer 1996), such a surge may be taken to mark the onset of regional mountain building and sustained high-angle thrusting.

2.3 Shortening in the Tanghenan Shan (Humbolt range) piedmont

The Tanghenan Shan, about 140 km southwest of Changma, is another of the great NW–SE-trending ranges of northeastern Tibet (Fig. 1). Like the Taxueh Shan and the Qilian Shan, it appears to be rising fast, reaching maximum elevations of ≈ 5700 m. It is bounded on either flank by Late Cenozoic faults and folds, roughly outlined by geological contours on available maps (Gansu Geological Bureau 1975) and clearly visible on Landsat images. On SPOT images, such recent tectonic features are particularly prominent across the northern foreland of the range, on the south side of the Yanchiwan intermontane basin (Fig. 9), where the surface morphology shares many of the tell-tale characteristics that typify active thrusting and fold growth in the Taxueh Shan foreland, and thus permits fairly elaborate analysis, even though we did not visit the area in the field.

The Yanchiwan basin is asymmetric. The northern, lowest half of the basin, at an altitude of about 3200 m, is drained by the Tang He river. Its 8–10 km wide floor is covered by marsh flats (Fig. 9a), rimmed in places by abandoned shorelines that imply the existence of a former lake, possibly of Early Holocene age. North of the river, the marshes abut a rejuvenated planation surface that dips 4°–5°S, exposing Precambrian and Palaeozoic rocks (Gansu Geological Bureau 1975; Defense Mapping Agency 1973, 1989). South of the river, they merge smoothly with the toes of contemporary fans that form the distal part of a bajada, comparable to that north of Taxueh Shan (Fig. 9a), which rises gently southwards to the Tanghenan range front. Using similar criteria to those in the Taxueh Shan piedmont, three principal fanglomerate units of increasing age, which we refer to by similar symbols (a3, a2, a1) may be distinguished (Figs 9a and b). Beige-coloured loess, possibly reworked by wash in places, and much thicker in the south than in the north, mantles broad areas of the main bajada surface (a2). Significant parts of the a2 surface may be younger than the Würm glacial retreat.

The bajada slope is broken into two distinct, 4–6 km wide steps by two conspicuous, NW–SE-trending zones along which fanglomerate terraces are strongly uplifted and incised (Figs 9a and b). As in the Taxueh Shan piedmont, both zones appear to be rows of hills separated by entrenched channels of contemporary streams (a3), which flow towards the northeast, orthogonal to the range. By comparison with the north hills, we interpret such hill rows to signal the emergence of two active, south-dipping thrust ramps (R1 and R2, Fig. 9b), roughly parallel to the range. The thrust traces follow the northern base of the hills, with the corresponding cumulative thrust scarps truncating the uplifted terrace patches. The

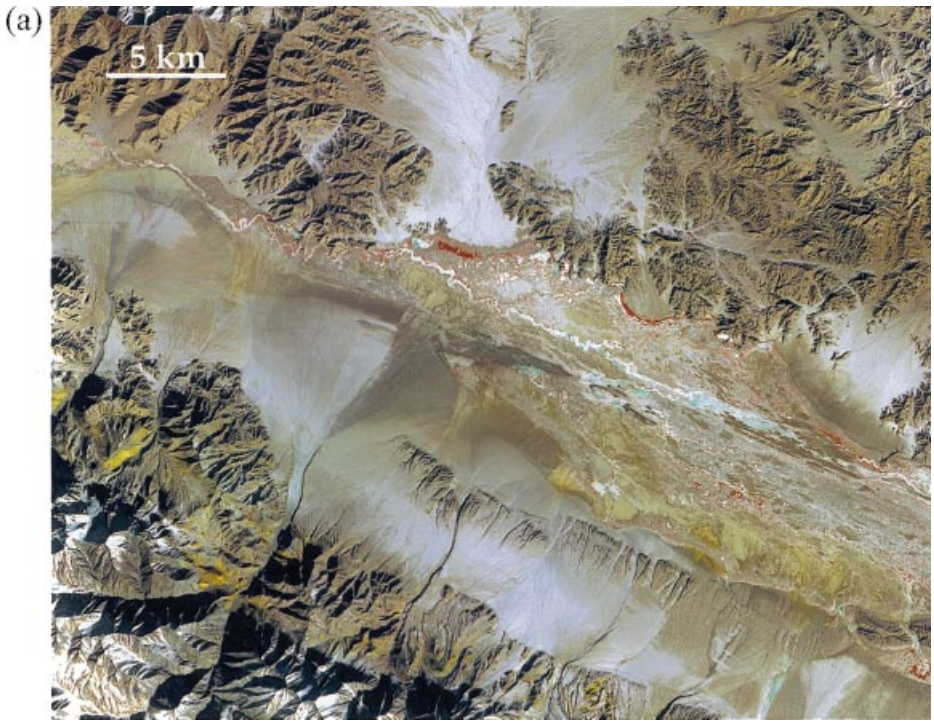

Figure 9(a). Part of multispectral SPOT scene KJ 238–271 (09/12/1986; pixel-size, 20 m). Northern piedmont of Tanghenan Shan. Thrust faulting and folding of fanglomerates is comparable to that seen on Taxueh Shan Piedmont.

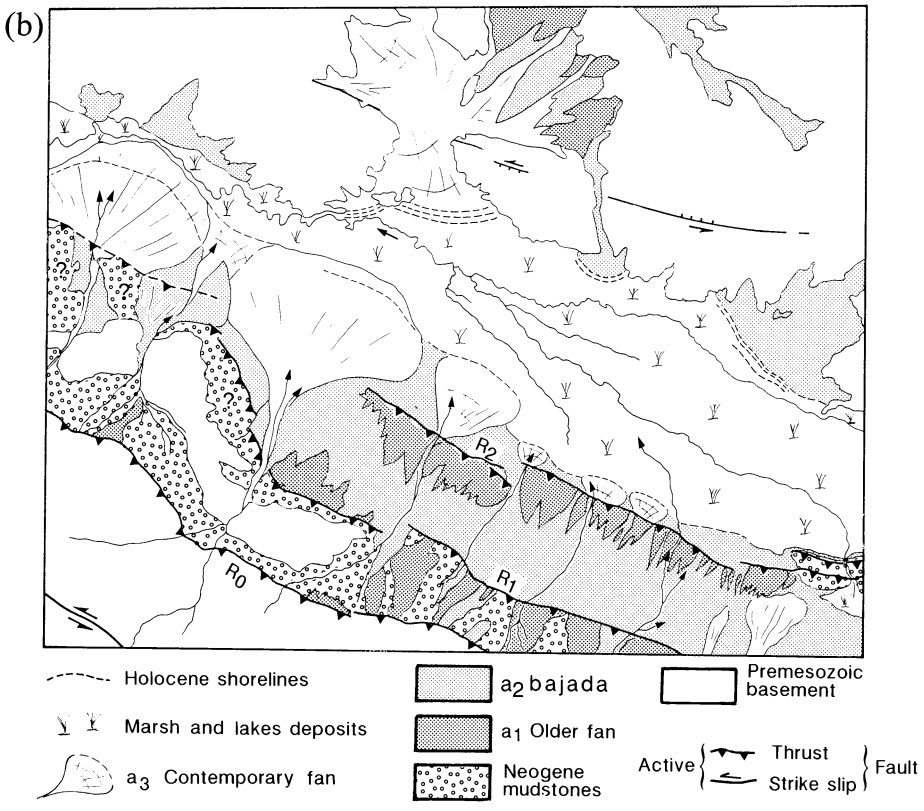

Figure 9(b). Sketch of Fig. 9(a). Fanglomerate surfaces a1 and a1–2 are uplifted and folded south of northern thrust ramp (R2), but only uplifted south of southern thrust ramp (R1).

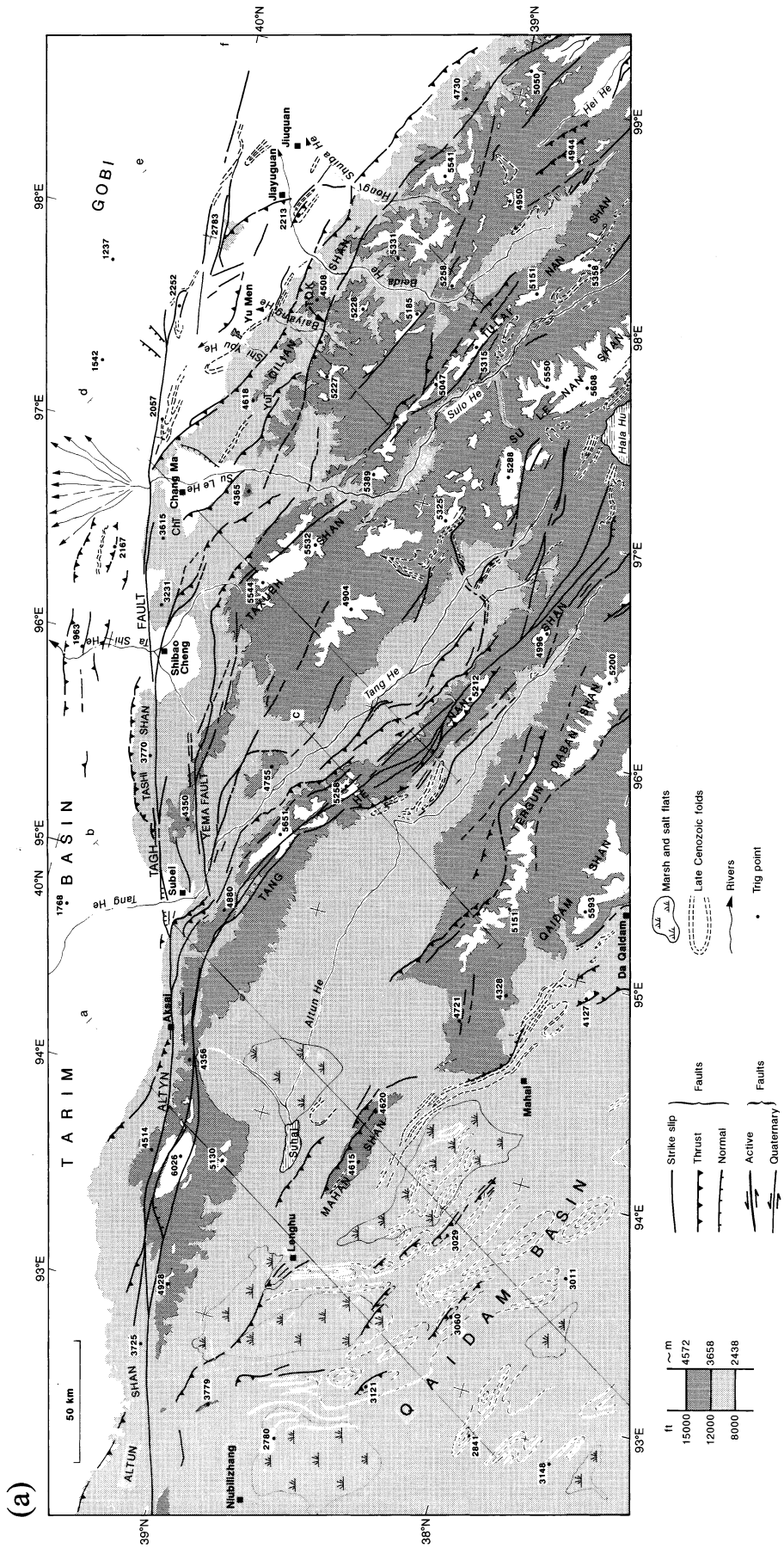

Figure 10(a). Relationship of Quaternary and active thrusts and strike-slip faults with topography in the NE corner of Tibet (improved from Peltzer *et al.* 1989 and Tapponnier *et al.* 1990a). Active faults are from fieldwork and augmented SPOT and Landsat coverage. Topography is from $1:10^6$ ONC chart G8. The location of sections in Fig. 10(c) is indicated. Note how all thrusts and associated ranges, which we refer to, collectively, as 'West-Qilian' ranges, splay from the Altyn Tagh fault zone.

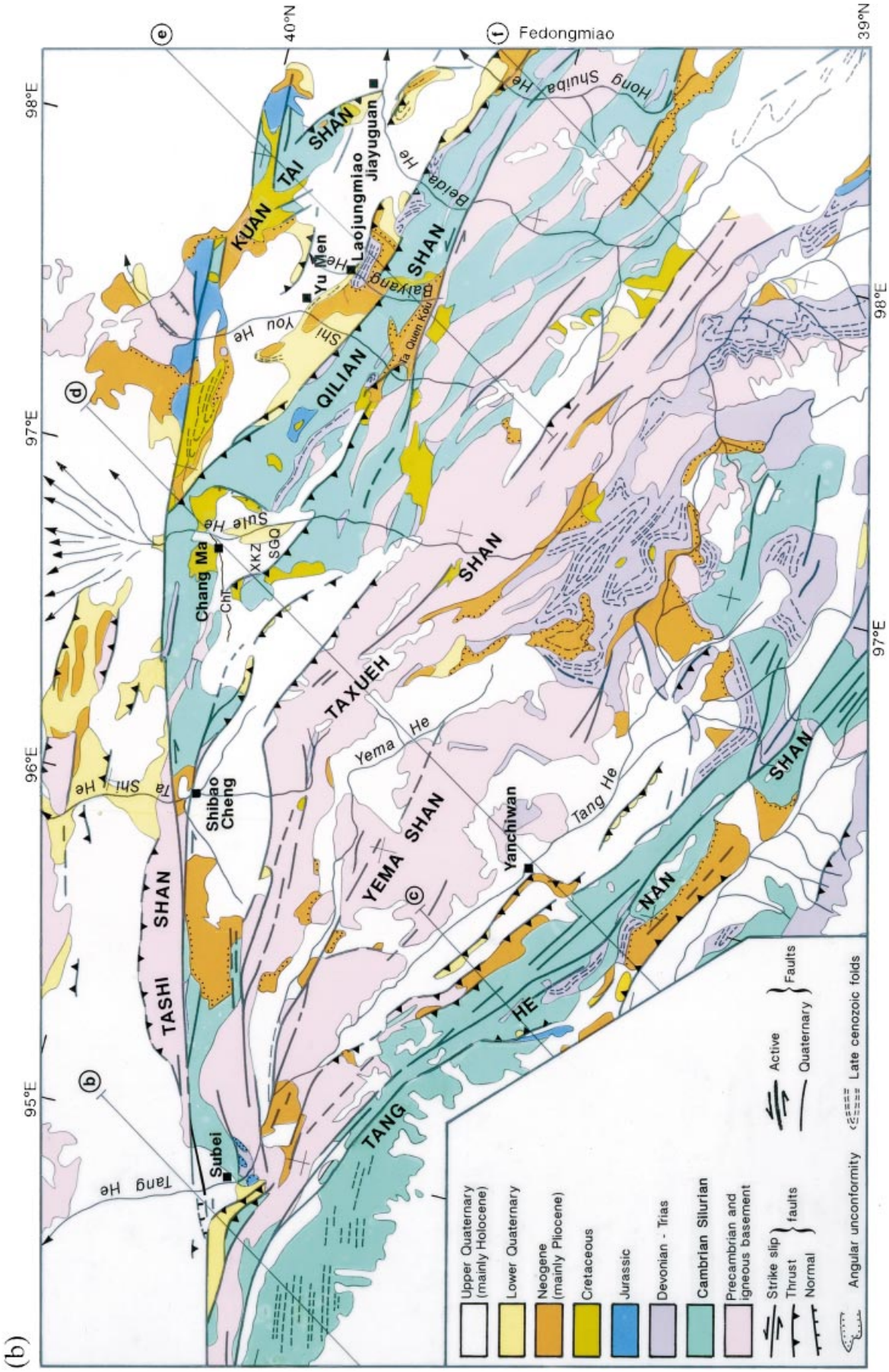

Figure 10(b). Plio-Quaternary faulting and geology of the NE corner of Tibet (based on Gansu Geological Bureau 1975 and improved from Peltzer *et al.* 1988). Pre-Devonian geology is greatly simplified. Emphasis is on distribution and structure of Mesozoic–Cenozoic series and Late-Cenozoic faulting.

observation that, in places, the two traces cut inset lateral terraces all the way to the seasonal flood channels implies that both are periodically rejuvenated by earthquake surface breaks. Hence, as in the Taxueh Shan, both thrust surfaces must somehow reach seismogenic depths. What can be assessed of the morphology and superficial stratigraphy from the images suggests, however, a major difference in their deep geometry.

South of the northern thrust ramp (R2), bottleneck cluses separate spearheaded tongues of uplifted terrace (a1) that merge upstream with the bajada surface (a2), a situation similar to that in the north hills, north of Taxueh Shan. Hence, R2 must reach the surface by slicing through the north limb of an asymmetric (north-facing), growing fault-propagation anticline. The core of that anticline, which includes steeply south-dipping, mostly upper-Neogene, pink-mudstone beds (N2, Gansu geological Bureau 1975), recognizable from their yellowish shade on the Landsat image (e.g. Avouac *et al.* 1993), is in fact exposed farther east along-strike across the Tang He marsh flats. From the length of the terrace tongues, the width of the anticlinal bulge is about 2–2.5 km, comparable to the width of its Neogene core where not hidden under the bajada apron. As for the Taxueh Shan north-hill ramp, we interpret this localized bulge to reflect the fact that R2 flattens southwards into a shallow south-dipping décollement (D, Fig. 7b). Taking R2 to dip at least as steeply as 45°S, in view of its linear trace and of the attitude of the Neogene beds, would imply a ramp-to-flat kink at least 1.5 km deep (Fig. 7b). Such a depth is consistent with the observation that the anticline folds a section of Late Cenozoic sediments that bottoms in the pink upper-Neogene mudstones brought to outcrop by R2 near the Tang He river.

South of the southern thrust ramp (R1), gently north-dipping, dark-grey Quaternary terraces (a1 and older) belonging to the proximal part of the bajada lie unconformably upon rocks with denser yellow hue on the Landsat image, which probably correspond to mostly early Neogene, deep-red sandstones (N1, Gansu Geological Bureau 1975; Xu *et al.* 1989). In contrast to what is observed south of R2, the terraces are uplifted all the way to the slope break marking the base of the steep range front, another 5 km farther south. The sharpness and continuity of that break, which follows the main tectonic contact placing Ordovician rocks on top of Neogene and Quaternary clastics on the geological map (Gansu geological Bureau 1975), implies that the range-front base itself coincides with the emergence of an active thrust ramp (R0, Figs 7b and 9b). The uplift of the a1 fanglomerate terraces between R1 and R0 appears to be relatively uniform, because the side cliffs of the contemporary drainage channels keep roughly the same height across the entire R0–R1 fault step (Fig. 9). This suggests wholesale uplift of the basement wedge between R0 and R1, without detectable, short-wavelength, contemporary surface folding on the image of Fig. 9(a). Thus, although topographic profiles might reveal slight surface warping across the entire width of that wedge, the morphological features visible on the image suffice to conclude that R1 extends much deeper than R2.

The section of Fig. 7(b) outlines the overall thrust geometry that we find most plausible north of Tanghenan Shan. Since it emplaces lower-Palaeozoic onto Neogene and Quaternary rocks, the thrust ramp along the range front (R0) has probably absorbed a few kilometres of late Cenozoic shortening and produced, given its fairly linear trace and hence probably steep dip (>45°), an even greater amount of uplift. When compared to that north of Taxueh Shan on the images, the Tanghenan Shan range-front ramp seems more active. As in the Taxueh Shan, however, a large fraction of the contemporary thrusting appears to be taken up north of the range, by ramps R1 and R2 within the foreland. We interpret this to reflect slip partitioning between two splays (R0 and F) of a deeper thrust ramp (F′) responsible for the large-scale uplift of that range. With the dips taken in Fig. 7(b) and the distance between the surface traces of R0 and R1, those two splays would merge at a depth of approximately 12 km, isolating the R0–R1 basement wedge, whose wholesale rise leads to fairly uniform surface uplift of the bajada step closest to the range. Further partitioning of slip occurs at the junction between R1 and D, possibly near the base of the Neogene, permitting a final slip fraction to reach the surface along the trace of R2, the farthest and probably most recent localization of the Tanghenan Shan piedmont thrust, 8–9 km north of the range. Note that the composition of slip at the junction between F, R1 and D (inset vector diagram, Fig. 7b) is precisely that which can be ruled out under the south-hills anticline, north of Taxueh Shan (Fig. 6e). Although the deep geometry of the section in Fig. 7(b) is different from that in the Taxueh Shan, it also implies many kilometres of cumulative late Cenozoic throw on the Tanghenan Shan thrust. Moreover, since the ranges' topographic and structural reliefs appear to be similar, and since the aspect of cumulative foreland thrust scarps on the SPOT image implies roughly comparable postglacial shortening and uplift rates, the ages of the two mountains may not be very different.

In summary, active shortening of surface deposits in the basins separating the ranges of northeastern Tibet results in patterns of uplift, warping and folding that permit first-order reconstruction of the geometries of SE-dipping seismogenic thrusts down-section (Fig. 7). To a degree, the geometries shown in sections 7(b) and (a) may be seen to represent two successive stages of the migration of young thrusts that root beneath the ranges into forelands with fairly dynamic contemporary sedimentation. In either case, localized, kilometre-wide foreland anticlines, whether of fault-propagation or fault-bend type, appear to reflect flat-to-ramp bends at rather shallow depths. At the scale of each range, the active thrusts flatten underneath the foreland sediments, which makes them break the surface far from the mountains, all the farther as the foreland flexural fill is thicker (e.g. Avouac *et al.* 1993; see also Armijo *et al.* 1986, for splaying normal faults), but plunge steeply into the deeper crust beneath the range-front slope breaks.

While similar thrust systems are commonly exposed in fossil foldbelts, it is rarer to witness them at work, in the act of migrating (Ikeda 1983) and dynamically creating relief in such a clear way. Going beyond the scale of shallow thrusts along the foreland of a single range, we now investigate the distribution and interrelation of thrusts along different ranges, and what their fate might be at depths greater than 15 km.

3 REGIONAL ORGANIZATION OF LATE-CENOZOIC FAULTING AND ORIGIN OF THE MOUNTAIN RANGES OF NE TIBET

In addition to the examples seen on the north sides of the Taxueh and Tanghenan Shan, there is prominent evidence for Quaternary thrusting at the foot of many other 'West-Qilian'

ranges, and along folds in the Qaidam basin. The maps of Figs 10(a and b) and the sections of Fig. 10(c) show the relationship of such thrusting to the regional topography and geology. The surface signatures of growing folds and the traces of Quaternary thrusts and other faults over this large area ($\approx 600 \times 250$ km^2) are derived from detailed analysis of nearly complete SPOT and Landsat coverage of the region, with reference to localities studied in the field.

3.1 Surface deformation

3.1.1 Extent of coeval thrusting and folding

Qilian Shan and Gobi: Active thrust faulting keeps on creating young, vigorous relief far northeast of the Taxueh Shan. 10 to 20 km north of the north-hills anticline, the southwest-dipping Changma thrust, and its eastward stepover, the Yuerhong thrust, both activated by the 1932 Changma earthquake, sharply bound one rising subrange of the Qilian Shan. In a sharply incised stream gully east of Sange Quan (Figs 10 and 11a), for instance, the former of these thrusts is seen to heave a slice of strongly sheared Cretaceous red-beds, itself overthrust by Cambrian slates, onto Holocene gravels. The fresh slickensides we exhumed on the main, N115°E-striking, 40°S-dipping fault plane imply nearly pure reverse faulting, with slip towards N30°E, perpendicular to the range front (inset, Fig. 11a, Table 2). Discrete, subsurface offsets of the gravel wedge that mantles the scarp, and sheared phacoids, suggest additional thrust slip on hanging-wall sandstone beds parallel to that plane. A large fraction, if not all, of the scarp height (≈ 2.4 m) formed during the 1932 earthquake (see discussion in Meyer 1991 and Meyer *et al.* 1991).

Another 20–30 km northwards, the ≈ 400 km long front of the main Qilian range is also a prominent site of Quaternary folding and overthrusting. Foreland-facing thrust scarps cut the surface of postglacial piedmont fans along much of the length of the range (e.g. State Seismological Bureau 1993; Meyer 1991; Tapponnier *et al.* 1990a). Where we were granted access, sections along river valleys incising the north flank of the range clearly display the style of recent deformation of Neogene and Quaternary rocks.

Such is the case, for instance, of the Hongshuibai He valley section, south of Jiuquan (Figs 10a,b and c). At Fedongmiao, upstream from ENE-striking, north-facing scarps that cross the apex of fans near the top of the Holocene bajada, the ≈ 20 m high cliff on the east side of the valley exposes a prominent, N70°E-striking, shallow SE-dipping thrust that emplaces pink, schistose Pliocene mudstones on top of flat, Mid-Pleistocene conglomerates (Fig. 11b). A smaller, steeper thrust splays upwards from that master thrust to offset, by a few metres, the base of the unconformable, Late-Pleistocene terrace on top of the cliff. South of the branch-line with that splay ramp, the dip of the master thrust steepens to 25°SE. The more intense, approximately EW-striking schistosity near that junction, and slickensides on the master-thrust plane where steeper (inset, Fig. 11b, Table 2), imply slip towards N25–30°E, with a left-lateral component.

Farther upsection in the deeper river canyon, fairly thick, consolidated, well-bedded Early Pleistocene conglomerates (Xiyu fm., Q1) lying conformably upon the Pliocene mudstones are strongly folded, with dominant SW-dips of up to 50° (photograph, Fig. 11c). Numerous small thrust faults, several of them along bedding planes, hence reflecting flexural slip (inset, Fig. 11c, Table 2), affect these south-dipping conglomerates. They bear slickensides compatible with N20°E shortening (Table 2). We interpret that deformation and the attitude of the Q1 conglomerates to reflect steepening, on a 40–50°SE-dipping ramp (Fig. 11c), of the underlying foreland thrust that used to break the surface at Fedongmiao (Fig. 11b). The corresponding ramp anticline is separated from the range front by a N–Q1 synclinorium, unconformably capped by flat Q3–4 terraces, with hinge faulting and folding and steeply north-dipping Neogene beds along its southern limb. Overall (Fig. 11c), the Qilian-front thrust geometry deduced from surface evidence in the Hongshuiba He valley thus resembles, both in scale and style, that inferred for foreland thrusts north of the Tanghenan and Taxueh Shan (Figs 7 and 10).

Even though the Qilian Shan, first great mountain wall south of the Gobi to stand above 5000 m, marks the northern boundary of the Tibet–Qinghai highlands, it is not the outer limit of active crustal deformation related to their growth. Crustal seismicity and active faulting extend farther towards the northeast (Figs 1 and 10a).

Just north of Yumen, an emergent, approximately N90–110°E-striking thrust ramp lifts terraces of the bajada south of Kuantai Shan above the current profiles of their parent streams (Figs 10 and 11d). This north-dipping thrust ramp, one of the rare exceptions we found amongst regionally south-dipping, Late-Quaternary overthrusts, is clearly active. Its hanging wall displays all the attributes, defined in the Taxueh Shan north hills (Figs 3 and 4), that characterize youthful, growing fault-propagation anticlines. In the field, the

Figure 11(a). Detailed sections of ground-breaking thrusts, and late Quaternary slip-kinematics at sites along the Qilian and Kuantai Shan northern range fronts (see Figs 10a,b for location). Section of Changma thrust in gully east of Sange Quan. SE-looking view (top) and interpretative sketch (below) show thrust of Cambrian slates and Cretaceous redbeds imbricates onto Holocene gravels. Steep scarp above thrust formed during 1932 Changma earthquake. Inset stereogram (lower-hemisphere projection) indicates attitudes of active thrust plane and fresh slickensides on it. (**b**). Fedongmiao, Hongshuibai He valley, Qilian foreland. SE-looking view (top) and sketch (below) of steep, Late-Pleistocene thrust ramping from shallower dipping contact emplacing schistose Miocene mudstones (N2) on top of Mid-Pleistocene conglomerates (Q2). Inset (as in 11a) shows attitudes of lowermost thrust, slikensides on it, and cleavage above it. (**c**). Hongshuibai He section. NW-looking photograph (top) of folded, 50°SW-dipping, Early Pleistocene conglomerates (Q1) upstream from Fedongmiao. Overall section (below) involves steepening of main active thrust on blind-ramp under N2–Q1 anticline north of the Qilian range front. Stratigraphic thicknesses are from Gansu Geological Bureau (1975), and Xu *et al.* (1989). Slickensides on fault planes in Q1 (most of them due to bedding slip) are represented on inset diagram. (**d**). North Yumen thrust. View of emergent, N-dipping thrust ramp, folding south Kuantai Shan bajada fans. Detail of panchromatic SPOT scene KJ 242–270 (07/10/87). Note the striking similarity with Taxueh Shan north-hills anticline, despite opposite vergence. (**e**). Jiayuguan. Southern extension of the Great Wall Citadel fault. NW-looking view of sheared Q2 conglomerates (top). The interpretative sketch shows sharp, steep contact between folded Cretaceous red-beds and Holocene conglomerates. Slickensides on the local shear plane (inset diagram) indicate oblique right-lateral slip, with uplift of the southwest wall on a NNW-striking fault.

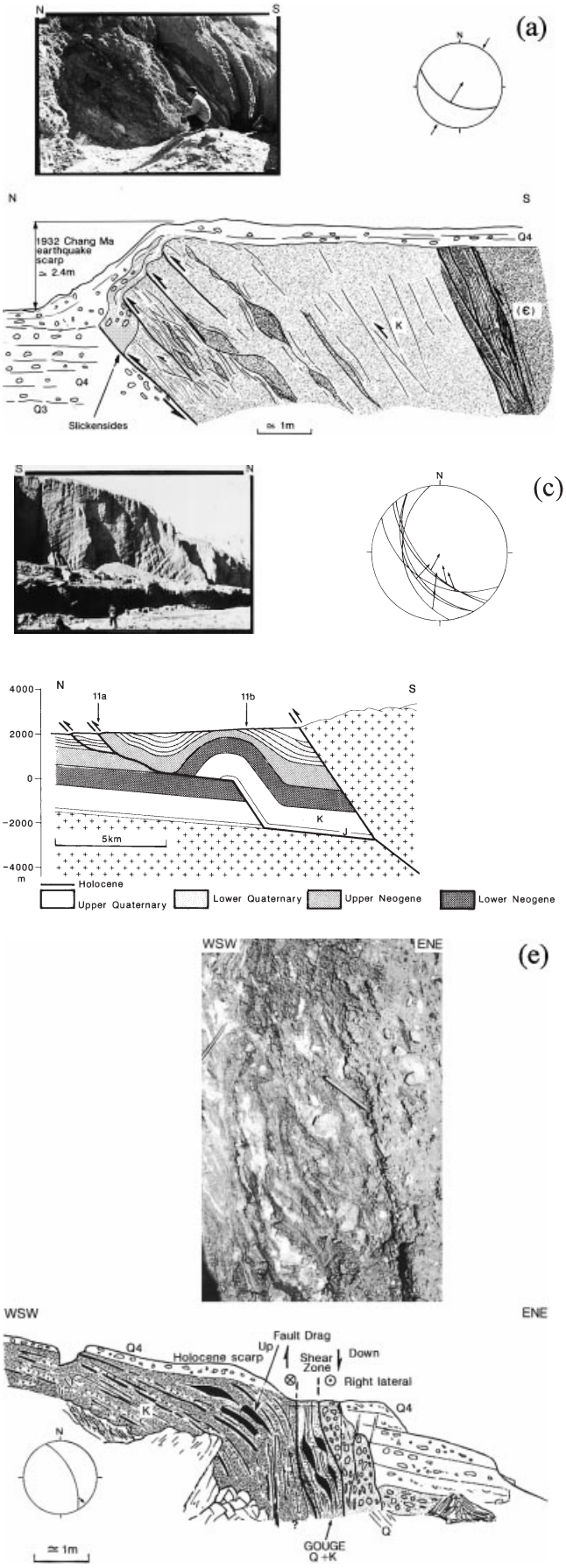
(a)
N
S
1932 Chang Ma earthquake scarp ≃ 2.4m
Q4
(€)
K
Q3
Slickensides
≃ 1m
(b)
S_1:70-90
55-60S
F
N2
Q4
Q3
Q2
(c)
11a
11b
4000
2000
0
−2000
−4000
m
5km
Holocene
Upper Quaternary
Lower Quaternary
Upper Neogene
Lower Neogene
(d)
1 km
Yumen
(e)
WSW
ENE
Fault Drag
Up
Down
Shear Zone
Holocene scarp
Right lateral
GOUGE
Q +K

Table 2. Quaternary slickensides on faults in and north of Qilian Shan. Most slip directions imply N20–30°E orientated shortening (Fig. 11).

Location	Strike	Dip	Pitch	Sense
Chang Ma	N120E	40S	76NW	I
Jiayuguan	N155E	65N	38SE	D
Hongshuibai He faults	N70E	25S	43S	I
	N150E	36S	75S	I
	N135E	5S	50S	I
	N150E	40S	45S	I
	N170E	32W	20S	I
	N140E	8S	80S	I
	N120E	40S	50S	I

thrust trace bears eroded, but unambiguous, south-facing seismic scarplets (20–30 cm high), across all but the most recent gravel deposits at the southern outlets of the stream cluses. We infer such scarplets to result from a single, fairly recent, historical earthquake, possibly the $M \approx 6$, 1785 April 18 event whose epicentre has been located 10–20 km northeastwards, near Xinminbao (Gu *et al.* 1989).

Though not of great height ($\approx$2800 m), the entire Kuantai Shan, north of the Jiuquan-Yumen road (Fig. 10), is undergoing current uplift, relative to the Gobi, above a SW-dipping thrust responsible for the commanding position of the Jiayuguan citadel, westernmost fortified watchpost along China's Great Wall. The citadel sits on the NE edge of a basement block that rises gently northwestwards to form the bulk of the mountain. Locally, the heaved basement (mostly isoclinally folded Ordovician greywackes, unconformably capped by a veneer of red Cretaceous sandstones) is mantled by Late-Pleistocene fanglomerates that are uniformly tilted several degrees towards the southwest (Figs 10a and b). North of the citadel walls, the height of the NE-facing, cumulative Quaternary fault scarp reaches about 30 m.

As might be expected from its N150–160°E average strike in map view, however, the Jiayuguan fault is not as simple a thrust as those documented in and south of the Qilian Shan. Where exposed south of the Lanzhou–Urumqi railroad, it reaches the surface as a nearly vertical zone of sheared clay-gouge and conglomerates separating deformed Cretaceous red-beds from postglacial gravels (Fig. 11e). Drag-folding of the red-beds, locally capped by a very thin terrace, against the shear zone, and non-coaxial strain-tails in the wake of phacoids within that zone, do corroborate uplift of the southwest wall. However slickensides on warped, N155°E-striking, 38°NE-dipping bedding planes near this zone imply a component of dextral slip (inset, Fig. 11e, Table 2). Hence, we interpret the fault to act locally as a right-lateral ramp connecting a 'purer', more westerly striking, SW-dipping thrust north of Kuantai Shan, with another prominent Quaternary thrust south of Jiuquan. We infer recent movement on this latter thrust, also SW-dipping, to have caused the growth of the large, asymmetric, Neogene–Quaternary anticline that forms the $\approx$2200 m high hills visible southeast of the Jiayuguan citadel, about 20 km north of the Qilian range front (Figs 10a and b). On the SPOT image, this thrust, in turn, appears to connect with the Qilian Shan frontal thrust just west of Fedongmiao, through another, N160°E-striking, right-lateral ramp (Figs 10a and b).

Bypassing the Kuantai Shan to the north, the Altyn Tagh fault zone continues eastwards at least 300 km into the Gobi-Alashan desert, to Yabrai Shan and possibly farther, across a strategic region straddling the Gansu–Neimongol provincial border. Along and south of that zone, ESE-trending push-up folds exposing pink-ochre Pliocene mudstones or dark grey Quaternary conglomerates, more modest anticlines warping bajada fans, and youthful, 50–150 km long ranges bounded by recent thrusts are clear whether on Landsat and SPOT images or from the air (Figs 1 and 10; also Fig. 1a in Tapponnier *et al.* 1990a). Most prominent among such ranges are the N120°E-trending Heli Shan (up to $\approx$2200 m a.s.l.) and Longshou Shan (up to $\approx$3600 m a.s.l.), which mark the northern boundary of the Hexi corridor ($\approx$1500 m a.s.l., on average). From the air, north-facing cumulative scarps north of the Longshou Shan display the particularly steep and sharp morphology that typifies the emergence of active thrusts elsewhere. Some may have ruptured on the occasion of the $M \approx 7.2$, 1954 February 11 earthquake or of its strongest, $M \approx 6$ aftershock, north of Shantan (Fig. 1) (State Seismological Bureau 1993). Farther northeastwards in the Tengger desert, other earthquakes recorded this century (Gu *et al.* 1989), including the $M \approx 7$, 1954 July 31 event, show predominant strike-slip, consistent with approximately NE–SW shortening (e.g. Tapponnier & Molnar 1977) (Fig. 1).

Hence, even though Late-Cenozoic crustal thickening has clearly been more modest north than south of the Qilian Shan, 'incipient' relief growth and active thrusting may be traced about 150 km northeast of the highland front into the Gobi platform. Such incipient thrusting appears to be still mostly NE-vergent and compatible with NE–SW regional shortening.

Suhai and Qaidam basins: Chiefly northeast-vergent thrusts and growing folds, trending N110–150°E, also characterize ongoing deformation across regions well southwest of the Tanghenan Shan (Figs 1 and 10). Even though folding of Neogene beds is clear south of the central part of the Tanghenan Shan, the westernmost, $\approx$100 km long, south flank of the mountain shows little evidence of active, south-vergent thrust faulting (Fig. 10). The surface traces of north-vergent range front thrusts, on the other hand, are remarkably sharp at the foot of the western Tergun Daban and Mahan Shan, south of the vast bajadas of the Suhai basin.

One of the thrusted basement wedges of the Mahan range appears to continue under the thick, Oligocene–Holocene deposits of the northwesternmost Qaidam basin. The corresponding thrust, which has carried Neogene rocks to outcrop, emerges along a north-facing cumulative scarp that divides the marshy flats west of Lenghu (Fig. 10a) and is responsible for the development of the Lenghu anticline (Fig. 10c, section a). As interpreted by Bally *et al.* (1986) and shown, to scale, in Fig. 10(c), one seismic-reflection profile across this anticline reveals chiefly post-Early-Pliocene growth above a south-dipping ramp offsetting the Palaeozoic basement by several kilometres. Hence, regardless of the complexity in the anticline core, due in part to conjugate, Early Miocene, reverse faulting (Bally *et al.* 1986, Fig. 14d), both the mechanism and timing of growth resemble those typifying active, northeast-vergent ramp anticlines in the West Qilian ranges (Fig. 7b; Meyer 1991; Tapponnier *et al.* 1990a).

South of Lenghu, within the $\approx$200 km wide Qaidam basin, landforms become much smoother, and maximum relief much less, with ridges only $\approx$150–200 m higher than the basin surface, $\approx$2700 m a.s.l. (Figs 1 and 10a). Two principal factors,

both a consequence of internal drainage, conspire to generate such flatness, hence the striking morphological contrast between that vast, gentle plain and the rugged topography of the 'West-Qilian' ranges.

First, basement highs and lows in the Qaidam are everywhere hidden beneath an enormous thickness of Cenozoic fluvio-lacustrine sediments (generally between 10 and 15 km, e.g. Bally *et al.* 1986; Gu & Di 1989). Up to two-thirds of this sedimentary pile ($\approx$8–10 km) is of Miocene to Quaternary age. The thickness of Eocene–Oligocene deposits (up to $\approx$2–3 km), particularly in the northwestern half of the basin (Gu & Di 1989), is much greater than north of the Taxueh Shan (Fig. 10c, sections a and b).

Second, because the mountain-locked Qaidam plain is the ultimate sink for many of the rivers that drain the surrounding relief, and its surface a local base level, much of it has been repeatedly flooded by a large lake (e.g. Phillips *et al.* 1993). Today, broad salt flats, marshes and small residual lakes remain (Figs 1 and 10a). Abandoned shorelines at $\approx$2800 m a.s.l., whether near Golmud to the south or Lenghu to the north, and wavecut cliffs around rising anticlines, attest to recurrent lake highstands during the wettest episodes of the Pleistocene and Holocene. Thus the extraordinary flatness of the surface of the basin probably results from smoothing by uniform shallow deposition in that lake and abrasion of residual relief along its shores.

Despite the great sediment thickness, and hence the broad width of most folds and probable tapering of certain faults before they reach the surface, clear, if discontinuous, thrust scarps cut young superficial deposits in the northeastern Qaidam, generally along the north limbs of anticlines (Fig. 10a). The thrust traces usually trend N120–130°E. Three zones with N150–160°E-striking beds, south and west of Mahan Shan, may correspond to right-lateral ramps in the basement underneath, similar to that along the Jiayuguan citadel fault. With the exception of thrusts along the steep Nan Qilian and Qaidam Shan range fronts, the dominant vergence of emergent thrusts and ramp anticlines in the western part of the Qaidam is towards the northeast, even, surprisingly, near the southwest-sloping, northeastern edge of the basin.

Most of the thrusts at the south edge of the Qaidam, along the Kunlun range (Burhan Budai Shan), do not reach the surface. They remain beneath the sediments they warp, except in the westernmost corner of the basin, where the basement shallows between the Qiman and Altyn Tagh. Cenozoic deposits in the Kunlun foreland are especially thick, even on top of hidden, upthrust basement wedges (Bally *et al.* 1986) (Fig. 10c, section b). This is the area where Middle-Tertiary sediments, in particular, are thickest, with the main Oligocene depocentre near 92°E (Métivier 1996). Although deposition keeps smothering surface evidence of active deformation, sustained seismicity, and fault-plane solutions with nodal planes striking mostly N90–150°E (Fig. 1) imply a crustal shortening regime similar to that in the West-Qilian ranges, albeit on blind thrusts.

In summary, between the Kunlun range and the Gobi desert (90–102°E), contemporaneous thrusting governs the growth of approximately SW-striking mountain ranges or of sediment-drowned basement highs over a distance of as much as $\approx$1000 km along the Altyn Tagh fault and more than 300 km southeastwards from it (Figs 1 and 10). The vergence of the active, parallel thrusts is towards the northeast, with few exceptions. In general, slip on the thrusts is also towards the northeast ($\approx$N30°E where accurately measured), roughly perpendicular to the ranges. The overall geometry of the thrust network is remarkably regular despite its grand scale, with well-organized steps, oblique ramps, and connections reminiscent of those that typify thin-skinned fold belts in sedimentary covers (e.g. Boyer & Elliot 1982). Perhaps the most remarkable connections, discussed below, are those between the thrusts and the left-lateral Altyn Tagh fault, the longest active strike-slip fault of Asia.

3.1.2 Links between West Qilian–Qaidam thrusts and the Altyn Tagh strike-slip fault

Our mapping of the active West-Qilian and Qaidam thrusts shows that they terminate at the Altyn Tagh fault. They are not truncated and offset by it. Rather, they appear to branch from it, often through oblique, more easterly striking splays (Peltzer *et al.* 1989) (Figs 10a and b). Accordingly, most of the NW–SE-trending basement wedges uplifted by such thrusts taper and veer as they come to abut the fault. None continues northwest of it, and there is in fact no evidence for NE–SW shortening in regions located just north of the fault, between 85° and 105°E. This contributes to making this fault the sharpest structural and morphological discontinuity of central Asia.

There are youthful, rising mountain ranges north of the Altyn Tagh fault, notably, west of 85°E, the Tashi and Altyn ranges (Figs 1 and 10a). However these ranges, and Quaternary thrusts along their fronts or across their forelands, tend to strike roughly parallel to the fault (N70–80°E, Fig. 10a). Such thrusts show little evidence of systematic, left- or right-lateral components of slip, and those that limit the ranges usually merge with the fault where such ranges pinch out, to the east and west (Figs 1 and 10). Mountain ranges north of the Altyn Tagh fault thus form completely fault-bounded wedges or flakes of Tarim basement, thrust towards the NNW, orthogonal to the fault, a result of crustal-scale slip partitioning (e.g. Gaudemer *et al.* 1995) along the edge of the Tarim block (Matte *et al.* 1996).

The abrupt change in the mean trend of ranges and thrusts south and north of the fault is quantitatively depicted in Fig. 12(a), where the angles between range crests or Qaidam fold axes and the fault are plotted as a function of distance from it, in 25 km steps. On average, thrusts just north of the Altyn Tagh fault strike about 40° counterclockwise from thrusts south of it. That angle is seldom less than 20°, and exceeds 60° in the western part of the Qaidam basin (Fig. 12a). In the eastern two-thirds of the Takla Makan desert, evidence of Quaternary surface deformation vanishes $\approx$100 km north of the Altyn Tagh fault (Figs 1, 10 and 12a). The fault thus separates two regions with markedly different shortening directions and styles, whose crusts have suffered very different amounts of Late-Cenozoic strain, as corroborated by the low level of instrumental seismicity in the Tarim (Gu *et al.* 1989), a consequence of the high strength of this ancient block's lithosphere (e.g. Molnar & Tapponnier 1981).

Current movement on the Altyn Tagh strike-slip fault appears to be intimately related to motions on the adjacent, active thrusts. This is a kinematic consequence of the geometry of the fault traces, which merge at certain points. The Kuantai and Qilian range-front thrusts, for instance, meet with the Altyn Tagh fault north of Jiayuguan and Changma, respectively

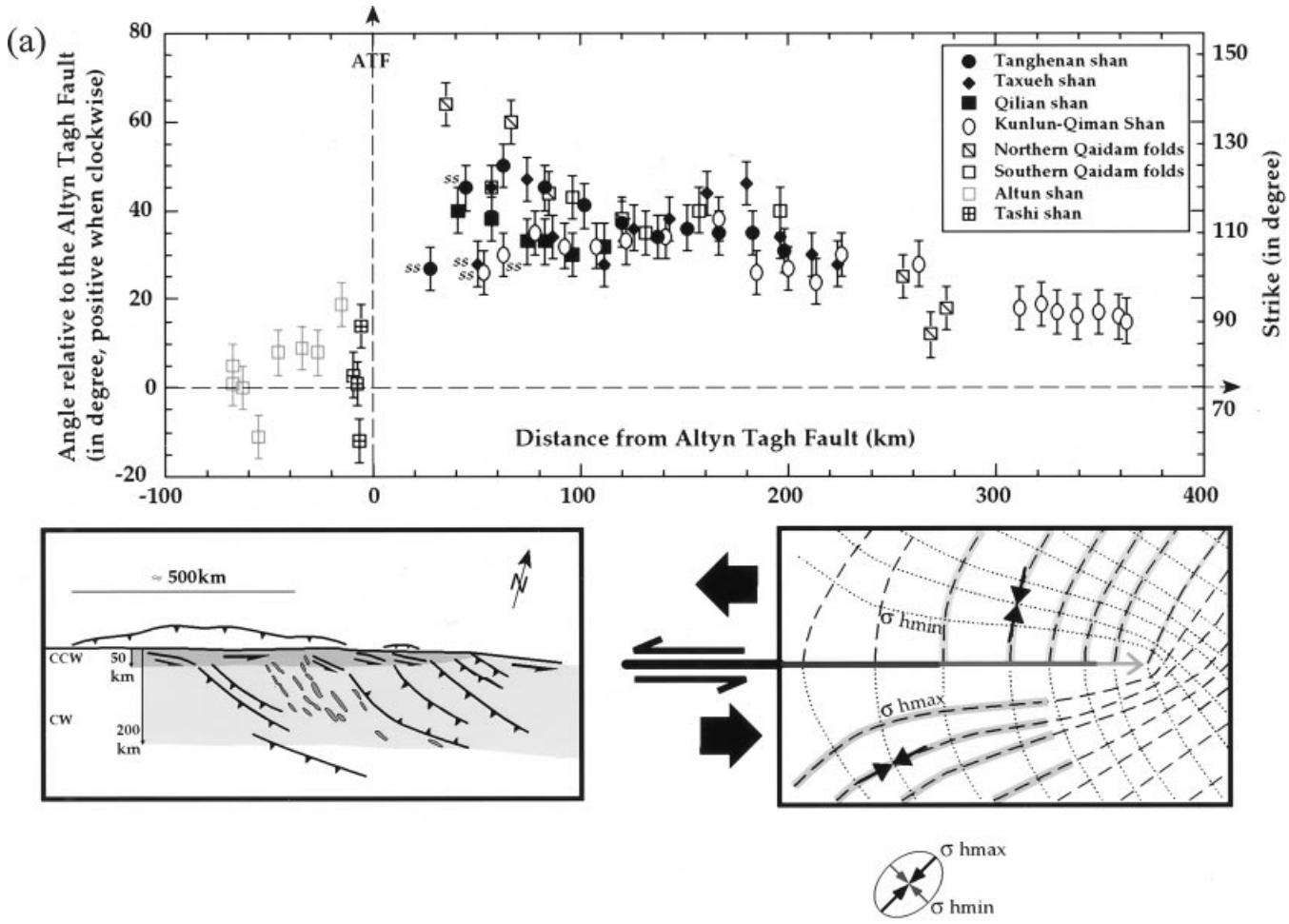

Figure 12(a). Contrast in trends of growing folds and mountain ranges south and north of the Altyn Tagh fault. The diagram is derived from ONC Digital Elevation Model by plotting the measured strike difference between the fault and 25 km long segments of range crests, and fold axes in the Qaidam basin, as a function of the distance of the segment centre from the fault. Errors in angles are estimated to be $\pm 5^{\circ}$. Bottom left inset depicts schematically zones with counterclockwise and clockwise swings in trends near and away from fault, dark and light grey shades, respectively. Bottom right inset shows the expected deviation of maximum principal stress trajectories, relative to regional stress (ellipse beneath), near the tip of propagating, sinistral strike-slip fault.

(Figs 10 and 12b). Both veer by $\approx 20^{\circ}$ counterclockwise over a distance of ≈ 20 km east of such junctions. At the Qilian thrust junction, the Altyn Tagh fault also changes strike, quite abruptly, by $\approx 16^{\circ}$ clockwise. Given the angle between the two faults prior to the junction ($\approx 54^{\circ}$), and assuming the blocks they separate to be rigid, a left-slip rate of ≈ 4 mm yr^{-1}, as deduced from Holocene fan and channel offsets west of the junction (Meyer *et al.* 1996), would result in ≈ 3 mm yr^{-1} of left-slip and 1.6 mm yr^{-1} of thrust-perpendicular slip east of the junction (Fig. 12b). That the strike-slip fault trace bends at this junction, becomes fainter east of it, and that both the direction ($\approx$N30°E) and rate of thrusting are consistent with those estimated for ranges of greater height to the south, suggest that, to first order, the rigidity assumption holds.

Branching of the major thrusts west of the Sule He is less simple, and generally involves oblique splays of the Altyn Tagh fault. The surface break of the 1932 Changma earthquake, for instance, has only been unambiguously traced to about 15 km of the fault, along the Changma thrust. The last 6 km stretch of the break follows a N160°E-striking dextral ramp (Meyer 1991), before veering and disappearing in the Changma river valley. Breaks to the north or west have not been found. The westernmost Changma thrust segment may continue farther westwards along that valley, north of uplifted terraces, then step northwards along exhumed basement, closer to the Altyn Tagh fault (Fig. 10b), but such continuation and the existence of a clear junction remain to be established. The Shibaocheng fault (Fig. 10), a prominent, oblique splay of the Altyn Tagh that heads straight towards the Changma thrust zone and bears recent, if discontinuous, seismic scarplets (Meyer 1991), might act as an alternative link, but its NE dip is opposite to that of all the other segments of the zone. Thus, if transfer of motion presently occurs between the Altyn Tagh and the Changma thrusts, it does so in a complex manner.

The south-dipping thrusts of the Taxueh range foreland do not continue across the Shibaocheng basin (Fig. 10). Instead, they merge with the active, lateral ramp that bounds the range south of the basin. Westwards, this sinistral ramp joins the Yema fault. For about 120 km, both run roughly parallel to the Altyn Tagh fault before meeting with the Tanghenan Shan front thrusts south of Subei. As they pass this meeting point towards the northwest, these thrusts veer clockwise, in

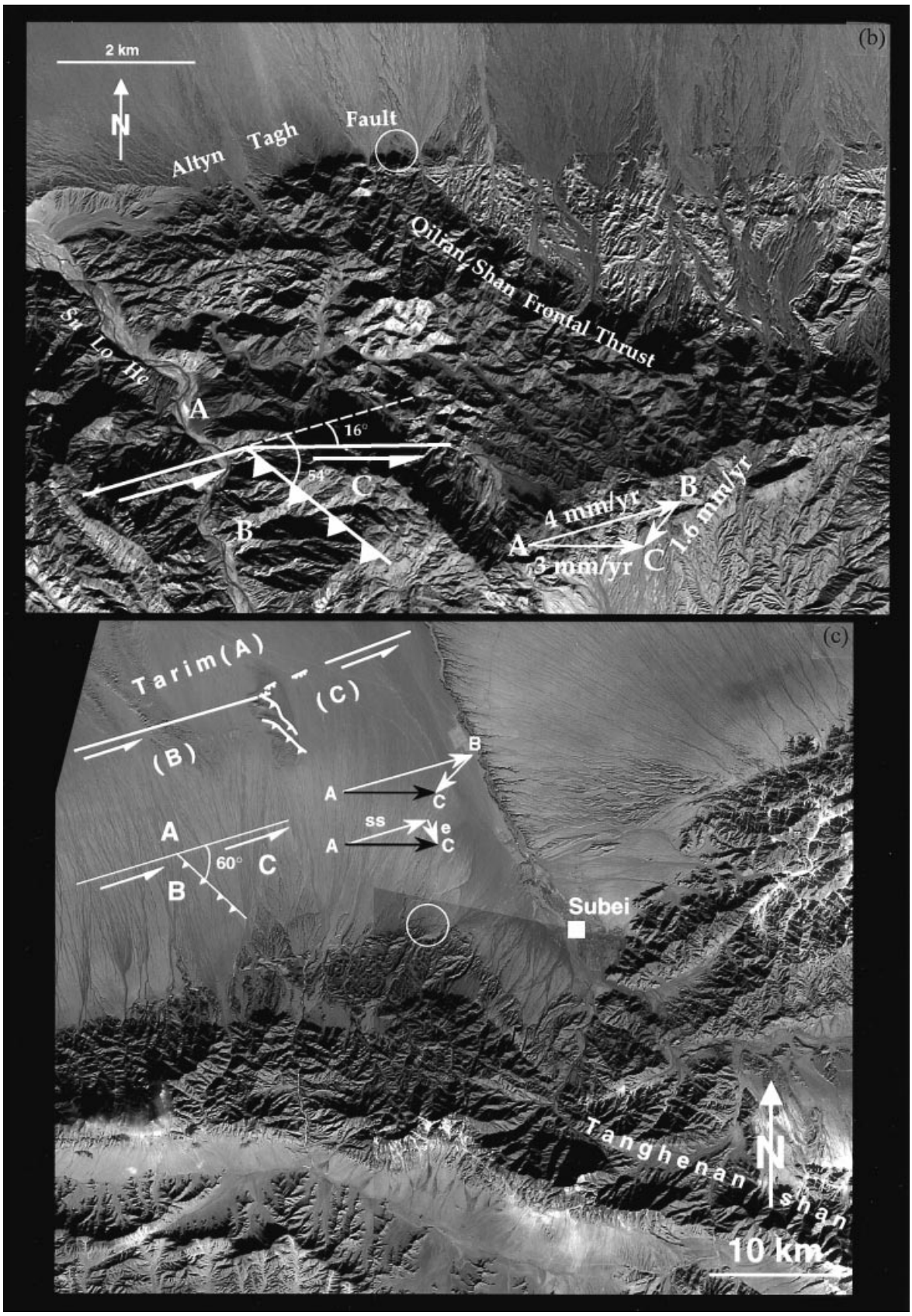

Figure 12(b). Kinematics of Sule He triple junction (white circle), between the Altyn Tagh fault and Qilian Shan front thrust. A, B and C stand for Tarim, Qilian and Hexi blocks, respectively. Left-slip rate between B and A is from Meyer *et al.* (1996). (**c**). Kinematics of the Subei triple junction (white circle), between the Altyn Tagh fault and Tanghenan Shan front thrust. A, B and C stand for Tarim, Tanghenan and Subei blocks, respectively; e and ss are extensional and strike components of the slip-vector (AC) on the segment of Altyn Tagh fault NE of junction.

qualitative agreement with triple-junction kinematics (Fig. 10). The foremost of the Tanghenan Shan thrusts, in turn, meets with the Altyn Tagh fault about 15 km west of Subei (Ge *et al.* 1992). A transtensive component of slip, giving rise to normal fault scarps (Fig. 10), is visible along the strand of the fault east of that well-defined junction, as rigid kinematics would predict if slip on the thrust were not parallel to the fault (Fig. 12c).

Faults other than thrusts also branch from the Altyn Tagh fault. Instead of following the range fronts or cutting the foreland bajadas, the traces of these active faults remain within the uplifted relief, roughly parallel to the ranges, often close to their crest lines. Most appear to be dominantly left-lateral. The easternmost segment of the Changma fault zone (Peltzer *et al.* 1988; Meyer 1991), which continues at least $\approx$100 km east of Ta Quen Kou, offsetting the Beida He by $\approx$15 km (Fig. 10), and the Tanghenan Shan 'axial' fault, which stretch along the entire length of the range, are particularly prominent examples, but discontinuous left-lateral faulting is also clear along the Yemah, Taxueh and Tulainan Shan (Fig. 10a,b). That those left-lateral faults tend to parallel the range-front thrusts is simply accounted for by slip partitioning in the middle-upper crust (e.g. Gaudemer *et al.* 1995). The ranges are therefore akin to 'flower structures' (Fig. 10c, sections c,d). Hence, current deformation in the West-Qilian ranges is 3-D, with motion of crustal slivers relative to the Gobi directed to the east of N30°E.

In summary, recent faulting southeast of the northern Altyn Tagh fault forms a transpressive 'horsetail' of grand scale. The fault geometry and the evidence for slip partitioning require that a large fraction, but not all, of the sinistral displacement on that fault be absorbed by crustal thickening across the Qaidam and Qilian ranges (Figs 1, 10, and 12a), (Peltzer *et al.* 1989; Meyer 1991). Most of the active faults within this horsetail meet with, or branch from, one another. In only very few places is the accurate position of fault junctions difficult to pinpoint. Where triple junctions are clear, a quantitative understanding of the local surface kinematics and of slip transfer between faults is gained by assuming rigid block motion.

The width of the main branching or transition zone, across which the Qilian thrusts swing counterclockwise from their NW–SE trends as they approach the Altyn Tagh fault (Figs 10a and b; dark shade, bottom left inset, Fig. 12a) is 30–60 km, of the order of the thickness of the crust (40–60 km). We interpret this swing to reflect oblique motion, within the crust, on lateral ramps connecting the thrusts to the fault.

South of this thrust/strike-slip transition zone, on a greater scale, the angle between the ranges and the Altyn Tagh fault increases progressively as such ranges approach that zone northwestwards (Figs 1, 10, and 12a). From a value of $\approx$20° or less about 300 km away from the fault, this angle reaches $\approx$40° or more about 50 km from it, reflecting a swing opposite to that in the transition zone. The exact length scale of this swing is difficult to assess because thrust trends also vary along the fault from region to region, probably due to differences in structural heritage. Besides, as one moves farther southeast from the Altyn Tagh fault, the influence of other large left-lateral faults, such as the Kunlun and Haiyuan, becomes felt, and the dips of certain thrusts flip towards the northeast (Sulenan Shan, Qaidam Shan, Qinghainan Shan) (Fig. 1). Nevertheless, the width of the zone (light shade, bottom left inset, Fig. 12a) in which the clockwise swing of the Qilian ranges and thrusts as they near the Altyn Tagh fault is most clear is $\approx$200 km, of the order of the thickness of the lithosphere (150–180 km).

There is no unique way to interpret this latter swing. Gradients of shortening, leading to differential block rotation, which the existing palaeomagnetic database is still insufficient to prove or disprove (e.g. Frost *et al.* 1995; Halim *et al.* 1998), might be involved. Regional shear gradients parallel to, and north of, the Kunlun and Haiyuan faults might also play a role. Another plausible way to interpret the clockwise swing at this scale, as well as the particularly high angle between thrusts north and south of the Altyn Tagh fault, is to invoke reorientation, relative to the regional stress induced by plate motion, of the maximum horizontal stress near the tip of a propagating, lithospheric, sinistral fault (Fig. 12a, bottom right inset). In this case, the present geometry of the thrusts would be inherited from that due to elastic deformation at the time of their birth. Although both the finite thrust displacements and the regional deformation are much larger than the incipient strain resulting from elastic stresses, the long-term deformation may be viewed as the sum of the anelastic relaxations of repeated stress increments (King *et al.* 1988). This approach, which is successful at modelling finite relief growth by motion on dip-slip faults (Stein *et al.*1988; Armijo *et al.* 1996), is also valid for 3-D strain involving strike-slip faults. At the outcrop scale, reorientation of anelastic, compressional and extensional deformation features has been shown to result from stress concentrations at the tip of small strike-slip faults (e.g. Rispoli 1981).

Probably the most inescapable consequence of superficial fault connections within the Qaidam–Qilian horsetail is that the active faults form a 3-D system with intimate physical and kinematic links at depth. Since most of the faults tend to segment, divide and branch when their lengths exceed a few tens of kilometres, most of the 'organic' connections within the system ought to occur in the crust.

3.2 Deep crustal deformation

3.2.1 Ranges as large crustal ramp anticlines

Whatever the scale, the Late-Cenozoic growth of relief, in section, appears to have occurred by similar mechanisms. Irrespective of basement history, such growth seems to have been simply governed by fault-propagation or fault-bend folding, as observed in the sediments of the Taxueh and Tanghenan Shan forelands. Several examples of increasing size document the uniformity of such processes (Fig. 13).

North of the west Qilian range front, the Yumen anticline culminates at 2758 m, locally $\approx$600 m higher than the Hexi corridor. It forms a topographic ridge $\approx$40 km long, with an average width of $\approx$7 km (Fig. 10, Table 3), and folds a thick Neogene and Quaternary sequence. West of Yumen, the anticline is little eroded and Quaternary conglomerates outline its regular periclinal termination with steeper NE limb. To the east, erosion has exhumed the core of the anticline, exposing the Laojunmiao thrust which brings Permocarboniferous upon Neogene rocks (Fig. 10b) (Gansu Geological Bureau 1975). The thrust locally dips 40–60°S, and the $\approx$50°S-dipping Carboniferous strata that underlie unconformable, but still S-dipping, Mesozoic and Tertiary sandstones appear to have

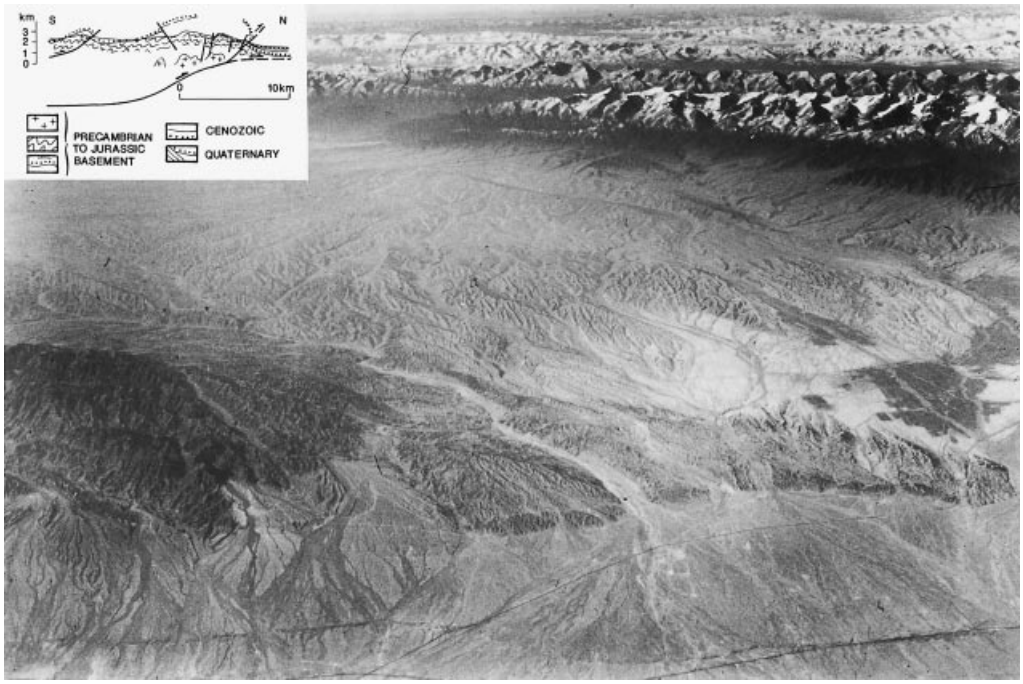

Figure 13(a). Oblique south-looking, aerial view of periclinal end of Yumu Shan mountain ridge, with snow-covered NE Tibetan ranges in background. A prominent Quaternary thrust, last activated by the 180 AD earthquake, bounds the Yumu Shan front. Inset is Yumu Shan section, with thrust ramping from deep décollement causing recent uplift. After Tapponnier *et al.* (1990a) and Meyer (1991).

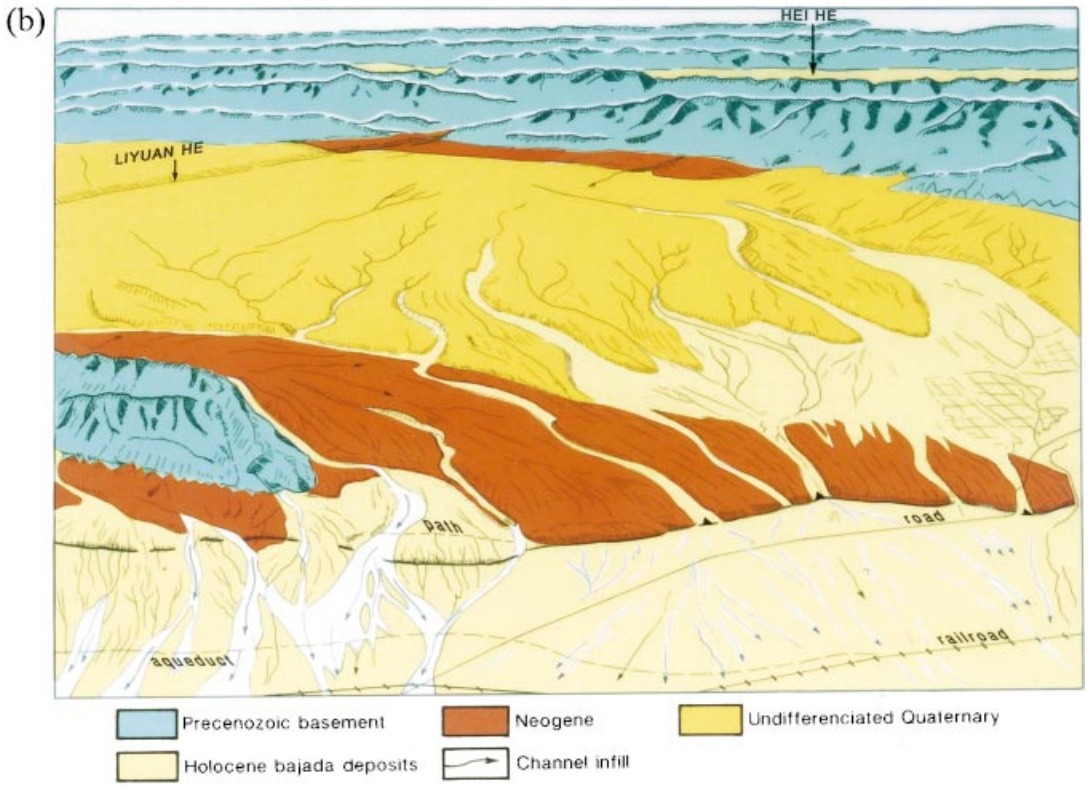

Figure 13(b). Sketch of photograph in Fig. 13(a).

simply ramped several kilometres upwards, parallel to the thrust, to overlie steep or overturned, schistose Miocene red-beds (Xu *et al.* 1989) (Fig. 10c, section e). The Yumen anticline is thus a typical fault-propagation fold, comparable in scale and style to those seen north of the Tien Shan (Avouac *et al.* 1993). It is ≈ 3.3 times the size of the north-hills anticline in the western Taxueh Shan piedmont (TXS NW, Table 3, Fig. 14).

Figure 13(c). East-looking view of south-dipping, Neogene red-beds immediately south of Tachi Shan crest.

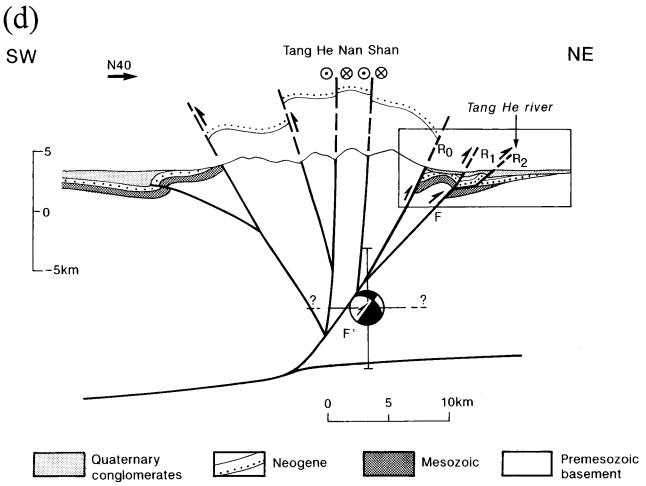

Figure 13(d). Schematic section of Tanghenan Shan mountain range at crustal scale. Depth and fault-plane solutions of the 1980 June 1 ($M_o = 1.5 \times 10^{17}$ N m) earthquake, which may have ruptured deep thrust ramp (F′) causing large-scale uplift of the range, are from Molnar & Lyon-Caen (1989). The box shows the location of Fig. 7(b).

Midway along the Gansu-Hexi corridor (Fig. 1), the Yumu Shan range is $\approx$60 km long and $\approx$9 km wide (Tapponnier *et al.* 1990a; Meyer 1991) (Table 3, Fig. 14). It rises to more than 3200 m, locally 1700 m above the Hei He plain. Although the Yumu Shan core is composed of Precambrian to Jurassic rocks with polyphase deformation, such rocks are wrapped by smoothly folded Plio-Quaternary beds (Figs 13a and b), (Gansu Geological Bureau 1975). The steep northern front of the range is marked by a south-dipping thrust fault (Fig. 13a), whose western segment last slipped during the 180 AD Luo Tuo Chen earthquake (Tapponnier *et al.* 1990a) ($M \approx 7.5$; Institute of Geophysics 1976; Gu *et al.* 1989; Fig. 1). The regular, asymmetric shape of the Plio-Quaternary envelope of the range, bounded on the north side by an active thrust ramp (Figs 13a and b), indicates that it too grew as a simple fault-propagation anticline, despite the more complex structure of basement rocks in its core (Tapponnier *et al.* 1990a; Meyer 1991). Although the Yumu Shan is 10 times the size of the north-hills anticline in the eastern Taxueh Shan piedmont (TXS NE), and large enough to qualify as a mountain range, both have the same length-to-width ratio ($\approx$6.7) (Table 3, Fig. 14).

Many, if not all, of the even larger ranges of northeastern Tibet appear to have grown as simply. Due south of the Yumu Shan, the eastern termination of the Qilian front range (Figs 13a and b) is outlined by Neogene beds wrapping the Palaeozoic core of the mountain. South of Xining, remnants of a 40°S-dipping monocline of Neogene red-beds and conglomerates, unconformable on Palaeozoic slates, are found at $\approx$4000 m a.s.l. just south of the crest of Tachi Shan (Figs 1 and 13c). The overall morphology and geology of the Tanghenan Shan (Figs 1 and 10a,b) also suggest that this great range, which is $\approx$235 km long, $\approx$30 km wide, and up to $\approx$5700 m high, has grown as a large anticline on top of S-dipping thrust ramps (Figs 10c, sections c, d, and 13d). The northern slope of the range, bounded by the most active thrusts (Figs 7 and 9), is generally steeper than its southern slope. On the southern side of the range, Neogene and/or Quaternary deposits, resting unconformably on Palaeozoic and Precambrian basement, generally dip gently south (Gansu Geological Bureau 1975). Despite strike-slip faulting along the range crest and some south-directed thrusting in the southeast, such a structure is chiefly consistent with north-vergent fault-propagation folding, after deposition of the Neogene sandstones and mudstones. This mountain-size anticline, which is $\approx$16.5 times larger than the western segment of the Taxueh Shan north hills, probably folds the crust down to a depth of $\approx$20 km, given its width and the dips (45–60°) of the thrust ramps R0 and F′ (Figs 7b and 13d). Such a picture is corroborated by the hypocentre depth (12 ± 4 km) of one earthquake (1980 June 1; 38.91°N, 95.60°E; Mo = 1.5 10^{17} N m), and by the strike and dip of its most likely fault plane (N128 $\pm$ 10°E, 53 + 7/−5° SW) as constrained by body-wave modelling (Molnar & Lyon-Caen 1989), which imply slip on F′ at mid-crustal depth (Fig. 13c). Despite the great difference in size, the length-to-width ratio of the Tanghenan Shan ($\approx$7.8) is only slightly greater than that of the western north-hills anticline ($\approx$7.4), (Table 3 and Fig. 14).

The available morphological, topographical, geological and seismological evidence thus suggests that the NW–SE-trending ripples, ridges and mountain ranges of northeastern Tibet (Fig. 1) correspond to growing ramp anticlines, folding rock layers of various thicknesses, up to that of the crust (e.g. Tapponnier *et al.* 1990a; Meyer 1991). Even at the largest scale, the asymmetry of the topography appears to be dictated by ramp dip. Such asymmetry is less prominent for mountains above hidden ramps. Mountains sharply bounded by emergent, fast-slipping, active thrusts are akin to crust-scale fault-propagation folds (e.g. Tanghenan Shan, central Qilian Shan, Yumu Shan), while others that, in spite of youthful relief, are less clearly bounded by contemporaneous thrusts (e.g. Tachi Shan, Yema Shan), or for which emergent thrust ramps have migrated kilometres away in the forelands (e.g. Taxueh Shan, Qinghainan Shan) are shaped more like crust-scale fault-bend folds.

3.2.2 Scaling law for mountain growth

The length versus width plot of Fig. 14 shows that, over a scale span of at least 40, the youthful topographic ridges that result from ongoing crustal shortening in NE Tibet, be they

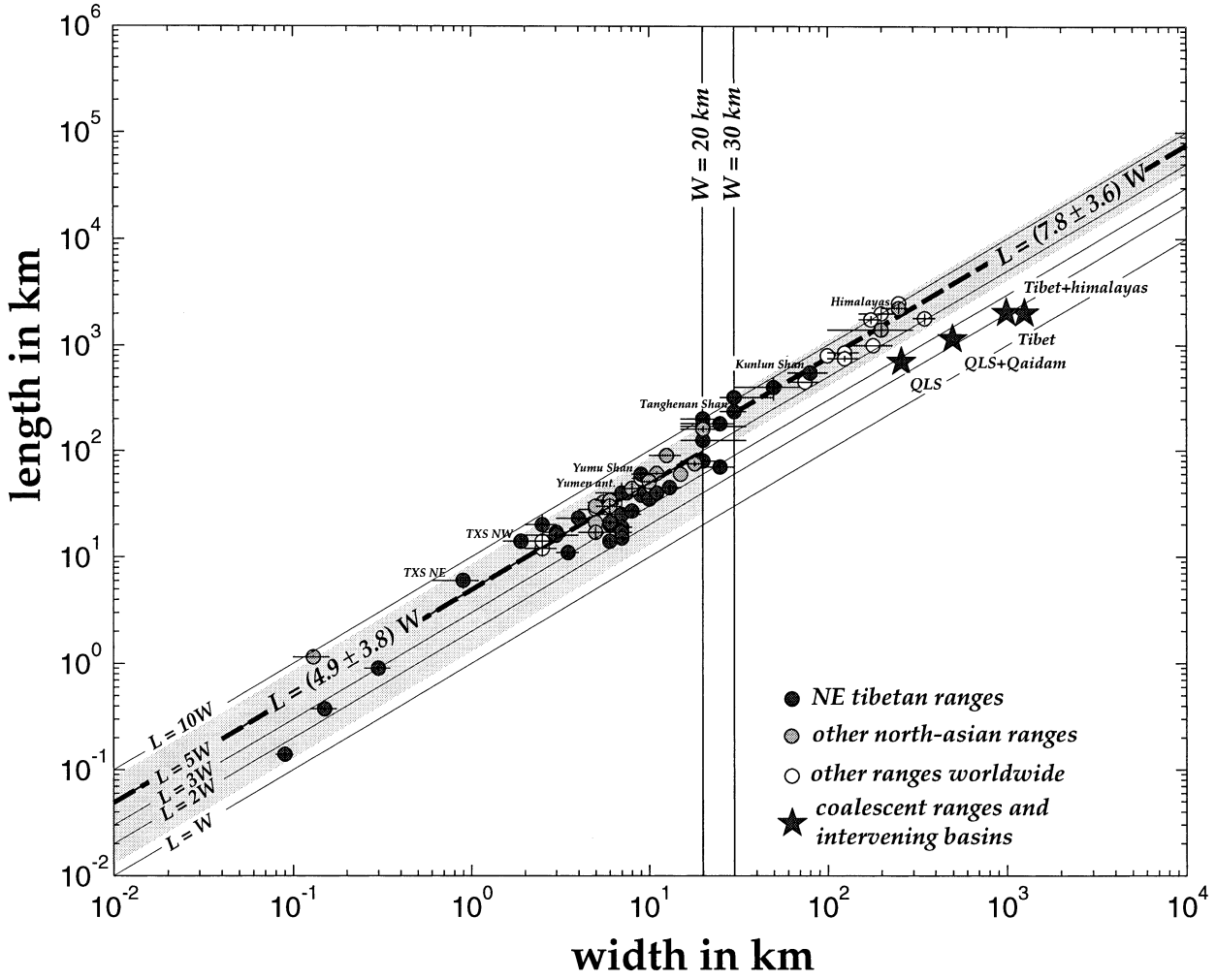

Figure 14. Scaling law for the growth of topography in young folds, ridges and ranges (from data set in Table 2). The bulk of data are from NE Tibet (filled circles and stars) and central Asia (shaded circles and stars). Data from rest of the world are represented by open circles.

smooth folds as in the Qaidam or jagged ranges north and south of it, keep a fairly scale-independent aspect ratio and thus appear to be approximately self-similar. Their sizes increase regularly from small piedmont 'whalebacks', such as the hills north of Taxueh Shan, with typical lengths of ≈ 10 km, widths of ≈ 2 km, and heights of ≈ 20 m, to great mountains (Kunlun or Burhan Budai range and main Qilian range) with lengths of 400–550 km, widths of 50–80 km and topographic relief of ≈ 3 km (Fig. 14 and Table 3).

Such length/width self-similarity seems to hold for other growing folds and ranges in the rest of eastern Asia and in the world, including very large collision ranges, and down to small strike-slip push-ups, over nearly four orders of magnitude in scale (Table 3 and Fig. 14). Fold and mountain heights do not scale with length or width as simply. Fold amplitudes or structural relief, and hence thrust displacement, might, but testing this inference would require better knowledge of sediment foreland thicknesses and amounts of denudation by erosion than available. Nevertheless, the width of the folds, ridges and ranges alike is most simply interpreted to reflect the depth reached by high-angle ramps underneath, be they shallow, seismogenic faults or deeper, localized ductile shear zones. Thrust faults would thus nucleate as fairly small, high-angle 'planes', then grow and coalesce (Jackson *et al.* 1996), as other faults do (e.g. Scholz *et al.* 1993; Cowie & Scholz 1992a,b,c), keeping a fairly constant length-to-depth ratio, from hundreds of metres to hundreds, and even thousands of kilometres, as cumulative throw increases on them.

At a more detailed level, there appears to be a change in scaling ratio for features with widths greater than 30 km. For a given width, folds and ridges narrower than ≈ 20 km tend to be shorter ($L/W = 4.9 \pm 3.8$), while ranges wider than ≈ 30 km tend to be longer ($L/W = 7.8 \pm 3.6$) (Fig. 14 and Table 3). We interpret this to reflect a cut-off within the mid-lower crust whose rheological layering acts as a mechanical barrier for further propagation of 40–60°-dipping thrust ramps downwards into the mantle, thus forcing trans-crustal thrusts and large ranges to grow faster along- than across-strike.

Recall that the data set we use is incomplete and the approach limited by tectonic boundary conditions. Large collision ranges, for instance, often end at pre-existing geological limits, such as continent–ocean boundaries, or at transform faults. Such truncation would tend to shorten their lengths. At the other end of the spectrum, the smallest-scale examples included are push-ups along strike-slip faults, hence biased either towards greater length because of slip-partitioning, or towards greater widths due to broad steps between strike-slip fault segments. This is apparent in the dispersion of values

Table 3. Aspect ratios, in map view, of topography of growing folds, ridges, and ranges due to recent shortening of continental crust in NE Tibet, Central Asia and other regions. Data from NE Tibet, Asia, Italy and Algeria are derived from topographic maps at scales of 1/100 000 and 1/1000 000 (ONC charts), combined with analysis of SPOT and Landsat images. Many features with widths <20 km were studied in the field. Data from California are from 1/62 500 topographic maps (Stein *et al.* 1992). Data for other large mountain ranges are from 1/1000 000 ONC charts and the Times Atlas of the World. The scaling law for growth of mountain belts derived from the data set is plotted in Fig. 14.

	Length (km)			Width (km)			Ratio L/W	References
	Average	Minimum	Maximum	Average	Minimum	Maximum		
Altynshan push up	0.14	0.12	0.16	0.09	0.08	0.10	1.6	0
Xorköl push up	0.375	0.35	0.40	0.15	0.125	0.175	2.5	0
West Xidatan push up	0.9	0.85	0.95	0.15	0.125	0.175	30	0
TXS northeast	6	5	7	0.9	0.6	1.1	6.7	0
TXS northwest	14	12	16	1.9	1.5	2.1	7.4	0
TXS southwest	17	15	20	3	2.5	3.5	5.7	0
THNS piedmont	20	18	25	2.5	2	3	80	0
Changma thrust (ChT) segment	25	22.5	29	7	5	9	3.6	0
Heiliangzi 1	19	17	21	70	60	80	2.7	0
Heiliangzi 2	17	15	19	70	60	80	2.4	0
Dafeng Shan	38	36	40	90	80	10	4.2	0
Wudijiang Liang	20	18	22	60	50	70	3.3	0
South Lenghu	45	42	48	13	11	15	3.5	0
Ebuoliang	35	33	37	10	90	11	3.5	0
Xiaoliang Shan 1	21	20	22	60	50	70	3.5	0
Xiaoliang Shan 2	27	26	28	80	70	90	3.4	0
Youdunzi 1	40	37	43	11	10	12	3.6	0
Youdunzi 2	23	22	24	40	30	50	5.75	0
Youdunzi 3	16	15	17	30	20	40	5.3	0
Youdunzi 4	11	10	12	3.5	30	40	3.1	0
Mang Ya	40	38	42	7.5	70	80	5.3	0
Shatuliang 1	15	14	16	70	6.5	7.5	2.1	0
Shatuliang 2	14	13	15	60	5.5	6.5	2.3	0
Yumen anticline	40	30	50	7	5	10	5.7	0
Yumu Shan	60	50	70	9	8	11	6.7	0
Sulenan Shan	95	80	115	25	20	30	2.8	0
Taxueh Shan (TXS)	80	70	100	20	15	25	40	0
Lungshou Shan	125	100	150	20	15	35	6.25	0
Tolainan Shan	170	150	190	20	15	35	8.5	0
Qiman Shan	180	180	180	25	15	30	7.2	0
Qinghai Shan	200	200	200	20	15	25	10	0
Tanghenam Shan (THNS)	235	220	250	30	25	35	7.8	0
Nan Qiman Shan	320	320	320	30	25	50	10.7	0
Qilian Shan	400	300	500	50	30	70	80	0
Kunlun Shan	550	500	600	80	60	100	6.9	0
Karakax push up	1.15	1.1	1.2	0.13	0.1	0.16	8.8	0
Kashifold1	30	30	30	6	5	7	50	1
Kashifold2	32.5	30	35	5.5	4.5	6.5	5.9	1
WuWei	90	90	90	12.5	10	15	7.2	1
Aksu 1	30	30	30	5	5	5	60	1
Aksu 2	21	21	21	5	5	5	4.2	1
Aksu 3	21	21	21	5	5	5	4.2	1
Tien Shan A1	61	59	63	11	9	13	5.5	1
Tien Shan A2	44	38	50	8	7	9	5.5	1
Tien Shan A3	51	50	52	10	9	11	5.1	1
Tien Shan A5	34	32	36	6	5	7	5.7	1
Tien Shan A6	17	15	19	5	4	6	3.4	1
Tien Shan A7	17	15	19	5	4	6	3.4	1
Tien Shan A9	30	25	35	6	5	7	50	1
Yecheng	160	150	170	20	15	25	80	0
Muztagh	60	60	60	15	15	15	40	0
Kongur	75	70	80	18	16	20	4.2	0
Tien Shan	1400	1200	1600	200	100	300	70	0
Himalayas	2250	2000	2500	250	200	300	90	0

Table 3. (*Continued*).

	Length (km)			Width (km)			Ratio L/W	References
	Average	Minimum	Maximum	Average	Minimum	Maximum		
Sara el Marouf	12	10	14	2.5	2	3	4.8	2
Lost hills	14	12	16	2.5	2	3	5.6	0
Montello	28	26	30	5	4	6	5.6	0
Kettleman Hill fold	55	50	60	9	8	10	6.1	3
Pyrénées	450	450	450	75	60	90	60	0
Appenines	800	800	800	100	100	100	80	0
Alps	1000	1000	1000	180	130	230	5.5	0
Atlas	2000	1800	2200	200	150	250	10	0
Caucasus	850	800	900	125	100	150	6.8	0
Zagros	1800	1600	2000	350	300	400	5.1	0
Sumatra (Barisan)	2500	2500	2500	250	250	250	10	0
New Zealand (Alps)	750	700	800	125	100	150	60	0
New Guinea	1750	1600	1900	175	150	200	10	0
whole Qilianshan (QLS)	700	600	800	260	240	280	2.7	0
NE edge of Tibet = QLS + Kunlun	1150	1000	1300	500	400	600	2.3	0
whole Tibet	2100	1800	2400	1000	900	1100	2.1	0
Tibet + Himalayas	2100	1800	2400	1250	1150	1350	1.7	0

below $W \approx 1$ km. Finally, our overall sampling is also biased, with a majority of features having lengths between 10 and 100 km and widths between 2 and 30 km (Table 3). Despite such imperfect sampling, however, and the preliminary nature of the plot in Fig. 14, folds in the continental crust appear to grow self-similarly as a result of increasing anelastic slip on thrusts from the start. They do not seem to result from finite-amplitude buckling, followed by breaking of layers of specific thicknesses (Martinod & Davy 1994; Burg *et al.* 1995).

3.2.3 *Crust/mantle decoupling on large regional décollement*

Taken together, the characteristics of ongoing deformation in the Qilian mountains and Qaidam imply that the crust is now decoupled from the underlying mantle over much of the region. The coeval kinematics, as well as the typical patterns and scale of surface segmentation and branching of the faults indicate that most of them form a 3-D, interconnected system restricted to a layer at most a few tens of kilometres thick, i.e. to the thickening crust (Fig. 15a). The limited widths of the topographic bulges of most ranges (up to ≈ 30 km), and the minimum cumulative throws (≈ 10 km) on the main thrust ramps beneath them, imply that such steep ramps flatten in the lower crust onto shallow-dipping décollements, making the process that folds 10–30 km thick slices of the crust in anticlines of mountain size analogous to that operating in thinner foreland sedimentary layers (e.g. Avouac *et al.* 1993). The cut-off in the L/W scaling law for range widths > 30 km further supports the inference that crustal thrust ramps do not extend straightforwardly into the mantle. The dominant northeastward vergence of thrusts from the Kunlun fault to the Gobi platform is consistent both with uniformly directed motion of the mantle relative to the crust, towards the southwest, and with the inference that, save perhaps along the Early Palaeozoic sutures, there is little shortening—if any—in the mantle, as expected in view of its Precambrian age, and hence great strength.

The organization and kinematics of faulting, the disposition of topographic ridges, and the gradual northeastward decrease in elevation across the northeast corner of Tibet are thus best interpreted to imply that its crust forms a large accretionary wedge. This deformed crust would be decoupled from the more rigid mantle lithosphere underneath over a vast (up to 500 km $\times$ 1000 km), mid- to lower-crustal décollement plunging on average at a shallow angle (≈ 5–10°) to the southwest (Figs 10c and 15b) (Bally *et al.* 1986; Tapponnier *et al.* 1990a; Meyer 1991).

The old age of the crust (≥ 400 Myr), and the recent onset of Cenozoic shortening (≤ 15 Myr) (Métivier 1996), makes the existence of a thick (≈ 20–30 km) weak layer at its base unlikely. A thick, weak lower crust would result in more undecided vergence for shallow thrusts. Upper-crustal thrust ramps thus probably do not vanish downwards into a ductile lower-crustal buffer. In any case, at any given time within the rheologically weak zone above the Moho, whose thickness in Precambrian–Lower Palaeozoic crust should not exceed 10–15 km (e.g. Molnar & Tapponnier 1981), strain is expected to localize further. Hence, it seems preferable to picture the deep, NE Tibetan décollement as a ductile shear zone several kilometres thick, resembling the Himalayan Main Central Thrust.

Scale notwithstanding, this process is similar to that generally observed in sedimentary fold and thrust belts. The whole NE corner of Tibet in fact seems to be little more than a leading imbricate thrust fan, involving the entire crust (Boyer & Elliott 1982) (Fig. 10c), laterally limited by strike-slip ramps, as commonly illustrated in sandbox experiments (e.g. Calassou *et al.* 1993) (Figs 10a and 15). If this interpretation, in our view the simplest compatible with extant geological evidence, survives testing by seismic imaging, NE Tibet would represent the thickest-skinned current example of fold and thrust tectonics in the world.

Only under the widest (≈ 80 km) mountain ranges (Kunlun, Altyn Tagh) are discrete, fairly steep, mantle thrusts likely to continue crustal thrusts downwards and offset the Moho. We thus infer the lithosphere to be cut under these two ranges, in close connection with strike-slip faulting (Figs 15a and b)

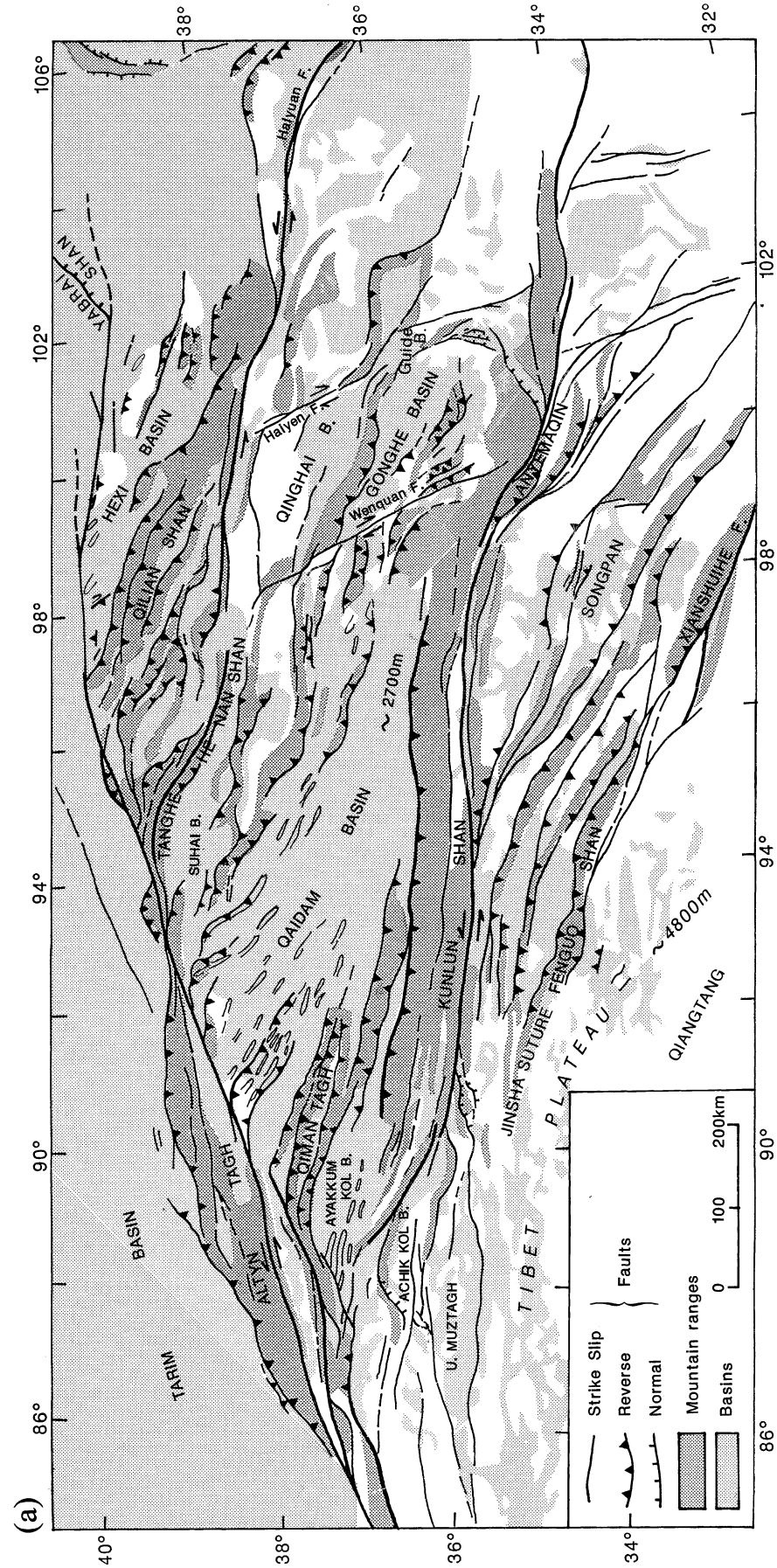

Figure 15(a). Morpho-tectonic sketch map of Cenozoic relief, faults and basins in the northeastern third of Tibet. High topography and basin flats are controlled by faulting. Faults with lengths < 100–200 km appear to be restricted to crust, while faults whose lengths reach 1000 km probably cut through lithosphere.

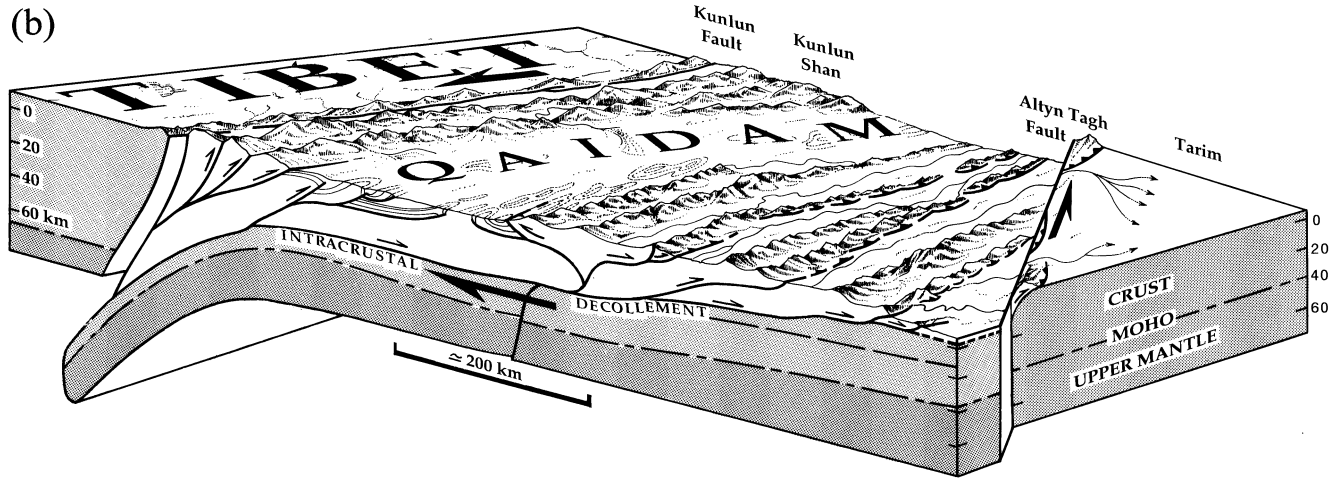

Figure 15(b). 3-D block diagram sketching inferred crustal deformation of the northeastern edge of the Tibet–Qinghai highlands. The long edge of block is orientated ≈N30°E. Although deformation is idealized, the front and back corners of the block may be taken to lie roughly at 91°E, 35°N, and 98°E, 40°N, respectively. Topographic relief is exaggerated. Dark shade is for upper mantle, light shade, for autochthonous crust. The bottom of the diagram does not coincide with the base of the lithosphere. Parallel mountain ranges separated by NW–SE basins formed as crustal anticlines on northeastwards-migrating thrust ramps splaying from large, shallow south-dipping décollement rooting into the mantle subduction zone south of Kunlun range (after Tapponnier *et al.* 1990a). Altyn Tagh and Kunlun sinistral faults are lithospheric, with slip-partitioning in the crust.

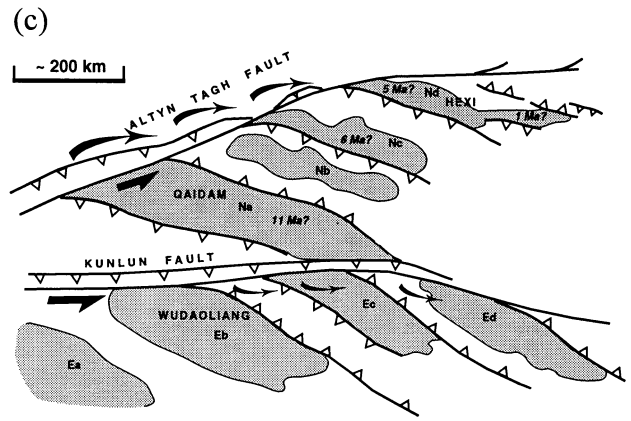

Figure 15(c). Schematic sketch of the strike-slip-controlled growth of northern Tibet. Most Cenozoic thrusts branch southeastwards from the Altyn Tagh and Kunlun faults. Thrusts parallel to strike-slip faults north of the Altyn and Kunlun ranges reflect crust-scale slip-partitioning. Basins south, and north of Kunlun are filled with mostly Palaeogene (Ea–d), and Neogene-Quaternary (Na–d) clastics, respectively. Sedimentation onset in basins south of the Altyn Tagh fault youngs towards the northeast, implying the propagation of fault and associated relief in that direction. Similar propagation related to eastward younging may exist in basins south of the Kunlun fault.

(Matte *et al.* 1996). In order to discuss the ultimate fate of the lithospheric mantle, it is paramount to estimate the amount of crustal shortening north of the Kunlun fault.

4 AMOUNT OF LATE-CENOZOIC CRUSTAL SHORTENING

4.1 Direct estimate, from reconstruction of the Qaidam–Hexi section

The evidence we have at hand permits only a rough assessment of strain between the Gobi platform and the Kunlun range, but a plausible lower bound of the amount of Tertiary shortening absorbed by crustal thickening may be estimated. The NE-stepping sections of Fig. 10(c) are all orientated N30°E, roughly perpendicular to the main ranges and folds, and parallel to the direction of slip on the thrusts where accurately measured (Fig. 11, Table 2). All are constructed by integrating 3-D information from topographic and geological maps at different scales, seismic reflection and borehole log data available to us (e.g. Xu, He & Yan 1989), and our field measurements and satellite image analysis. Given the scale, most small thrusts and folds are not represented. The sections are thus grossly simplified to include only major features. They broadly resemble the sections derived by Bally *et al.* (1986) from seismic profiles of the Qaidam, but there are differences due to the different line locations chosen, to our more accurate mapping of surface features and to our assessment of Quaternary and active strain. Like those constructed at a smaller scale in the ranges' forelands (Figs 7, 11c, and 13d), the crust-scale sections are not uniquely constrained by the available data set. In particular, the depths of the junctions between the thrust ramps and the décollement depend on the ramp dips, most of which are poorly known. The extrapolation below ≈15 km is most uncertain in the central and southern parts of the Qaidam basin where the basement lies underneath more than 10 km of sediments. Nevertheless, the growing topography provides a control unavailable in inactive mountain belts.

We have attempted to retrodeform in a crude way three typical sections (b, d and f, Fig. 10c; Table 4a), for which enough field and subsurface data are available. Such restoration is possible because much of the Lower-Palaeozoic basement was rather uniformly blanketed by fairly flat Late-Mesozoic and Tertiary sediments prior to Late-Cenozoic reactivation (Fig. 8). In many areas north of the Kunlun, only slight angular unconformities of stratigraphic horizons are visible between the Devonian and the Miocene, an indication of moderate tectonic strain with mostly localized faulting and basin sag during that period, as elsewhere in central Asia (e.g.

Table 4(a). Amounts of late-Cenozoic shortening for sections C1 and C2 in Figs 1 and 17, assuming isostatic compensation or elastic thicknesses of 45 and 80 km, and initial crustal thickness of 47.5 ± 5 km, following Avouac *et al.* (1993). Lengths and orientations of sections are indicated, as well as cross-sectional areas of excess crust due to thickening, and of sediments locally derived from erosion of relief (see text).

	Elastic thickness (km)	Crustal area (km^2)	Sediment area (km^2)	Shortening km To = 47.5 km	Shortening To = 47.5 ± 5 km
C1	0*	39597	844	213	
620 km	45	38400	844	188.5	188.5 ± 98 km
N 35	80	38389	844	188	
C2	0*	32741	4	144	
545 km	45	32574	4	141	141 ± 84 km
N35	80	32447	4	138	

Bally *et al.* 1986; Hendrix *et al.* 1992; Avouac *et al.* 1993; Gaudemer *et al.* 1995). Folding of Permo-Triassic, Jurassic or Cretaceous beds is often coaxial with that of adjacent Neogene strata (e.g. south flank of Taxueh Shan, Fig. 10b), implying that both result from the same Cenozoic, N30°E shortening episode. Hence, well-defined horizons from the upper Palaeozoic onwards may be used as restorable reference surfaces.

For sections e and f, which extend from the Kuantai Shan to the Taxueh-Tolainan Shan across the Hexi-Jiuxi basin and the Qilian Shan front, roughly parallel to the Baiyang and Beida He valleys (Figs 10a and b), oil-company seismic reflection and well logs give depth control (Xu *et al.* 1986). On section f, structural relief alone implies at least 10 km of throw on just the outer Qilian Shan thrusts. Restoration of the top of the Cretaceous or of the base of the Miocene yields $\approx$20–25 km of shortening across those thrusts (Fig. 10c). Use of the same reference surfaces along the whole 150 km long section implies that a minimum of 50–70 km of shortening (Table 4b) is taken up by large, discrete thrusts between the Tolainan Shan and the Gobi-Ala Shan platform, with $\approx$50 per cent of that amount absorbed in the 50 km wide Qilian range.

Section d crosses all the ranges south of the Qilian Shan to the Suhai basin, particularly the Taxueh and Tanghenan Shan (Figs 10a and b). In this region, the base of the Mio-Pliocene provides the best reference horizon (Fig. 10c). Sediment depths are less well known in the intermontane forelands south of the Hexi corridor than in the Jiuxi basin. Also, there are complexities related to the flower structure of the two main ranges. Nevertheless, both line and areal restorations yield a minimum of 35–45 km of N30°E-directed shortening (Table 4b), with about 30 per cent of the total in each range. We infer that small-scale thrusts related to complex oblique motion absorb additional, distributed shortening within the 'flower' structures.

Section b first crosses the NW terminations of the three ranges (Tergun Daba, Qaidam, and Mahan-Xitie Shan) that separate the Suhai and Qaidam basins, then the entire Qaidam basin all the way to the Kunlun fault, across the SE extension of the Qiman Tagh and the main Kunlun or Burhan Budai Range (Figs 10a and b). The base of the Pliocene and the top of the Mesozoic provide reference surfaces in the north and south, respectively (Fig. 10c). Restoration implies a minimum of $\approx$90 km of shortening on the major thrusts (Table 4b), with over half of it in the Kunlun and Qiman ranges. The uncertainty is large, as is that of the section from which it derives, but the amount of folding in the southern Qaidam basin suggests that this number is a very conservative estimate.

Taking into account small overlaps between the three sections, the western part of the wedge of Tibet caught between the Kunlun and Altyn Tagh faults (Figs 1, 10, and 15a,b) thus appears to have shortened by at least $\approx$150 km during the Late Cenozoic (Table 4b). We think this is a robust lower bound, not very different from the even cruder estimate (130–140 km) obtained by just summing the average structural relief ($\approx$10 km) across the 13–14 main ranges and basement highs between the Hexi corridor and the Kunlun fault. Recall, however, that this number concerns only the amount of N30°E shortening absorbed by thickening of the crust, and that most sections cannot be retrodeformed in a strict sense because sinistral components of faulting parallel to the ranges shift crustal material out of the section planes. Locally, the amount of displacement due to sinistral faulting appears to be similar to that of thrusting towards the NNE. The 15 km offset of the Beida He by the Taquen Kou fault in the Qilian Shan (Fig. 10), which may have accrued in only $\approx$3 Myr at the present rate ($\approx$5 mm yr^{-1}, Peltzer *et al.* 1988), provides a good example of such roughly balanced partitioning.

4.2 Bulk estimate, from regional mass-balance including erosion

It is also possible to estimate the minimum convergence between the Kunlun and the Gobi in the Late Cenozoic by regionally balancing the mass of crust thickened, including that transported by erosion and redeposited in adjacent basins. For this, one may follow the approach that Métivier & Gaudemer (1997) applied to the Tien Shan and its forelands. The boundaries of the region of interest here enclose the whole area between the Kunlun fault and the Tarim, Gobi-Ala Shan and Ordos stable platforms (Fig. 16a). The surface of that region is $\approx 5.4 \times 10^5$ km^2. For topography, we rely on the hypsographic DEM of the Defense Mapping Agency (1992), which is known with a resolution of 30 arc-seconds ($\approx$900 m). For the volume of the solid phase of Tertiary sediments deposited in the Qaidam-Gonghe, Hexi-Jiuxi and other basins north of the eastern Altyn Tagh fault and of Kuantai and Lungshou Shan, we use the number ($0.44 \pm 0.18 \times 10^6$ km^3) derived from subsurface data by Métivier (1996). Assuming conservation of crustal mass (i.e. negligible loss of crust into the mantle, and negligible loss of sediments outside the region, Métivier 1996), we may then derive the volume of rocks (V_{top})

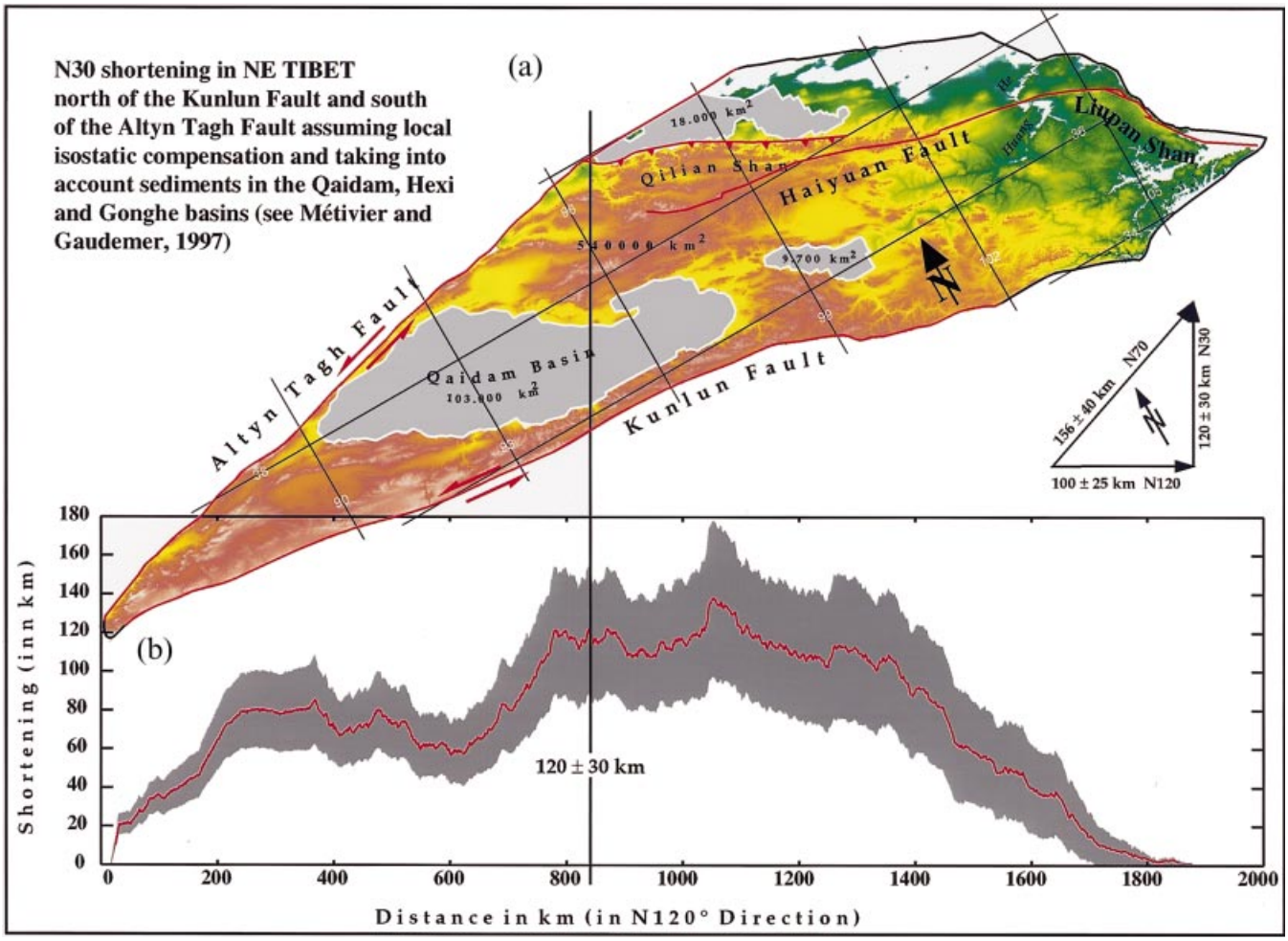

Figure 16(a). Digital elevation model of the area between the Kunlun fault, Altyn Tagh fault, Alashan and Liupan Shan (Defense Mapping Agency 1992). Areas shaded grey, with surface area indicated, are major Plio-Quaternary basins. Elevations are colour coded above 1500 m, with yellow, brown and white corresponding roughly to elevations above 3000, 4000 and 5000 m. (**b**). N30°E-directed shortening as a function of distance along N120°E strike. Local isostatic compensation is assumed, and sediment mass deposited in the Qaidam, Hexi and Gonghe basins (Métivier 1996) is taken into account. The zone shaded grey indicates uncertainty. The vector diagram (inset) depicts partitioning of motion between the Altyn Tagh and Qilian faults near 96°E, 39°N (see text for discussion).

that recent crustal thickening, outside Tertiary basins (grey shade, Fig. 16a), has heaved above the regional base-level—taken to stand at the elevation of the Gobi-Ala Shan platform, $\approx$1500 m a.s.l.:

$$V_{\mathrm{top}} = 1.06 \pm 0.16 \times 10^6 \ \mathrm{km}^3 . \qquad (1)$$

Assuming local isostatic compensation, crust and mantle densities of 2750 and 3300 kg m^{-3}, respectively, and taking the sedimentary mass into account, the excess volume of crustal rocks stored in the NE-Tibetan wedge as a result of shortening (V_{sh}) is thus

$$V_{\mathrm{sh}} = \frac{\rho_{\mathrm{m}}}{\rho_{\mathrm{m}} - \rho_{\mathrm{c}}} V_{\mathrm{top}} + V_{\mathrm{sed}} = 6.81 \pm 1.67 \times 10^6 \ \mathrm{km}^3 . \qquad (2)$$

Assuming that volume to result from shortening of a crust of initial thickness equal to that of the undeformed Gobi-Alashan platform ($H = 47.5 \pm 5$ km) (Ma 1987), the amount of surface-area reduction or shrinking (S_{sh}) in NE Tibet comes out to be

$$S_{\mathrm{sh}} = 1.43 \times 10^5 \ \mathrm{km}^2 .$$

This number represents $\approx$26 per cent of the present-day surface of the area selected in Fig. 16(a) (5.4×10^5 km^2), and $\approx$40 per cent of the surface ($\approx 3.5 \times 10^5$ km^2) now occupied by mountains above 2000 m a.s.l. within that area.

As a next step, one can estimate the variation of the amount of NNE shortening (*Sh*) as a function of distance (*d*) along a direction parallel to the NE-Tibetan ranges (N120°E). The excess crustal volume stored within vertical slices of width $w \approx 900$ m, orientated parallel to thrust slip, is computed from DEM elevation values along N30°E section-lines. Isostatic compensation is dealt with as above (2). To account for erosion and ensure mass conservation, sediment volumes accumulated in the basins are first sprinkled uniformly over drainage catchments (Métivier 1996). Although crude, this technique has little impact on the final results, since the sediment volume accounts for at most 7 per cent of the crustal volume stored in the ranges. The sum of the restored sediment and crustal rock volumes yields the surface shortened on each section. The curve relating shortening to distance along the N120°E direction (*Sh*(*d*), Fig. 16b) is then obtained by dividing that surface

by the initial crustal thickness chosen and section width:

$$Sh(d) = \frac{1}{Hw}\left(\frac{\rho_m}{\rho_m - \rho_c} V_{top}(d) + V_s(d)\right). \quad (3)$$

Given the uncertainties on V_{top}, V_{sed}, and H, and taking that on the compensation ratio $C = \rho_m/(\rho_m - \rho_c) = 6$ to be of the order of 0.5, the uncertainty on shortening (3) is

$$dSh = Sh\left[\frac{\left(\frac{dC}{C} + \frac{dV_{top}}{V_{top}}\right) CV_{top} + dV_{sed}}{V_{sh}} + \frac{dH}{H}\right], \quad (4)$$

typically of the order of ± 20 per cent (Fig. 16b).

With the fairly restrictive assumptions made, the shortening values in Fig. 16(b) should be considered very conservative lower bounds. Loss of sediments by transport outside the region may have been significant. The largest river, the Huang He, carries much of its load to NE China. Other large rivers such as the Sule and Tang He probably flowed west into Lop Nor during climatic intervals wetter than the present. The mass of thickened crust thus lost might reach several per cent. The presence of a large-scale décollement at the base of the middle-upper crust makes coupling between a 5–10 km thick slice of lower crust and the lithospheric mantle likely (Fig. 10c), which would increase shortening everywhere by as much as 10–20 per cent, respectively. Last but not least, the crust of the Qaidam, which at all times in the Neogene remained a deep depocentre, may have initially been thinner than that of the Gobi. Moreover, the mass balance calculations above do not take thickening of the Qaidam crust into account. Hence, overall, we suspect that such calculations underestimate shortening by a few tens of per cent on many sections.

Nevertheless, for most sections crossing the Qilian ranges, the amount of N30°E shortening derived from regional mass balance exceeds 100 km. In the westernmost 200 km, near the ranges' junctions with the Altyn Tagh fault, the lower bound obtained (120 ± 30 km, white line on Fig. 16; Table 4b) is on the low side of that (≈ 150 km) derived from retrodeformation of N30°E structural sections of the same area.

Simpler mass-balance calculations (Avouac *et al.* 1993) along two sections (C1 and C2, Fig. 1), for which local isostatic equilibrium of the topography, or flexural compensation with an elastic thickness of 45 km, is assumed, and for which densities of sediments, crust and upper mantle of 2.6, 2.8 and 3.3 g cm^{-3}, respectively, and an initial crustal thickness of 47.5 km are taken (Fig. 17), are consistent with extant estimates of Moho depths (Ma 1987; Wittlinger *et al.* 1996), and yield amounts of shortening of ≈ 190 and ≈ 140 km, corresponding to ≈ 30 and 26 per cent of the section lengths, respectively (Fig. 17a; Tables 4a and b). The uncertainty on such numbers, which depends critically on the initial thickness, is large, typically of the order of 30 per cent (Avouac *et al.* 1993), but, considering the slight difference in crustal density, both values are compatible with those found with the other two approaches.

4.3 Geodynamic consequences

Given the kinematic connections of thrusts beneath the Qilian ranges with the Altyn Tagh fault, and the rigidity of the Tarim, minimum amounts of shortening of 150, or 120 ± 30 km would imply at least 196, or 156 ± 40 km of Late-Cenozoic left-slip, respectively, on the N70°E-striking fault near 88°E (inset, Fig. 16b) (Table 4b). They also imply at least 126 km, or 100 ± 25 km of N120°E-directed displacement between the Kunlun range and the Gobi (Table 4b). That displacement, which corresponds to the fraction of slip on the Altyn Tagh fault not absorbed by crustal thickening, ought to have been taken up by sinistral slip partitioning within the ranges (inset, Fig. 16b). Note that such roughly balanced regional partitioning is in keeping with that found locally in the northwestern Qilian Shan, near the Beida He. Note also that, at the regional scale, significant clockwise rotation of ESE-trending crustal slivers due to slip on parallel sinistral faults is unlikely, because such rotation would be incompatible both with left-lateral boundary motions on the Altyn Tagh, Kunlun and Haiyuan faults, and with NNE shortening.

North of the Qaidam basin, most of the ESE motion of the Qilian crustal slivers ought to be transferred to the Haiyuan fault, which meets with the SE extremities of the Qilian ranges (Fig. 1) (Meyer 1991). The results obtained here are thus quantitatively compatible with the displacement, relative to the eastern Ala Shan platform, of the northeasternmost corner of Tibet near Lanzhou. Such displacement would have been of the order of ≈ 120 km east-southeastwards if its current rate (15 ± 6 mm yr^{-1} in the N105 $\pm$ 6°E azimuth) is extrapolated back to ≈ 8 Ma BP (Gaudemer *et al.* 1995), consistent with the $\approx 95 \pm 15$ km offset of the Yellow River course by the western Haiyuan fault zone (Figs 1 and 16a). The minimum displacement required to form the great bend of the river across the fault zone (40–80 km; Gaudemer *et al.* 1995) would be compatible with about half of the minimum amounts of partitioned slip found above, in keeping with the estimate derived from retrodeformation of section b (Fig. 10c) that at most half of the minimum shortening west of 97°E has been absorbed south of the Suhai basin. Neither the kinematic regime nor the minimum displacement values derived here accord with a maximum sinistral offset of ≈ 16 km on the Haiyuan fault since Precambrian time, as inferred from geological mapping in the loess-mantled country west of the Yellow River (Burchfiel *et al.* 1991).

Amounts of crustal shortening of 100–200 km above a décollement underlying much of the region shown in Fig. 16 require concurrent Late-Cenozoic shortening and foundering of the lithospheric mantle of that region south of the Kunlun range. Such strain would be most simply taken up by south-dipping mantle subduction, to depths of 200–300 km, along a deep thrust into which the décollement would root (Figs 10c, 15b and 16b) (Mattauer 1986a,b; Tapponnier *et al.* 1990a; Meyer 1991). Geological evidence points to two zones under which the mantle lithosphere of NE Tibet might plunge. One lies south of the Kunlun fault, beneath the Miocene to Quaternary plutonic–volcanic belt that stretches hundreds of kilometres west of Kusai Hu (≈ 93°E, Fig. 1) (Norin 1946; Deng 1989; Arnaud *et al.* 1992), past Ulugh Muztagh (Fig. 15a, Burchfiel *et al.* 1989a). The other is the Jinsha suture, the boundary between the Qiangtang continent and the Songpan terrane, a broad wedge of strongly folded Triassic flysch overlying attenuated basement (Sengör 1984; Mattauer *et al.* 1992; Wittlinger *et al.* 1996). Both zones actually converge near 94°E, to continue westwards parallel to one another, less than ≈ 100 km apart.

The tectonic setting of the Kunlun fault, a strike-slip fault that runs parallel to, and south of, the Kunlun range for more

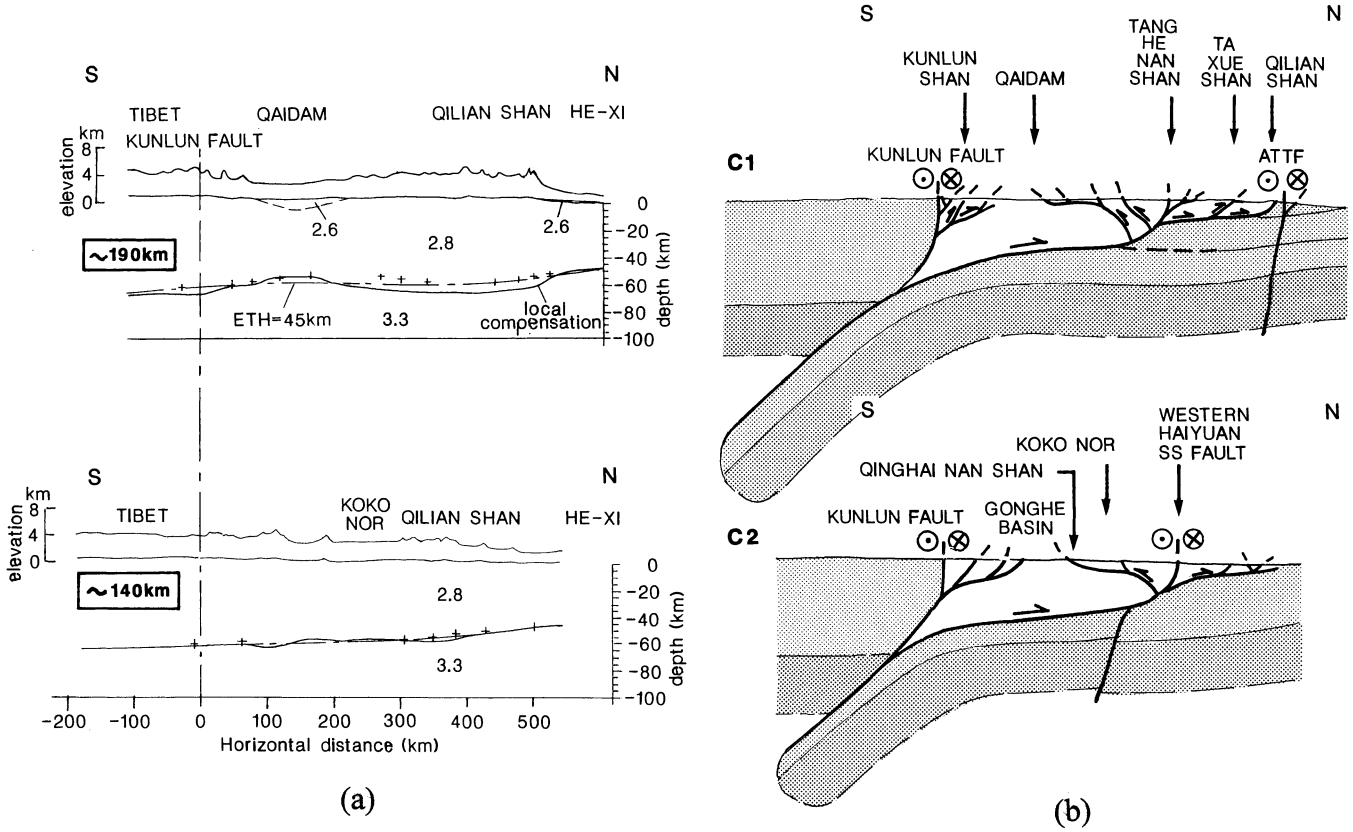

Figure 17(a). N35°-striking crustal sections between the Kunlun fault and He-Xi corridor (C1, C2, Fig. 1). Crosses are Moho depths inferred from geophysics (Ma 1987). Continuous and dashed lines are calculated Moho depths assuming local isostatic compensation and an elastic thickness of 45 km, respectively. Present-day crustal thickness is 47.5 km under the Gobi desert. Vertical exaggeration is 2. Topography drawn above sections is with a vertical exaggeration of 10. Numbers are densities (see text and Avouac *et al.* 1993). Bold numbers in boxes (see also Table 4) are minimum amounts of Late-Cenozoic shortening on each section. (**b**). Schematic sections of Cenozoic thrusting at lithospheric scale along C1 and C2. Bold lines represent major faults and kilometres-wide shear zones in the upper crust and lower crust and mantle, respectively. The geometry of faults is consistent with topography and Moho depths. Large décollement between undeformed mantle and lowermost crust, and shortened middle-upper crust is inferred to root into the subduction zone south of Kunlun. The bottom of sections does not coincide with the base of the lithosphere. Lithospheric mantle ought to plunge to depths at least equal to the bold numbers in Fig. 16(a).

Table 4(b). Summary of minimum amounts of late-Cenozoic shortening for sections in Figs 1, 10, 16 and 17, and cumulative offsets on the Altyn Tagh fault and N120°E-striking sinistral faults in Qilian Shan (see discussion in text).

N30°-directed shortening		
Section f	Figure 10(c)	>50–70 km
Section d	Figure 10(c)	>35–45 km
Section b	Figure 10(c)	>90 km
Composite b,d,f section	Figure 10(c)	>150 km
Bulk estimate from regional mass balance	Figure 16(b)	>120±30 km
Section C1	Figure 17(a)	>188.5±98 km
Section C2	Figure 17(a)	>141±84 km
Cumulative offset on the Altyn Tagh Fault at 88°E		
	Figure 16(b)	>156±40 km
	Figure 10(c)	>196 km
Cumulative sinistral slip partitioning on N120°E strike NE of 88°E		
	Figure 16(b)	>100±25 km
	Figure 10(c)	>126 km

than 1000 km (Fig. 15), along and north of the most recent, calcalkaline volcanic belt of Tibet, is analogous to that of the Barisan fault along the Sunda arc (e.g. Fitch 1972). A simple comparison with oblique plate convergence at active margins would thus suggest oblique subduction of the Qaidam mantle under the Kunlun, with slip partitioning in the crust (Figs 15a,b and 17b), (Matte *et al.* 1996). The Jinsha suture, the southern boundary of the thick, Songpan accretionary prism and western continuation of one branch of the sinistral Xianshuihe fault to the Fenguo Shan, might be another plausible locus of

partitioning (Figs 15a and 17b). The Songpan lithospheric mantle, which probably underlies a crust thinner and denser than elsewhere in Tibet, would then plunge under Qiangtang, as hinted at by the existence of a south-dipping zone with faster relative *P*-wave velocities down to $\approx$350 km south of Fenguo Shan (Wittlinger *et al.* 1996).

Tying the emplacement of Neogene igneous and volcanic rocks just south of the Kunlun range to subduction beneath it and crustal shortening north of it would imply rough coevality between these processes. The bulk ages of the earliest well-dated such rocks west of 94°E are between $\approx$8 and 13 Ma, about an average of 10.8 Ma (Burchfiel *et al.* 1989a; Turner *et al.* 1996). To first order, a minimum of $\approx$150 km of crustal shortening in the last $\approx$10 Ma would yield a minimum rate of crustal shortening of $\approx$15 mm yr^{-1} in the N30°E azimuth. If, concurrently, the northeastern wedge of Tibet encompassing the Kunlun, Qiman and Qilian ranges and the Qaidam, Gonghe and Suhai basins had reached its average elevation of 3500 m above the 1500 m-high Gobi desert in about 10 Myr, then the average rate of regional uplift would have been $\approx$0.2 mm yr^{-1}. The timing constraint derived from relating the Kunlun volcanics to continental subduction is comparable to that implied by sediment deposition in the Qaidam, which shows a marked increase after $\approx$11 Ma (Métivier 1996). More than 1.5 cm of yearly shortening, at present, across the many ranges and basement highs (>10) of the western Qaidam and Qilian Shan would be in keeping with the minimum shortening rate found across just one of them, the Taxueh Shan (1.5 mm yr^{-1}). This cumulative value would also be consistent with shortening rates inferred across other youthful mountains of the region (1–4 mm yr^{-1}; Tapponnier *et al.* 1990a; Zhang *et al.* 1990; Gaudemer *et al.* 1995). Finally, such timing and minimum cumulative shortening rate would be consistent with a minimum sinistral slip rate of $\approx$2 cm yr^{-1} on the Altyn Tagh fault near 88°E, in agreement with previous estimates (Peltzer *et al.* 1989; Ryerson *et al.* 1997).

5 SUMMARY AND IMPLICATIONS: GROWTH AND RISE OF THE TIBET PLATEAU

The work presented here is part of a decade-long effort to understand the mechanics of Late-Cenozoic shortening in the remote highlands of NE Tibet, an area where recent, coeval thrust faulting is more ubiquitous, and spreads over a greater surface than anywhere else in Asia or in other regions of plate convergence. An increase in our SPOT image coverage, access to many different field areas and the use of digital topography now enable us to draw, at the appropriate scale, a comprehensive picture of deformation between the Kunlun fault and the Gobi. Our results strengthen the view that current deformation processes over the entire NE quarter of Tibet, a surface of about 1/2 million square kilometres, provide the key to understanding the growth and uplift of the plateau, much more so than those responsible for the rise of its southern rim, the Himalayas.

5.1 Plateau building: role of coeval crust/mantle décollements and strike-slip faults

The whole region north of the Kunlun fault is the site of vigorous mountain and fold growth. Such youthful reliefs grade from hill to range size. In general, the rising ridges trend $\approx$N120°E. All, including the largest, appear to be ramp anticlines. Their lengths scale with their widths ($L/W \approx 5$–8), and hence probably with the ramp depths and cumulative throws. Near the Altyn Tagh fault, most of the thrust ramps dip south. Many of the largest mountain ranges, especially near the edges of the Tarim and Gobi deserts, appear to be rising simultaneously today. They have comparable widths and heights, usually 20–50 and 4–6 km, respectively. They are roughly parallel, generally a few tens of kilometres apart, separated by piggy-back basins presently in the stage of fairly rapid sedimentary infilling. Most of the basins form local base-levels, with little or no fluvial outlet (Suhai, Ala Hu). Typical rates of throw or shortening on the thrusts appear to be of the order of a few millimetres per year, and typical amounts of cumulative displacement on the largest thrusts reach 10–20 km. Most of the relief growth north of the Kunlun fault appears to postdate 11 million years. Farther north, the large ranges south of the Hexi corridor probably rose in less than 6 million years. Smaller ones along the eastern part of that corridor may be of Quaternary age only, implying northeastward younging of deformation (Fig. 15c).

In map view, the thrusts form a remarkably organized network, both geometrically and kinematically. Westwards, most of them bend into the sinistral Altyn Tagh fault. Towards the east, those north of the Suhai basin similarly merge with the sinistral Haiyuan fault. Those northeast of the Qaidam basin or bounding the Gonghe and Qinghai basins, by contrast, are cut and truncated by the NNW-trending, dextral, Wenquan and Haiyen faults (Fig. 15a). In the west, but probably also elsewhere, triple-junction vector sums help predict transfer and loss of coeval slip between fault segments that meet, implying small strains within the blocks such faults separate. Oblique motion across several large ranges appears to be partitioned between inner, range-parallel, sinistral faults, and outer thrusts with NNE to NE slip (Figs 15b and 16b). Steep thrust ramps, whether emergent or not, appear to flatten into shallow south-dipping décollements, at different depths within the crust. Active thrusts have migrated up to $\approx$15 km into the mountain forelands, in discrete steps, as previously documented over horizontal distances of at most $\approx$3 km in northern Japan (Ikeda 1983). The youngest ramp anticlines thus fold gently sloping, contemporaneous fanglomerates for great distances across piedmont bajadas, which yields spectacular geomorphic snapshots of fold growth, with bottleneck cluses in the drainage incising spearheaded, almond- or teardrop-shaped terrace tongues, depending on whether the thrust ramps break the ground surface or not.

The overall picture is strikingly reminiscent of the thrust organization commonly found in thin-skinned sedimentary fold and thrust belts (e.g. Boyer & Elliott 1982), but the scale is gigantic. Here, ramp anticlines reach mountain-range size and can fold layers of crust 20 km thick or more. Much of the crust seems to be decoupled from the mantle at the scale of NE Tibet. The ongoing deformation suggests that a vast (500×1000 km), active, lower-crustal décollement underlies the Qilian ranges, Qaidam basin and other regions between the Kunlun fault and the Gobi, and deepens southwestwards to root into a deep mantle megathrust, south of the Kunlun range. Beneath that décollement, the lithospheric mantle apparently remained rigid, except along ancient sutures. Hence, the crust of NE Tibet thickened while the mantle did not, forming

a huge acccretionary wedge, probably the broadest and thickest of its kind on the planet. First-order estimates of amounts of crustal shortening in that wedge imply that the mantle subducted obliquely southwestwards to depths of at least 200–300 km, beneath and south of the Songpan terrane (Figs 16 and 17). Some lower crust may have remained attached to the foundering mantle (Figs 15b and 16b). The thickness of the lower-crustal layer thus underthrust is unknown, but if it exceeded 10 km then the amounts of surface shortening and mantle subduction would be increased by more than 20 per cent. We relate the Miocene to Quaternary volcanism and plutonism along the south flank of the Kunlun to such oblique subduction of lower crust and mantle into the Tibetan asthenosphere (see also Matte *et al.* 1996).

The importance of large décollements within the crust has long been pointed out (e.g. Boyer & Elliott 1982; Bally *et al.* 1986; Mattauer 1986a,b; Beanland & Berryman 1989; Tapponnier *et al.* 1990a; Mattauer *et al.* 1992; Cook & Warsek 1994; Lacassin *et al.* 1996; Yeats *et al.* 1997), and the mechanical comparison of thrust belts with accretionary wedges has led to substantial advances in the understanding and modelling of mountain ranges (e.g. Davis *et al.* 1983; Dahlen *et al.* 1984a, 1984b; Malavieille 1984; Mattauer 1986a,b; Molnar & Lyon Caen 1988). What makes the thrusts and décollements discussed here unique is their coevality over a particularly vast surface, their 3-D interaction with particularly large strike-slip faults, and the geomorphic consequences of the growth of a particularly thick-skinned wedge inside a continent. All of these characteristics have a direct bearing on plateau—rather than mountain—building. Also, the fact that faulting is recent and active, and hence that coevality can be rigorously established, allows interaction and growth processes to be deciphered in unrivalled fashion. It is possible to watch the system at work, and to unravel its evolution in ways that are out of reach in more ancient orogens.

The horsetail geometry of large thrusts south of the northeastern stretch of the Altyn Tagh fault implies that the NE Tibetan highlands have grown obliquely, in connection with propagation of that fault towards the NE. Such propagation must predate regional mountain building, because the strike-slip fault now extends much farther east into the Gobi–Ala Shan platform (to at least $\approx 102^{\circ}$E) than does the present boundary of the highlands along the Hexi corridor (Figs 1 and 15a). As the fault grew, it appears to have successively shed thrusts at high angle towards the SE (Figs 12 and 15c), slicing and weakening the crust. The fault subsequently bypassed those thrusts, its propagation rate being probably much faster than its slip rate (e.g. Briais *et al.* 1993; Armijo *et al.* 1996; Manighetti *et al.* 1997). The timing of propagation is still poorly constrained, but the northeastward younging of the onset of rapid sedimentary infilling in the basins south of the fault (Na to Nd, Fig. 15c) offers a lead (Métivier 1996). Taking changes in sedimentation rates to reflect enhanced mountain building in regions adjacent to the fault due to its growth would suggest a northeastward propagation rate of the order of 10 cm yr^{-1} or more (Fig. 15c), at least five times its present, minimum slip rate near 90°E (2 cm yr^{-1}) (Peltzer *et al.* 1989).

While we interpret thrusts south of the Altyn Tagh fault to have initially formed in a large process zone (e.g. Armijo *et al.* 1996) at the tip of the fault, they subsequently continued to grow and develop, shortening the crust north of the Kunlun to absorb part of the NE-directed motion of Tibet relative to Siberia (e.g. Avouac & Tapponnier 1993; Peltzer & Saucier 1996). The exceptional width of the zone of active overthrusting in NE Tibet thus appears to result from fast propagation of a large strike-slip fault. Such strike-slip-controlled mountain growth is unlike that observed in narrower belts such as the Alps and Himalayas, where one major thrust tends to stop at the expense of a new, adjacent one because of the increase in gravitational potential energy (e.g. Molnar & Lyon Caen 1988). In NE Tibet, many large thrusts keep functioning together, building distant ranges of comparable elevation separated by broad basins: hence the remarkably vast area subject to coeval crustal thickening and the high, albeit unexceptional, elevation. In short, the process now at work across NE Tibet is better suited to creating a wide plateau (stars, Fig. 14) than a towering mountain belt. Rather than being sliced and stacked up to great height and depth over a relatively narrow width, the crust thickens more moderately over a huge surface.

5.2 Early propagation of lithospheric strike-slip faults and diachronous crustal thickening domains in Tibet

That the Altyn Tagh fault limits all the thrusts of the region (Fig. 15a) supports the inference that it formed first, and rapidly cut through the entire lithosphere. The crust north of the fault would have otherwise shortened much more than it did. In effect, established strain softening and localization along the fault prevented areas north of it from yielding to the shortening regime already well underway in the south. Although the mechanical strength of the Tarim block (e.g. England & Houseman 1985), as well as elements of the tectonic fabric inherited from Precambrian and early Palaeozoic times probably played a role in guiding the initial path of the strike-slip fault, we infer lithospheric localization to be the most plausible interpretation of a change in style, direction and amount of deformation as radical as that observed across the fault (Figs 10, 12, and 15). A recent tomographic profile near 90°E, which reveals a steep, low-*P*-wave velocity anomaly down to ≈ 150 km beneath the Altyn Tagh fault (Wittlinger *et al.* 1998), appears to confirm that it is a lithospheric shear zone rather than just a crustal ramp, as inferred by many (e.g. Burchfiel *et al.* 1989b).

That strike-slip faults propagate readily in the lithospheric mantle may explain why large-scale extrusion played an essential role throughout the Indian collision history (e.g. Peltzer & Tapponnier 1988; Lacassin *et al.* 1997), as demonstrated by the existence of another large Tertiary shear zone along the Ailao Shan and Red River in south China (e.g. Tapponnier *et al.* 1990b; Leloup *et al.* 1995; Schärer *et al.* 1994). The age and nature of either of these zones makes the popular view that strike-slip faulting is a late and shallow—hence minor—side-effect of continental thickening during collision (e.g. Dewey *et al.* 1988; England & Houseman 1986; England & Molnar 1990) untenable.

Like the Ailao Shan–Red River shear zone, the Altyn Tagh fault illustrates a simple tenet of continental tectonics. Scaling laws and kinematics require that fault zones and mountain belts that stretch continuously for lengths of many hundreds to thousands of kilometres, as plate boundaries do, root into lithospheric cuts, while shorter features that are more segmented, at the scale of tens to less than two hundred kilometres (Fig. 14), only or principally affect the crust. On the map of

Fig. 15(a), for instance, only the Altyn Tagh fault and Altyn Range, the Kunlun fault and Kunlun Range, and the Haiyuan fault and North Qilian Range are long and continuous enough to reflect slicing of the lithospheric mantle beneath. Concurrently, only those long fault zones have slip rates that reach or exceed 1 cm yr^{-1} (e.g. Zhang *et al.* 1988; Lasserre *et al.* 1997; Ryerson *et al.* 1997; Van Der Woerd *et al.* 1998). This simple principle guided the construction of sections in Figs 16(b), 17(b) and 18(b), and may be used to unravel large-scale continental deformation anywhere.

The map of Cenozoic relief and faults of northern Tibet (Fig. 15a) draws attention to remarkable similarities between the Kunlun and the Altyn Tagh faults. Most of the thrusts south of the Kunlun fault, between the Fenguo Shan and Anyemaqin, strike 30–40° clockwise from this fault, as do the Qilian thrusts relative to the Altyn Tagh fault, south of it (Fig. 12a). North of the Kulun fault, by contrast, thrusts tend to parallel this fault, implying that the Kunlun and Qiman Shan are just mature counterparts of the Altyn Range (Fig. 15c). Thrusts south of the Kunlun are older, however, since they typically emplace Triassic flysch over Lower- to Mid-Tertiary red-beds, and only a few of them remain active. This, together with erosion, including longer and more extensive glacial abrasion, explains the much smaller relief observed there than north of the Qaidam. As in the Qilian Shan, however, the overall landscape is still one of broad basins separated by long ranges oblique to the Kunlun fault, which veer and terminate along it. It is thus tempting to infer that, like the Altyn Tagh fault, the Kunlun fault propagated towards the east (Fig. 15c), forming a major Mid-Tertiary lithospheric boundary, and contributed to the initiation of the building of the north-central part of the Tibet Plateau, south of the Kunlun Range, in a way analogous to that later triggered in the Qaidam and Qilian Shan by propagation of the Altyn Tagh fault. In keeping with this interpretation, one would predict eastward younging of the onset of sedimentation in the Tertiary intramontane basins south of the Kunlun fault (Ea to Ed, Fig. 15c).

Relative fault orientations in southeastern Tibet and Yunnan suggest that, even earlier during the Tertiary, similar coupling between thrusts and lithospheric strike-slip shear took place southwest of the Xianshuihe and Red-River faults (Lacassin *et al.* 1996, 1997). This further suggests that the now rather uniform expanse of high topography that is generally referred to as 'The Tibet–Qinghai Plateau' is in fact composed of three distinct Cenozoic domains, corresponding to different lithospheric blocks separated by oblique-slip boundaries (Tapponnier *et al.* 1986), whose crust thickened and whose elevation rose above 4000 m a.s.l. in three successive, northward younging steps (Fig. 18). Possibly, there might exist no orogenic plateau as broad as Tibet without strike-slip shear zones propagating rapidly through the lithosphere. And it might be no coincidence that the largest plateau on Earth is associated with the largest intracontinental strike-slip faults.

The map of Fig. 15(a) also reveals similarities in the bends connecting the Altyn Tagh fault with the western Haiyuan and Kunlun faults. Both faults trend $\approx 30°$ more easterly than the Altyn Tagh and veer clockwise near it. Both lie south of rhomb-shaped, thrust-bounded mountain zones, about 400 km long and 200 km wide, that harbour broad basins in their centres—the Tang He-Yema He basin between the Tanghenan and Qilian Shan, and the Ayakkum Kol basin between the Qiman Tagh and Kunlun Shan. The scales, geometry and styles of faulting in both zones are comparable enough to suggest a similar origin. We interpret such faulting to have formed within fairly long-lived, right-stepping push-ups coinciding with restraining bends related to deviated propagation of branches of the Altyn Tagh fault along pre-existing, weak lithospheric discontinuities—the Kunlun and Qilian sutures—that it ultimately cut and displaced. Such deviated propagation is commonly observed in analogue indentation experiments (Peltzer & Tapponnier 1988). If a similar rhomb-shaped connection existed north of Fenguo Shan between the Kunlun and Xianshuihe faults (Fig. 15a), a similar deviation might have occurred there, for the later fault roughly follows the Jinsha suture. At a greater scale, the entire area encompassing the Qaidam basin and Qilian Shan might be thought of as having originated in a similar fashion, but although this area stands within a very large restraining bend of the Altyn Tagh–Haiyuan fault system (Fig. 1, 15a), the three main strike-slip faults that bound it all remain active, and that bend is now becoming outgrown by the continuing propagation of the Altyn Tagh fault towards the northeast.

5.3 Smooth, high topography, and infilling of rhomb-shaped basins closed by tectonic catchment cut-off

The most striking element of the landscape of northeastern Tibet is the existence of immense, relatively flat, Tertiary basins that stand nearly 3000 m a.s.l. (Figs 10, 15 and 16). Many such basins are rhomb- or triangular-shaped, because they are bounded by Late-Cenozoic faults with different strikes. Most of the highest basins have no present fluvial outlet, and thus form local base levels. Such is the case, for instance, for the western Gonghe, Qinghai, Ala Hu, Suhai, Qaidam, Ayakkum Kol, and Achik Kol basins. A few other basins, although surrounded by towering ranges on all sides, are still drained by large rivers, such as the Tang He, Sule He, and Huang He, whose incision power has kept pace with the growth of the mountain barriers. But even these rivers, whose flow swells and shrinks in tune with climate change, have had difficulties maintaining a steady outlet towards the lowlands peripheral to Tibet. This is best illustrated by the kilometre-thick Quaternary deposits that the Huang He, greatest river of northern Tibet, has accumulated in the eastern Gonghe and Guide basins, upstream from the forbidding, hundreds-of-metres deep canyons with impassable vertical walls that it has incised across the Qinghainan and Tachi Shan.

It thus appears that damming of rivers by fast tectonic uplift of the ranges above the Late-Cenozoic thrusts has cut off catchment outlets, isolating the vast, now internally drained basins of northeastern Tibet, and will continue to do so as the mountains rise higher and the faults propagate farther. In this process, the role of transpressive strike-slip faults is essential. Because such faults typically strike at angles of 20°–50° from the thrusts, they provide an efficient way to sever drainage parallel to the ranges and isolate rhomb-shaped, completely mountain-locked basins. Local, fairly high base-levels, all disconnected from the adjacent lowlands, are thus created. Subsequently, such levels are free to evolve independently, but can only rise further with the influx of debris from the surrounding mountains, until they reach the residual elevation of the eroding ranges between them. We infer that it is the ultimate coalescence of such base-levels that yields the high,

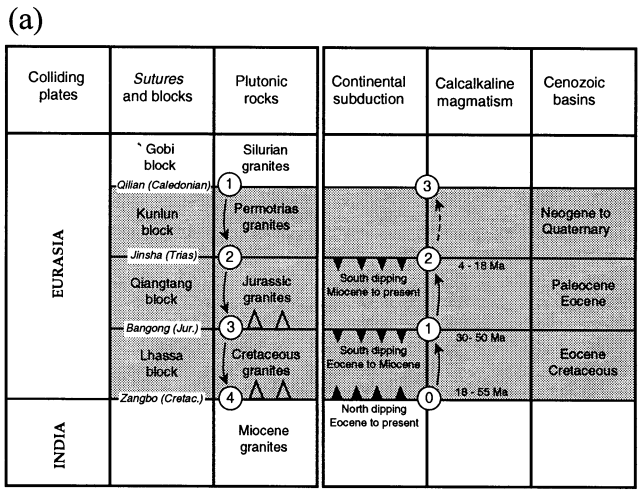

Figure 18(a). Diagram summarizing major stages of the Phanerozoic tectonic evolution of Tibet (modified from Bourjot 1991). Left: between Palaeozoic and Early Tertiary, accretion of Cathaysian and Gondwanian blocks resulted in the southward growth of the Tibetan collage from the initial central Asian core. Suturing of blocks followed mostly north-dipping subduction of Tethysian oceanic lithosphere. Right: in contrast, since Cretaceous, depocentre migration in Tibetan basins implies northward relief growth and successive reactivation of Mesozoic sutures, as India penetrated into Asia. We infer that India's collision triggered discrete, short-lived, south-dipping subduction of lithospheric mantle, particularly along the Bangong–Nujiang and Jinsha–Kunlun sutures, resulting in calcalkaline magmatism and volcanism.

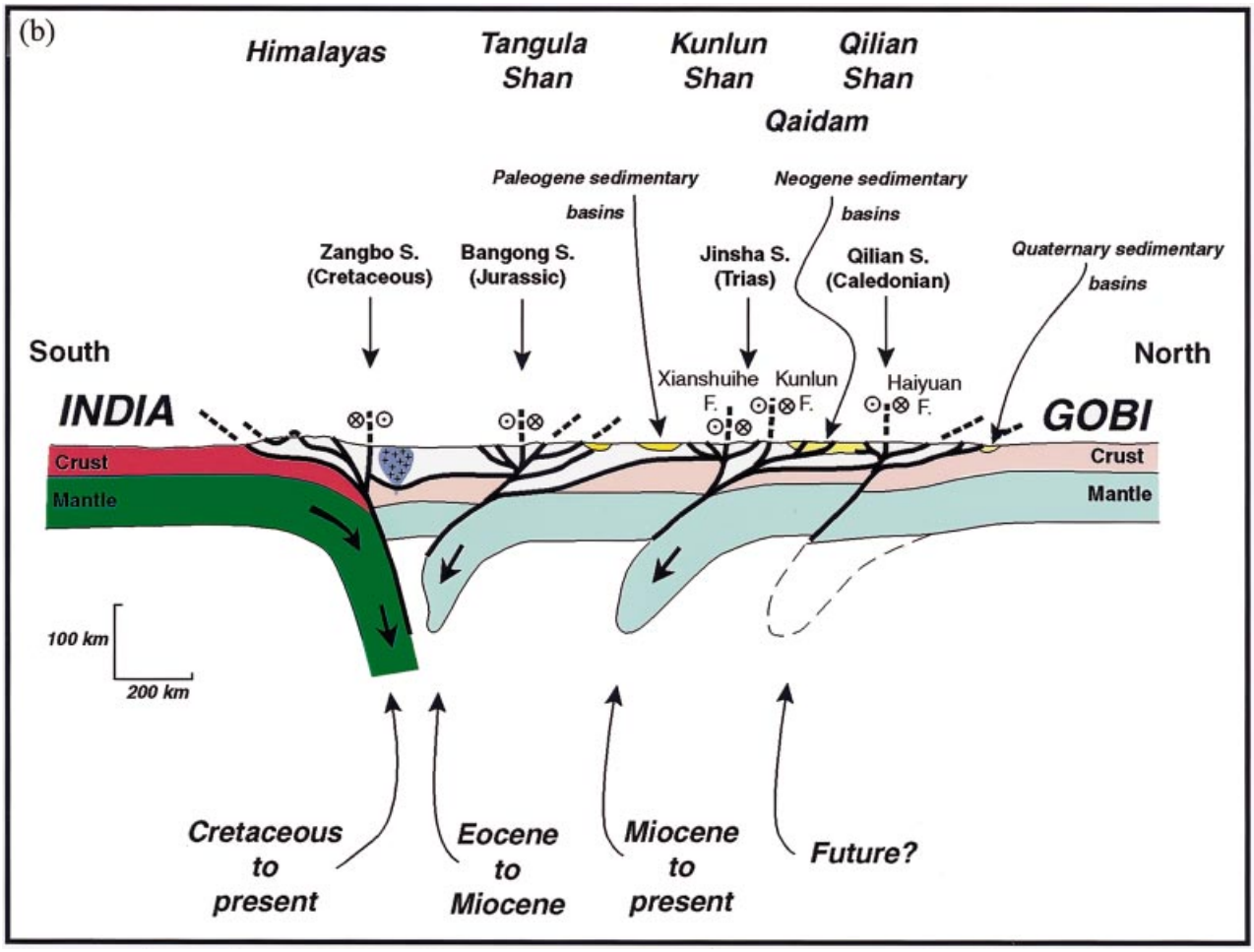

Figure 18(b). Interpretative section across the entire Tibet plateau, illustrating northward outgrowth by successive accretion of thickening crustal wedges above décollements rooting into south-dipping, lithospheric-mantle subduction zones, initiated along older sutures (modified from Bourjot 1991). Bold lines are major Cenozoic faults and shear zones, as in Fig. 17(b). Strike-slip faults 1000 km long are coupled with oblique mantle subduction.

but remarkably smooth and flat topography that characterizes the surface of the Tibet Plateau.

The interplay, presently seen at work north of the Kunlun, between tectonic uplift of distant, narrow ranges, and erosion and sedimentation within doomed catchments may thus provide a simple mechanism for flattening the surface of orogenic plateaus over broad areas. Northeastern Tibet is home to the clearest examples of small, smooth-surfaced, high plateaus in a state of swift growth and rise that we have seen. The most prominent of all is the Qaidam, which is entirely rimmed by Cenozoic faults and 5–6000 m high ranges, and whose base-level already reaches an average elevation of nearly 3 km a.s.l. over a surface of $\approx 103\,000\,km^2$ (Figs 1, 15 and 16). The exceptionally rapid Plio-Quaternary infilling of that basin, at rates equal to or greater than present-day ones in the Ganges plain or Bengal fan, requires tectonic cut-off of an oulet that used to drain, probably into the Huang He, the catchments that subsequently fed the huge volumes of sediments accumulated in the basin (Métivier 1996). In a sense, elevation rise and surface smoothing by dammed sedimentation is akin to 'bathtub' infilling, but with decreasing relief, and hence diminishing erosion rates along the mountainous edges of the tub, acting to slow down sediment infill and prevent overspill.

Large parts of the Tibet Plateau south of the Kunlun have in fact more to do with basins than with mountains, and probably acquired their smooth morphology through that infilling process. Although this may seem a paradox, both the geology (Geological Publishing House 1988) and topography (Fielding *et al.* 1994) imply that much of the vast and flat 'plain' that forms the roof of the world is better described, despite its 4–5000 m elevation, as a mosaic of coalescent basins separated by far-apart ranges than as a continuum of closely packed mountains. This view is consistent both with the variable Moho depths, beneath crustal domains that apparently experienced different amounts of thickening, found in local seismic studies of central and northern Tibet (Hirn *et al.* 1984; Wittlinger *et al.* 1996), and with the recent discovery of significant oil reserves in the middle of the plateau (Xu Zhiqin, personal communication). It implies also that large regions of Tibet, particularly in the north, are underlain by thick piles of low-density rocks, which may in large part account for the very low crustal velocities revealed by recent seismic tomography experiments (Wittlinger *et al.* 1996).

We infer 'bathtub' infilling to have played an important part in the formation of other fairly broad, if less high, orogenic plateaus that harbour large, internally drained basins surrounded on all sides by rising mountains, such as the Altiplano in the Andes, or Central Iran. Ductile flow of the lower crust (e.g. Owens & Zandt 1997) may be involved in smoothing Moho depth irregularities, and hence surface topography (e.g. Fielding *et al.* 1994; Avouac & Burov 1996) within Tibet and other plateaus. However, while such a deep-seated mechanism is physically plausible, and may contribute to making surface elevation even more uniform by raising certain areas at the expense of others, it ought to intervene at a later stage, and uncontroversial evidence for it has yet to be found.

Throughout northern Tibet, whether north or south of the Kunlun range, we found little evidence of a large rebound of the topography that might testify to convective removal of the lower part of the lithosphere (e.g. England & Houseman 1989). The existence of such an instability, invoked to explain, simultaneously, a rapid uplift of Tibet to greater height than today's, the shift to the now widespread extension on top of the Plateau, and the triggering of the monsoon in the Mid-Miocene (Molnar *et al.* 1993)—all phenomena whose 'sudden', coeval onset is doubtful—requires that the lithospheric mantle first thickens (England & Houseman 1986) before some of it can detach and sink. Since our observations suggest subduction rather than thickening of the lithospheric mantle under northern Tibet, and since no process other than those we document in the crust seems needed to build the relief to current Tibetan heights gradually, we find convective rebound to be implausible.

5.4 Sequential, south-directed subduction of Asian lithospheric mantle in response to India's push

That the lithospheric mantle of inner Asia might subduct southwestwards along the Kunlun, under the edge of northern Tibet, is neither surprising nor inconsistent with generally accepted models of lithospheric convergence in other large mountain ranges such as the Alps or Himalayas (e.g. Lyon-Caen & Molnar 1984). But such subduction did not follow closure of a recent ocean basin. It was triggered anew sometime in the Miocene by the stresses that India applies to the rest of the Asian continent, and probably corresponds to only the most recent stage of a process that has repeated itself, by jumping northwards at least twice, since collision began, 55 or 60 million years ago (Fig. 18).

The simple logic here is that the topographic bulge of crust thickened by the impingement of India must have had, from the start, a northern edge. Initially, such an edge probably lay rather close to the Zangbo suture, albeit north of the Gangdese batholith. This northern edge would have provided a particularly favourable place for north-vergent thrusts to develop. Increasing amounts of crustal shortening on such thrusts would have forced the mantle of lowlands farther north to plunge southwards under that edge. Concurrently, Tibet's Palaeozoic and Mesozoic accretion history, which resulted in blocks and sutures younging towards the south (e.g. Sengör 1984; Chang *et al.* 1986; Matte *et al.* 1996) (Fig. 18b) would have fostered sequential triggering of south-directed subduction north of the Gangdese. Each suture, forming a lithospheric cut with the oldest, and hence densest and strongest block to the north, would have provided, in turn, an appropriate starting point for mantle underthrusting, with a tendency for the north side to plunge southwards (Figs 18a and b). The Cenozoic growth of the high plateau would thus have been characterized by mantle subduction polarities generally opposite to those that presided in the Palaeozoic and Mesozoic assemblage of Tibetan terranes by collage of far-travelled blocks along the southern rim of Laurasia.

Crustal shortening might have started also in regions well north of the former plateau boundaries, as observed today in the Tien Shan, north of the Tarim basin. This might have led to north-directed foundering, beneath such outlying regions, of the mantle of strong intervening blocks. It is possible, for instance, that the Qiangtang-Songpan and Qaidam mantles plunged under the Kunlun and Qaidam Shan, in the Eocene and Early Miocene, respectively. However, the ultimate incorporation of these blocks and regions into the growing highland mass implies that north-dipping mantle subduction, if any, should have been short-lived, and soon replaced by subduction dipping inwards beneath the northern topographic edge of the

highlands. At all times, the situation would have tended to evolve towards that of today, which appears to be characterized by inward downwelling of cold mantle beneath all the outer boundaries of the plateau, as suggested by surface-wave tomography (Griot 1997).

The sequential evolution that we find mechanically most plausible and most consistent with extant geological evidence is outlined in Fig. 18(a) (Bourjot 1991). The northward younging of Tertiary red-bed basins suggests a succession of at least two distinct accretionary forelands north of the Gangdese. Along and north of the Tanggula range, Palaeogene red-beds, now strongly folded, cover the Jurassic and Cretaceous sediments of the Lhassa and Qiangtang blocks (Geological Publishing House 1988; Chang *et al.* 1986). Remnant patches of roughly coeval red-beds also unconformably cover the Songpan flysch farther north. North of the Kunlun range, by contrast, the greatest thicknesses of Cenozoic, molassic deposits are of Neogene age. We thus infer that south-dipping subduction of the Asian mantle first developped in the Eocene a few hundred kilometres north of the initial contact between India and Asia, along the western, deeper part of the Bangong-Nujiang suture, together with strong crustal shortening in the Tanggula range and sinistral shear along the shallower trace of that suture (Matte *et al.* 1996). At that time, thrusting probably spread far into the Qiangtang and Songpan blocks, as observed now north of the Kunlun. One significant difference may have been the persistence of greater residual topography from Late Mesozoic orogenic episodes in that region than farther north. Later, as the Songpan terrane became part of the collisional highlands, south-dipping mantle subduction developed along the western Jinsha and Kunlun suture in the Early Miocene, a northward jump of a few hundred kilometres, leading to accretionary growth of the plateau along the Kunlun and in regions farther north, coupled with continuing sinistral slip on the western Altyn Tagh–Kunlun, and Xianshui He faults. The eastern Altyn Tagh and Haiyuan faults developed even later in the Mio-Pliocene, to yield a situation that may ultimately lead to mantle subduction under the Qilian Shan, the present-day outer limit of the Tibet–Qinghai highlands. Overall, successive jumps of the northern edge of the Plateau and of the site of mantle subduction thus appear to have followed the successive activation of strike-slip faults by India's penetration into Asia (Peltzer & Tapponnier 1988; Lacassin *et al.* 1997).

Clearly, the first-order model shown in Fig. 18 is not unique, and should be seen as little more than a working hypothesis. It includes, however, first-order tectonic features that are overlooked in all attempts to model Tibet as a uniform entity. In particular, it accounts for the three $\approx$E–W belts of greatest topographic elevation and tectonic strain within the plateau, the Tanggula, Kunlun and Qilian ranges, where prominent Cenozoic folding and thrusting are intimately associated with strike-slip faulting: such belts are inferred to correspond to the three main, discrete, diachronous sites of mantle deformation between the Himalayas and the Gobi since collision began. Hence, this model offers a more realistic path towards understanding the structure and tectonic history of Tibet than the many scenarios based on steady consumption of the lithospheric mantle along one or at most two zones through the entire collision span (e.g. Willet & Beaumont 1994; Westaway 1995; Royden 1996; Nelson *et al.* 1996; Owens & Zandt 1997). Also, it appears to rest on more realistic processes—fault growth and suture reactivation—than those underlying models in which finite-amplitude buckling is surmised to trigger both widespread, coeval mountain growth and mantle downwelling (e.g. Molnar *et al.* 1993; Jin *et al.* 1994; Martinod & Davy 1994; Burg *et al.* 1995), neither of which prediction seems to be supported by observations (Figs 14, 15 and 18).

5.5 Plate-like tectonics versus diffuse deformation during continental collision

With regard to the mechanics of large-scale continental deformation during collision, the most significant implication of the interpretation shown in Fig. 18 is that, while crustal strain in Tibet is distributed and may seem complex, an impression also conveyed by the widespread shallow seismicity, deformation at the lithospheric mantle level may have been simpler, and comparable to plate tectonics. At any time, such deep deformation may have involved only a few long, oblique mantle megathrusts, akin to oblique subduction zones, which formed by reactivation of ancient sutures, the most ready-made lithospheric cuts. The relative motions of large, strong mantle blocks along these deep boundaries would merely be concealed by the more complicated behaviour of the decoupled crust at shallower levels. Crustal slip partitioning would occur above such boundaries, as at oblique convergent margins.

Together with modelling of the contemporaneous kinematics, which implies little internal strain within blocks between large, fast-slipping faults (e.g. Avouac & Tapponnier 1993; Peltzer & Saucier 1996), the conclusions we reach on lithospheric mantle motions beneath Tibet suggest that one might have to revise the now ingrained view that plate tectonics dramatically fail when applied to continental interiors in general and to the India–Asia collision zone in particular (e.g. Molnar 1988). Buried plate tectonics might take place under and around Tibet.

Rapid, early, strike-slip fault propagation, development of thrusts in the wake of the propagating fault-tips, large-scale crust/mantle decoupling on broad décollements, development of subcrustal mantle subduction along pre-existing sutures, and tectonic pirating of drainage catchments, followed by rapid infilling of the resulting captive basins by low-density sediments seem to be the main processes needed to build continental orogenic plateaus of Tibet's size.

This conceptual framework is radically different from that of dynamic models in which the continental lithospheric mantle is taken to behave as an integral part of a thickening, thin viscous fluid sheet, with no decoupling or strain localization (e.g. England & Houseman 1986; Houseman & England 1986). Should the interpretation consistent with our analysis of the Cenozoic crustal deformation be corroborated by seismic imaging and measurements of palaeo-elevation changes, then such models, and their most speculative consequence—wholesale, rapid plateau rebound to an elevation well in excess of today's (England & Houseman 1989; Molnar *et al.* 1993)—might have to be dismissed. The thin viscous sheet approach might still be applicable to strain in the crust (Holt *et al.* 1995; Royden 1996) but mantle-plate motions involving both strike-slip and subduction should be taken into account.

Although the large-scale section we propose (Fig. 18) differs from that of Mattauer (1986a,b), who suggested that lithospheric mantle now plunges south under both the Kunlun and the Qaidam, that suggestion was important. For there is a key

difference between the birth of a new mantle subduction zone inside a large, long-welded, continental plate, a mechanism he dubbed 'continental subduction', and the mere continuation of subduction during collision. In the latter case, the lithospheric mantle of the continent initially attached to the subducting oceanic plate is simply pulled under the other's, as India's mantle was north of the Indus–Zangbo suture (Molnar & Lyon-Caen 1988). In the former, boundary forces must play a role in triggering the process.

As deformation keeps migrating towards the northeast, the Qilian Shan may become a site of continental subduction. The present length of the Haiyuan fault and the fact that it continues into one of the largest rifts of Asia, along the Wei He valley (inset, Fig. 1) (Peltzer *et al.* 1985; Gaudemer *et al.* 1995), implies that it is already a deep lithospheric cut, and overthrust flakes of crust comparable to those north of the western Kunlun fault have already formed in the Tianjin and Mibo Shan (Zhang *et al.* 1990) (Fig. 15). Should mantle subduction develop along that deep cut (Fig. 18), then the Tibet Plateau might continue to grow for millions of years, through appropriation of its now peripheral basins by new outer ranges, north of the topographic barrier that now bounds it south of the Gobi desert.

ACKNOWLEDGMENTS

We thank the State Seismological Bureau in Beijing, the Lanzhou Institute of Seismology (China), the Institut National des Sciences de l'Univers (INSU, CNRS, Paris, France), and the French Ministery of Foreign Affairs for financial and logistical support. Without continued funding by programs DBT, IST-Tectoscope, Mecalith and IDYL, this work could not have been accomplished. Particular gratitude goes to Dr J. C. Rossignol and G. Aubert, and to Dr Gu Ping and Chen Zhangli, who coordinated the development of our cooperation program on the French and Chinese sides, respectively. We had numerous and fruitful discussions with G. King, J. Vanderwoerd, M. Brunel, Xu Zhiqin, Xu Xiwei, R. Armijo, R. Lacassin, N. Arnaud, and F. Roger. We also thank Xiang Hongfa, Xiang Guangzhong, Dai Huagang, Cai Shuahua, Yin Kelun, Chen Hongfei and Zhao Xiaochen whose contributions in the field were greatly appreciated. Peter Molnar's and Rick Ryerson's thorough reviews helped improve the original manuscript. G. Aveline and J. Dyon are responsible for the quality of the figures. This is IPGP contribution No. 1519.

REFERENCES

Argand, E., 1924. La tectonique de l'Asie, *Proc. Conf. 13th Int. Geol. Congr.,* 171–372.

Armijo, R., Tapponnier, P., Mercier, J.L. & Tonglin, H., 1986. Quaternary extension in southern Tibet: field observations and tectonic implications, *J. geophys. Res.,* **91,** 13 803–13 872.

Armijo, R., Tapponnier, P. & Tonglin, H., 1989. Late Cenozoic right-lateral strike-slip faulting in southern Tibet, *J. geophys. Res.,* **94,** 2787–2838.

Armijo, R., Meyer, B., King, G.C.P., Rigo, A. & Papanastassiou, D., 1996. Quaternary evolution of the Corinth Rift and its implication for the late Cenozoic evolution of the Aegean, *Geophys. J. Int.,* **126,** 11–53.

Arnaud, N.O., Vidal, P., Tapponnier, P., Matte, P. & Deng, W.M., 1992. The high K^2O volcanism of northwestern Tibet; geochemistry and tectonic implications, *Earth planet. Sci. Lett.,* **111,** 351–367.

Avouac, J.P. & Burov, E., 1996. Erosion as a driving mechanism of intracontinental mountain growth, *J. geophys. Res.,* **101,** 17 747–17 769.

Avouac, J.P. & Tapponnier, P., 1993. Kinematic model of active deformation in central Asia, *Geophys. Res. Lett.,* **20,** 895–898.

Avouac, J.P., Meyer, B. & Tapponnier, P., 1992. On the growth of normal faults and the existence of flats and ramps along the El Asnam active fold and thrust system, *Tectonics,* **11,** 1–11.

Avouac, J.P., Tapponnier, P., Bai, M., You, H. & Wang, G., 1993. Active thrusting and folding along the northern Tien Shan and late Cenozoic rotation of the Tarim relative to Dzungaria and Kazakhstan, *J. geophys. Res.,* **98,** 6755–6804.

Bally, A.W., Chou, I.M., Clayton, R., Heugster, H.P., Kidwell, S., Meckel, L.D., Ryder, R.T., Watts, A.B. & Wilson, A.A., 1986. Notes on Sedimentary basins in China, Report of the American Sedimentary Basins Delegation to the People's Republic of China, August 17–September 8, *open file report* 86–327, USGS.

Bard, E., Hamelin, B., Fairbanks, R.G. & Zindler, A., 1990. Calibration of the ^{14}C timescale over the past 30000 years using mass spectrometric U-Th ages from Barbados corals, *Nature,* **345,** 405–410.

Beanland, S. & Berryman, K.R., 1989. Style and episodicity of late-Quaternary activity on the Pisa-Grandview fault zone, Central Otago, New Zealand, *NZ J. Geol. Geophys.,* **32,** 451–461.

Bourjot, L., 1991. Relation entre structure lithosphérique profonde et déformations de surface au Tibet, *PhD thesis,* Université Paris VII.

Boyer, S.E. & Elliot, D., 1982. Thrust systems, *Am. Assoc. Pet. Geol. Bull.,* **66,** 1196–1230.

Briais, A., Patriat, P. & Tapponnier, P., 1993. Updated interpretation of magnetic anomalies and seafloor spreading stages in the South China Sea, implications for the Tertiary tectonics of SE Asia, *J. geophys Res.,* **98,** 6299–6328.

Burchfiel, B.C., Molnar, P., Zhao, Z., Liang, K., u, Wang, S., Huang, M. & Sutter, J.F., 1989a. Geology of the Ulugh Muztagh area, northern Tibet, *Earth planet. Sci. Lett.,* **94,** 57–70.

Burchfiel, B.C., Deng, Q., Molnar, P., Royden, L.H., Wang, Y., Zhang, P. & Zhang, W., 1989b. Intracrustal detachments within zones of intracintinental deformation, *Geology,* **17,** 478–452.

Burchfiel, B.C., Zhang, P., Wang, Y., Zhang, W., Jiao, D., Song, F., Deng, Q., Molnar, P. & Royden, L.H., 1991. Geology of the Haiyuan fault zone, Ningxia-Hui autonomous region, China, and its relation to the evolution of the northeastern margin of the Tibetan Plateau, *Tectonics,* **10,** 1091–1110.

Burg, J.P., Davy, P. & Martinod, J., 1995. Shortening of analogue models of the continental lithosphere: new hypothesis for the formation of the Tibetan plateau, *Tectonics,* **13,** 475–483.

Calassou, S., Larroque, C. & Malavieille, J., 1993. Transfer zones of deformation in thrust wedges; an experimental study, *Tectonophysics,* **221,** 325–344.

Chang Chenfa *et al.,* 1986. Preliminary conclusions of the Royal Society and Academia Sinica 1985 geotraverse of Tibet, *Nature,* **323,** 501–507.

Chen, Y.T., Xu, L.S., Li, X. & Zhao, M., 1996. Source process of the 1990 Gonghe, China, earthquake and tectonic stress field in the northeastern Qinghai-Xizang (Tibetan) Plateau, *Pageoph.,* **146,** 697–715.

Cook, F.A. & Varsek, J.L., 1994. Orogen-scale décollements, *Rev. Geophys.,* **32,** 37–60.

Cowie, P.A. & Scholz, C.H., 1992a. Displacement-length scaling relationship for faults: data synthesis and discussion, *J. struct. Geol.,* **10,** 1149–1156.

Cowie, P.A. & Scholz, C.H., 1992b. Growth of faults by accumulation of seismic slip, *J. geophys. Res.,* **97,** 11 085–11 095.

Cowie, P.A. & Scholz, C.H., 1992c. Physical explanation for the displacement-length relationship of faults using post-yield fracture mechanics model, *J. struct. Geol.,* **14,** 1133–1148.

Dahlen, F.A., 1984. Noncohesive critical Coulomb wedges; an exact solution, *J. geophys. Res.,* **89,** 10 125–10 133.

Dahlen, F.A., Suppe, J. & Davis, D., 1984. Mechanics of fold-and-thrust belts and accretionary wedges; cohesive Coulomb therory, *J. geophys. Res.,* **89,** 10 087–10 101.

Davis, D., Suppe, J. & Dahlen, F.A., 1983. Mechanics of fold and thrust belts and accretionary wedges, *J. geophys. Res.,* **94,** 347–354.

Defense Mapping Agency, 1973. Operational Navigational Chart Series, Scale 1/1 000 000, *Sheet G8,* 3rd edn, St Louis, USA.

Defense Mapping Agency, 1989. Operational Navigational Chart Series, Scale 1/500 000, *Sheets G8A G8B,* 1st edn, St Louis, USA.

Defense Mapping Agency, 1992. *Digital Chart of The World,* Faifax, USA.

Deng, W.M., 1989. Cenozoic volcanic rocks and intracontinental subduction in the northern Alhi, Xizang, (Tibet), *Acta Petrol. Sin.,* **3,** 1–11.

Dewey, J.F. & Burke, K.C., 1973. Tibetan Variscan and Precambrian basement reactivation: products of continental collision, *J. Geol.,* **81,** 683–692.

Dewey, J.F., Shackleton, R.M., Chang Chengfa & Yiyin, S., 1988. The tectonic evolution of the Tibetan Plateau, *Phil. Trans. R. Soc. Lond.,* A, **327,** 379–413.

Duplessy, J.C., Shackelton, N.J., Fairbanks, R.G., Labeyrie, L.D., Oppo, D. & Kallel, N., 1988. Deepwater source variations during the last climatic cycle and their impact on the global deepwater circulation, *Paleoceanography,* **3,** 651–655.

Ekström, G., 1987. A broad-band method of earthquake analysis, *PhD thesis,* Harvard University, Cambridge, MA.

England, P., 1993. Convective removal of thermal boundary layer of thickened continental lithosphere; a brief summary of causes and consequences with special reference to the Cenozoic tectonics of the Tibetan Plateau and surrounding regions, *Tectonophysics,* **223,** 67–73.

England, P.C. & Houseman, G., 1985. Role of lithospheric strength heterogeneities in the tectonics of Tibet and neighbouring regions, *Nature,* **315,** 297–301.

England, P. & Houseman, G., 1986. Finite strain calculations of continental deformation, 2. comparison with the India-Asia collision zone, *J. geophys. Res.,* **91,** 3664–3676.

England, P. & Houseman, G.A., 1989. Extension during continental convergence, with application to the Tibetan Plateau, *J. geophys. Res.,* **94,** 17 561–17 579.

England, P. & Molnar, P., 1990. Right-lateral shear and rotation as the explanation for strike-slip faulting in eastern Tibet, *Nature,* **344,** 140–142.

Fairbanks, R.G., 1989. A 17 000-year glacio-eustatic sea level record: influence of glacial melting rates on the Younger Dryas event and deep-ocean circulation, *Nature,* **342,** 637–642.

Fielding, E., Isacks, B., Barazangi, M. & Duncan, C.C., 1994. How flat is Tibet?, *Geology,* **22,** 163–167.

Fitch, T.J., 1972. Plate convergence, transcurrent faults, and internal deformation adjacent to southeast Asia and the western Pacific, *J. geophys. Res.,* **77** (23), 4432–4460.

Frost, G.M., Coe, R.S., Meng, Z., Peng, Z., Chen, Y., Courtillot, V., Peltzer, G., Tapponnier, P. & Avouac, J.P., 1995. Preliminary early Cretaceous paleomagnetic results from the Gansu corridro, China, *Earth Planet. Sci. Lett.,* **129,** 217–232.

Gansu Geological Bureau, 1975. *Geologic map of Gansu,* scale 1/1 000 000, 6 sheets, Lanzhou, Geological press, Ministry of Geology, Beijing.

Gaudemer, Y., Tapponnier, P., Meyer, B., Peltzer, G., Shunmin, G., Zhitai, C., Huagung, D. & Cifuentes, I., 1995. Partitioning of crustal slip between linked active faults in the eastern Qilian Shan, and evidence for a major seismic gap, the 'Tianzhu gap', on the western Haiyuan Fault, Gansu (China), *Geophys. J. Int.,* **120,** 599–645.

Ge, S., Bai, M., Li, Y., Liu, G., Zhen, Q., Zheng, J. & Zhu, S., 1992. *Active Altyn fault zone,* Seismological Press, Beijing.

Geological Publishing House, 1988. *Geological Map of Qinghai-Xizang Plateau and Adjacent Areas,* Science Press, Beijing, China.

Griot, D.A., 1997. Tomographie anisotrope de l'Asie centrale à partir d'ondes de surface, *PhD thesis,* l'Université Paris VII-Denis Diderot, Université ParisVII.

Gu, Gongxu & Di, 1989. Mechanism of formation of the Qaidam basin and its control on petroleum, in *Chinese Sedimentary Basins,* ed. X. Zhu, Series ed. K.S. Hsü, Elsevier, Amsterdam.

Gu, Gongxu, Tinghuang, L. & Zheniliang, S., 1989. *Catalogue of Chinese earthquakes (1831 BC–1969 AD),* Science Press, Beijing, China.

Guo, S. & Xian, H., 1985. *Active faults and scarps due to faulting in Late Cenozoic era in Gaotai and Yumu Shan area, Gansu,* State Seismological Bureau (in Chinese).

Halim, N., Cogné, J.P., Chen, Y., Atasiei, R., Besse, J., Courtillot, V., Gilder, S., Marcoux, J. & Zhao, R.L., 1998. New Cretaceous and Lower Tertiary paleomagnetic results from Xining-Lanzhou basin, Kunlun and Qiangtang blocks (China): implications on the geodynamic evolution of Asia, *J. geophys. Res.,* in press.

Hendrix, M., Graham, S., Carrol., A., Sobel, E., McKnight, C., Shulei, B. & Wang, Z., 1992. Sedimentary record and climatic implications of recurrent deformation in the Tien Shan: Evidence from Mesozoic strata of the north Tarim, south Dzungar, and Turpan basin, northwest China, *Geol. Soc. Am. Bull.,* **104,** 53–79.

Hirn, A., Lepine, J., Jobert, G., Sapin, M., Wittlinger, G., Xu, Z.X., Gao, E.Y., Jing, W.X., Teng, J.W., Xiong, S.B., Pandey, M.R. & Tater, J.M., 1984. Crustal structure and variability of the Himalayan border of Tibet, *Nature,* **307,** 23–25.

Holt, W.E., Li, M. & Haines, A.J., 1995. Earthquake strain rates and instantaneous relative motions within central and eastern Asia, *Geophys. J. Int.,* **122,** 569–593.

Houseman, G.A. & England, P.C., 1986. Finite strain calculations of continental deformation 1. Method and general results for convergent zones, *J. geophys. Res.,* **91,** 3651–3663.

Ikeda, Y., 1983. Thrust-front migration and its mechanism–Evolution of intraplate thrust fault systems, *Bull. dept Geog. Univ. Tokyo,* **15,** 125–159.

Institute of geophysics, 1976. *The catalog of strong shocks of China,* Academia Sinica, Beijing.

Jackson, J., Norris, R. & Youngson, J., 1996. The structural evolution of active fault and fold systems in central Otago, New Zealand: evidence revealed by drainage patterns, *J. struct. Geol.,* **18,** 217–234.

Jamison, W.R., 1987. Geometric analysis of fold development in overthrust terranes, *J. struct. Geol,* **9,** 207–219.

Jin, Y., McNutt, M.K. & Yongsheng Zhu, 1994. Evidence from gravity and topography data for folding of Tibet, *Nature,* **371,** 669–672.

King, G.C.P. & Vita-Finzi, C., 1981. Active folding in the Algerian earthquake of 10 October, 1980, *Nature,* **292,** 22–26.

King, G.C.P., Stein, R.S. & Rundle, J.B., 1988. The growth of geological structures by repeated earthquakes. 1. Conceptual framework, *J. geophys. Res.,* **93,** 13 307–13 318.

Lacassin, R., Armijo, R. & Tapponnier, P., 1993. Can ramp to flat bends on thrust induce transport parallel extension? the exemple of the himalayan thrust wedge, in *Proc. Conf. in Late orogenic extension in mountain belts,* pp. 114–115, Document du BGRM, 219.

Lacassin, R., Schärer, U., Leloup, P.H., Arnaud, N., Tapponnier, P., Liu Xiaohan, & Zhang Liansheng, 1996. Tertiary deformation and metamorphism SE of Tibet: the folded tiger-leap décollement of NW Yunnan (China), *Tectonics,* **15,** 605–622.

Lacassin, R., Maluski, H., Leloup, P.H. & Tapponier, P., 1997. Tertiary diachronic extrusion and deformation of western Indochina: structural and $^{40}Ar/^{39}Ar$ evidence from NW Thailand, *J. geophys. Res.,* **102,** 10 013–10 037.

Lasserre, C., Gaudemer, Y., Tapponnier, P., Lu, T., Liu, B., Morel, P.-H., Ryerson, F.J., King, G.C.P. & Ruegg, J.C., 1997. Multidisciplinary study of the seismic 'Tianzhu gap' along the Haiyuan fault (Gansu, China): constraints on slip rate, *Terra Nova,* **9,** 305, Abstract supplement.

Lee, W.H.K., Wu, F.T. & Jacobsen, C., 1976. A catalogue of historical earthquakes in China compiled from recent Chinese publications, *Bull. seism. Soc. Am.,* **66,** 2003–2016.

Leloup, P.H., Lacassin, R., Tapponnier, P., Schärer, U., Dalai, Z., Xiaohan, L., Liangshang, Z., Shaocheng, J. & Trinh, P.T., 1995. The Ailao Shan-Red River shear zone (Yunnan, China), Tertiary transform boundary of Indochina, *Tectonophysics,* **251,** 3–84.

Lyon-Caen, H. & Molnar, P., 1984. Gravities anomalies and the structure of Western Tibet and the southern Tarim basin, *Geophys. Res. Lett.,* **11,** 1251–1254.

Ma, X., 1987. *Lithospheric dynamic map of China and adjacent seas with explanatory notes,* scale 1:4 000 000, Geol. Publish. House, Beijing, China.

Malavieille, J., 1984. Modélisation expérimentale des chevauchements imbriqués: application aux chaînes de montagnes, *Bull. Soc. géol. Fr.,* **26,** 129–138.

Manighetti, I., Tapponnier, P., Courtillot, V. & Gruszow, S., 1997. Propagation of rifting along the Arabia–Somalia plate boundary: The Gulfs of Aden and Tadjoura, *J. geophys. Res.,* **102,** 2681–2710.

Martinod, J. & Davy, P., 1994. Periodic instabilities during compression of the lithosphere; 2, Analogue experiments, *J. geophys. Res.,* **99,** 12 057–12 069.

Mattauer, M., 1986a. Intracontinental subduction, crust-mantle décollement and crustal-stacking wedge in the Himalayas and other collision belts, in *Collision Tectonics,* eds Coward, M.P. & Ries, A.C., Geol. Soc. Spec. Publ., 19, 37–50.

Mattauer, M., 1986b. Les subductions intracontinentales des chaînes tertiaires d'Asie; leurs relations avec les décrochements, *Bull. Soc. géol. Fr.,* **8,** 143–157.

Mattauer, M., Malavieille, J., Calassou, S., Lancelot, J., Roger, F., Hao Ziwen, Zhu Zhiqin & Hou Liwei, 1992. La chaîne triassique de songpan-Garze (Ouest Sechuan et Est Tibet): une chaîne de plissement-décollement sur marge passive, *Comptes Rendus à l'Académie des Sci. de Paris,* **314,** 619–626.

Matte, P., Tapponnier, P., Arnaud, N., Bourjot, L., Avouac, J.P., Vidal, P., Liu Qing, Yusheng, P. & Yi, W., 1996. Tectonics of western Tibet, between the Tarim and the Indus, *Earth planet. Sci. Lett.,* **142,** 311–330.

Métivier, F., 1996. Volumes sédimentaires et bilans de masse en Asie pendant le Cénozoïque, *PhD thesis,* Université Paris VII, France.

Métivier, F. & Gaudemer, Y., 1997. Mass transfer between eastern Tien Shan and adjacent basins (Central Asia): constraints on regional tectonics and topography, *Geophys. J. Int.,* **128,** 1–17.

Meyer, B., 1991. Mécanismes des grands tremblements de terre et du raccourcissement crustal oblique au bord Nord-Est du Tibet, *PhD thesis,* Université ParisVI, France.

Meyer, B., Avouac, J.P., Tapponnier, P. & Meghraoui, M., 1990. Mesures topographiques sur le segment SW de la zone faillée d'El Asnam et interprétation mécanique des relations entre failles inverses et normales, *Bull. Soc. géol. Fr.,* **t vi, 3,** 447–456.

Meyer, B., Tapponnier, P., Gaudemer, Y., Mercier, N., Valladas, H., Guo, S. & Zhitai, C., 1991. 1932 Chang Ma (M = 7.6) earthquake surface breaks and implications on regional seismic hazard, (Extended abstract), in *Proc. Conf. 1st INSU-SSB Workshop, Earthquakes: from source mechanism to seismic hazard,* Institut de Physique du Globe de Paris, Paris.

Meyer, B., Tapponnier, P., Gaudemer, Y., Peltzer, G., Guo, S. & Chen, Z., 1996. Rate of left-lateral movement along the easternmost segment of the Altyn Tagh Fault, east of 96°E (China), *Geophys. J. Int.,* **124,** 29–44.

Molnar, P., 1988. Continental tectonics in the aftermath of plate tectonics, *Nature,* **335,** 131–137.

Molnar, P. & Lyon-Caen, H., 1988. Some simple physical aspects of the support, structure, and evolution of mountain belts, *Geol. Soc. Am. Spec. Paper,* **218,** 179–207.

Molnar, P. & Lyon-Caen, H., 1989. Fault plane solution of earthquake and active tectonics of the Tibetan plateau and its margins, *Geophys. J. Int.,* **99,** 123–153.

Molnar, P. & Tapponnier, P., 1975. Cenozoic tectonics of Asia: effects of continental collision, *Science,* **189,** 419–426.

Molnar, P. & Tapponnier, P., 1978. Active tectonics of Tibet, *J. geophys. Res.,* **83,** 5361–5375.

Molnar, P. & Tapponnier, P., 1981. A possible dependence of tectonic strength on the age of the crust in Asia, *Earth planet. Sci. Lett.,* **52,** 107–114.

Molnar, P., England, P. & Martinod, J., 1993. Mantle dynamics, uplift of the Tibetan Plateau, and the Indian monsoon, *Rev. Geophys.,* **31,** 357–396.

Nelson, K.D. *et al.* 1996. Partially molten middle crust beneath southern Tibet: Synthesis of project INDEPTH results, *Science,* **274,** 1684–1688.

Ni, J. & Barazangi, M., 1984. Seismotectonics of the Himalayan collision zone; geometry of the underthrusting Indian Plate beneath the Himalaya, *J. geophys. Res.,* **89,** 1147–1163.

Norin, E., 1946. Geological explorations in western Tibet, in *Reports of the scientific expedn to the Northwestern Provinces of China under the Leadership of Dr. Sven Hedin,* Publ. 29 III, Geology 7, Trycheri Aktiebolaget Thule, Stockholm, 214 pp.

Owens, T.J. & Zandt, G., 1997. Implications of crustal property variations for model of Tibetan plateau evolution, *Nature,* **387,** 37–40.

Peltzer, G. & Saucier, F., 1996. Present-day kinematics of Asia derived from geologic fault rates, *J. geophys. Res.,* **101,** 27 943–27 956.

Peltzer, G. & Tapponnier, P., 1988. Formation and evolution of strike-slip faults, rifts, and basins during India-Asia collision: an experimental approach, *J. geophys. Res.,* **93,** 15 085–15 172.

Peltzer, G., Tapponnier, P., Zhang, Z. & Xu, Z., 1985. Neogene and Quaternary faulting in and along the Qiling Shan, *Nature,* **317,** 500–505.

Peltzer, G., Tapponnier, P., Gaudemer, Y., Meyer, B., Guo, S., Yin, K., Chen, Z. & Dai, H., 1988. Offsets of late Quaternary morphology, rate of slip, and recurrence of large earthquakes on the Changma fault (Gansu, China), *J. geophys. Res.,* **93,** 7793–7812.

Peltzer, G., Tapponnier, P. & Armijo, R., 1989. Magnitude of late Quaternary left-lateral displacements along the northern edge of Tibet, *Science,* **246,** 1285–1289.

Philip, H. & Meghraoui, M., 1983. Structural analysis and interpretation of the El Asnam earthquake of October 10, 1980, *Tectonics,* **1,** 17–49.

Phillips, F., Zreda, M., Ku, T., Luo, S., Qi, H., Elmore, D., Kubik, P. & Sharma, P., 1993. $^{230}Th/^{234}U$ and ^{36}Cl dating of evaporite deposits from the western Qaidam basin, China: implications for glacial-period dust export from central Asia, *Geol. Soc. Am. Bull.,* **105,** 1606–1615.

Qinghai Geological Bureau, 1983. *Geological map of Qinghai,* Xining, Geological press, Ministry of Geology.

Rispoli, R., 1981. Stress fields about strike-slip faults inferred from stylolites and tension gashes, *Tectonophysics,* **75,** T29–T36.

Royden, L., 1996. Coupling and decoupling of crust and mantle in convergent orogens: implications for strain partitioning in the crust, *J. geophys. Res.,* **101,** 17 679–17 705.

Ryerson, F.J., Finkel, R.C., Meriaux, A., Caffee, M.W., Peltzer, G., Farr, T., Chadwick. O. & Clarke, D.H., 1997. *Rapid Slip on the Altyn Tagh Fault—Karakax Valley Segment,* Geol. Soc. Am., Abstracts with Programs, A-143.

Schärer, U., Lian-Sheng, Z. & Tapponnier, P., 1994. Duration of strike-slip movements in large shear zones: the Red River belt, China, *Earth planet. Sci. Lett.,* **126,** 379–397.

Scholz, C.H., Dawers, N.H., Yu, J.-Z., Anders, M.H. & Cowie, P.A., 1993. Fault growth and fault scaling laws: Preliminary results, *J. geophys. Res.,* **98,** 21 951–21 961.

Sengör, A.M.C., 1984. *The Cimmeride Orogenic System and the Tectonics Of Eurasia,* Geol. Soc. Am., Special Paper, 195.

State Seismological Bureau., 1993. *The Qilian Mountain–Hexi Corridor Active Fault System,* eds Guo S., Chen Z., Xiang H., Dai H., Seismological Press, Beijing.

Stein, R. & Ekstrom, G., 1992. Seismicity and geometry of a 110-km-long blind thrust fault; 2, Synthesis of the 1982–85 California earthquake sequence, *J. geophys. Res.,* **97,** 4865–4883.

Stein, R. & King, G.C.P., 1984. Seismic potential revealed by surface folding: the 1983 Coalinga, California, Earthquake, *Science,* **224,** 869–872.

Stein, R.S., King G.C.P. & Rundle J.B., 1988. The growth of geological structures by repeated earthquakes. 2. Field examples of continental dip-slip faults, *J. geophys. Res.,* **95,** 13 319–13 331.

Suppe, J., 1983. Geometry and kinematics of fault-bend folding, *Am. J. Sci.,* **283,** 684–721.

Tapponnier, P. & Molnar, P., 1977. Active faulting and tectonics in China, *J. geophys. Res.,* **82,** 2905–2930.

Tapponnier, P., Mercier, J.L., Armijo, R., Han, T. & Zhou, J., 1981. Field evidence for active normal faulting in Tibet, *Nature,* **294,** 410–414.

Tapponnier, P., Peltzer, G. & Armijo, R., 1986. On the mechanics of the collision between India and Asia, in *Collision Tectonics,* eds Coward, M.P. & Ries, A.C., Geol. Soc. Spec. Publ., **19,** 115–157.

Tapponnier, P., Meyer, B., Avouac, J.-P., Gaudemer, Y., Peltzer, G., Guo, S., Xiang, H., Yin, K., Chen, Z., Cai, S. & Dai, H., 1990a. Active thrusting and folding in the Qi Lian Shan, and decoupling between the upper crust and mantle in northeastern Tibet, *Earth planet. Sci. Lett.,* **97,** 382–403.

Tapponnier, P., Lacassin, R., Leloup, P.H., Scharer, U., Zong, D., Wu, H., Liu, X., Ji, S., Zhang, L. & Zhong, J., 1990b. The Ailao Shan-Red River metamorphic belt: Tertiary left-lateral shear between Indochina and South China, *Nature,* **343,** 431–437.

Times Atlas of the World, 1978. 5th edn, John Bartholomew & Son Limited, Edinburgh.

Turner, S., Arnaud, N., Liu, J., Rogers, N., Hawkesworth, C., Harris, N., Kelley, S., Van Calsteren, P. & Deng, W., 1996. Post-collision, shoshonitic volcanism on the Tibetan Plateau: Implications for convective thinning of the lithosphere and the source of ocean island basalts, *J. Petrol.,* **37,** 45–71.

Van Der Woerd, J., Ryerson, F.J., Tapponnier, P., Gaudemer, Y., Finkel, R., Meriaux, A.S. & Caffee, M., 1998. Zhao Guoguang, He Qunlu, Holocene left-slip rate determined by cosmogenic surface dating on the Xidatan segment of the Kunulun Fault (Qinghai, China), *Geology,* in press.

Wang, J. & Derbyshire, E., 1987. Climatic geomorphology of the northeastern part of the Qinghai-Xizang plateau, People's Republic of China, *Geograph. J.,* **153,** 59–71.

Westaway, R., 1995. Crustal Vol. balance during the India-Eurasia collision and altitude of the Tibetan plateau: A working hypothesis, *J. geophys. Res.,* **100,** 15 173–15 192.

Willet, S.D. & Beaumont, C., 1994. Subduction of Asian lithospheric mantle beneath Tibet inferred from models of continental collision, *Nature,* **369,** 642–645.

Wittlinger, G., Masson, F., Poupinet, G., Tapponnier, P., Jiang Mei, Herquel, G., Guilbert, J., Achauer, U., Xue Guanqi, Shi Danian & Team, L.K., 1996. Seismic tomography of northern Tibet and Kunlun: Evidence for crustal blocks and mantle velocity contrasts, *Earth planet. Sci. Lett.,* **139,** 226–279.

Wittlinger, G., Tapponnier, P. & Poupinet, G., submitted. Jian Mei, Shi Danian, Herquel G. & Masson, F., 1998. Tomographic evidence for lithospheric shear along the Altyn Tagh Fault (China), *Science,* in press.

Xu, W., He, Y. & Yan, Y., 1989. Tectonic characteristics and hydrocarbons of the Hexi Corridor, in *Sedimentary Basins of the World, 1, Chinese Sedimentary Basins,* pp. 53–62, ed. Hsü, K.J., Elsevier, Amsterdam.

Yeats, R.S., 1983. Large-scale Quaternary detachments in Ventura basin, southern California, *J. geophys. Res.,* **88,** 569–583.

Yeats, R.S., 1986. Faults related to folding with examples from New Zealand, *Royal Soc. NZ Bull.,* **24,** 273–292.

Yeats, R.S., Clark, M.N., Keller, E.A. & Rockwell, T.K., 1981. Active fault hazard in southern California: ground rupture versus seismic shaking, *Geol. Soc. Am. Bull.,* **92,** 189–196.

Yeats, R.S., Sieh, K. & Allen, C.R., 1997. *The Geology of Earthquakes,* Oxford University Press, New York.

Zhang Peizhen, Molnar, P., Burchfiel, B.C., Royden, L., Wang Yipeng, Deng Qidong, L. & Song Fangmin, 1988. Bounds on the holocene slip-rate on the Haiyuan fault, north-central China, *Quat. Res.,* **30,** 151–164.

Zhang Peizhen, Burchfiel, B.C., Molnar, P., Zhang Weiqi, Jiao Dechen, Deng Qidong, Wang Yipeng, Royden, L. & Song Fangmin, 1990. Late Cenozoic tectonic evolution of the Ningxia-Hui autonomous region, China, *Geol. Soc. Am. Bull.,* **102,** 1484–1498.

Zhang Peizhen, Burchfiel, B.C., Molnar, P., Zhang Weiqi, Jiao Dechen, Deng Qidong, Wang Yipeng, Royden, L. & Song Fangmin, 1991. Amount and style of late Cenozoic deformation in the Liupan Shan area, Ningxia autonomous region, China, *Tectonics,* **10,** 1111–1129.

Zhao, W. & Morgan, W.J., 1985. Uplift of Tibetan Plateau, *Tectonics,* **4,** 359–369.

Zhao, W.J., Nelson, K.D. & Project INDEPTH Team, 1993. Deep seismic reflection evidence for continental underthrusting beneath southern Tibet, *Nature,* **366,** 557–559.